AD_____

AWARD NUMBER: DAMD17-98-1-8515

TITLE: Influence of Bone Remodeling Inhibition on the Development of Experimental Stress Fractures

PRINCIPAL INVESTIGATOR: Mitchell B. Schaffler, Ph.D.

CONTRACTING ORGANIZATION: Mount Sinai School of Medicine
New York, New York 10029

REPORT DATE: November 2005

TYPE OF REPORT: Final Addendum

PREPARED FOR: U.S. Army Medical Research and Materiel Command
Fort Detrick, Maryland 21702-5012

REPORT DOCUMENTATION PAGE

Form Approved
OMB No. 0704-0188

1. REPORT DATE *(DD-MM-YYYY)*	**2. REPORT TYPE**	**3. DATES COVERED** *(From - To)*
01-11-2005	Final Addendum	1 Oct 2004 – 31 Oct 2005

4. TITLE AND SUBTITLE

Influence of Bone Remodeling Inhibition on the Development of Experimental Stress Fractures

5a. CONTRACT NUMBER

5b. GRANT NUMBER
DAMD17-98-1-8515

5c. PROGRAM ELEMENT NUMBER

6. AUTHOR(S)

Mitchell B. Schaffler, Ph.D.

E-Mail: mitchell.schaffler@mssm.edu

5d. PROJECT NUMBER

5e. TASK NUMBER

5f. WORK UNIT NUMBER

7. PERFORMING ORGANIZATION NAME(S) AND ADDRESS(ES)

Mount Sinai School of Medicine
New York, New York 10029

8. PERFORMING ORGANIZATION REPORT NUMBER

9. SPONSORING / MONITORING AGENCY NAME(S) AND ADDRESS(ES)
U.S. Army Medical Research and Materiel Command
Fort Detrick, Maryland 21702-5012

10. SPONSOR/MONITOR'S ACRONYM(S)

11. SPONSOR/MONITOR'S REPORT NUMBER(S)

12. DISTRIBUTION / AVAILABILITY STATEMENT
Approved for Public Release; Distribution Unlimited

13. SUPPLEMENTARY NOTES

14. ABSTRACT

Stress fractures result from repetitive loading and have been regarded as a mechanical fatigue-driven process. However, a number of studies indicate implicate increased bone remodeling in the pathogenesis of stress fractures. Our experiments tested the hypothesis by pharmacological inhibition of bone remodeling will slow the accumulation of microdamage and diminish the severity of the stress fracture. Using a bisphosphonate (BIS) to suppress remodeling in the rabbit tibial stress fracture model, we found that antiresorptive therapy reduced the intensity of the stress fracture response in this model.(^{99m}Techneitum uptake reduced by approximately 50 percent, size of the resulting fracture callus reduced by about 30-50% in BIS-treated animals) and a trend toward reduced bone microdamage accumulation. These data are consistent with the hypothesis that bone remodeling contributes to the pathogenesis of stress fracture. However, variability in this model was greater than expected, limiting our ability to move forward with this animal model. We also report on the results of novel model for stress fracture healing, using adult rats, developed under the aegis of this program.

15. SUBJECT TERMS
Stress fracture, animal model, bisphosphonate

16. SECURITY CLASSIFICATION OF:			**17. LIMITATION OF ABSTRACT**	**18. NUMBER OF PAGES**	**19a. NAME OF RESPONSIBLE PERSON**
a. REPORT	**b. ABSTRACT**	**c. THIS PAGE**			USAMRMC
U	U	U	UU	84	**19b. TELEPHONE NUMBER** *(include area code)*

TABLE OF CONTENTS

INTRODUCTION

Stress fractures result from repetitive loading and have been regarded as a mechanical fatigue-driven process. However, histopathological data and experimental data from our laboratory suggests that increased remodeling precedes the occurrence of bone microdamage and stress fractures, suggesting a central role for increased intracortical remodeling in the pathogenesis of stress fractures. Thus, we propose that stress fracture occurs through a positive feedback mechanism, in which increased mechanical usage stimulates focal bone turnover, resulting in a local increase in porosity. Microdamage accumulation and stress fractures result from continued cyclic loading of this transiently osteoporotic bone. These experiments test the hypothesis that pharmacologically inhibiting the bone remodeling response will attenuate severity of the stress fracture response in an animal model (the rabbit tibial stress fracture model). To test the hypothesis that reactive remodeling within the cortex drives the development of stress fractures, the effect of remodeling suppression using a bisphosphonate on the accumulation of bone microdamage and diminishing the severity of stress fracture was examined. Tissues were assessed using bone scintigraphy, histomorphometry and biomechanical studies. The Hypotheses and Specific Aims were as follows:

Hypothesis 1*: Pharmacological prevention of increased intracortical resorption will attenuate the development of stress fracture resulting from continued mechanical loading*.

Aim 1: To determine at the whole bone level whether bisphosphonate inhibition of intracortical remodeling attenuates the bone scintigraphy changes (i.e. increases in focal ^{99m}Technetium uptake) that characterize the development of stress fracture.

Hypothesis 2*: With repetitive mechanical loading, pharmacological inhibition of bone resorption results in decreased microdamage accumulation in compact bone. A secondary hypothesis is that inhibition of activation of intracortical resorption will maintain mechanical integrity of bone*

Aim 2: To determine at the tissue level whether bisphosphonate inhibition of intracortical remodeling decreases the accumulation of cortical bone microdamage that occurs at stress fracture sites.

Hypothesis 3*: Pharmacological prevention of increased intracortical resorption in response to repetitive loading will maintain mechanical integrity of long bones.*

Aim 3: To use biomechanical testing of experimentally loaded rabbit tibiae to determine directly how increases in intracortical remodeling (porosity), and pharmacological prevention of that increase in remodeling, influence the structural-mechanical properties of long bones.

In this grant period, we tested these hypotheses in the rabbit tibial stress fracture model, which was developed in our laboratory. Tibiae in this loading model develop a stress fracture lesion after several weeks of daily loading. Increased ^{99m}Tc uptake, increased internal remodeling of bone, increased bone microdamage, all of which are associated with stress fractures in humans, are all present in this model.

Our objectives in these experiments were to use the rabbit tibial stress fracture model:

- To determine at the whole bone level whether bisphosphonate inhibition of intracortical remodeling attenuates the increase in focal bone reaction at the periosteal surface.
- To determine at the tissue level whether bisphosphonate inhibition of intracortical remodeling decreases the accumulation of cortical bone microdamage which occurs at the site of stress fracture, and
- To determine how stress fracture compromises mechanical properties of long bones and whether pharmacological inhibition of remodeling can offset that functional deficit.

RESEARCH SUMMARY

Rabbit Stress Fracture Studies

Description of the model: We developed an experimental animal model for stress fractures in rabbits, using repetitive impulsive loading (RIL) of hindlimbs. Microfractures of trabecular bone are a well-established consequence of the RIL model. Adapted for use in diaphyseal bone, this model reproduces the scintigraphic and radiographic changes typically observed with stress fractures, including progressive increase in ^{99m}Tc uptake in bone, periosteal callus formation and presence of microscopic cracks within the bone. In this model, hindlimbs of skeletally mature New Zealand white rabbits (1 year old, 4-5 kg) were loaded to produce tibial diaphyseal stress fractures. Briefly, right hindlimbs were subjected to repetitive impulsive loading, using a cam-driven loading device. Loading is at 1.5X body weight, for 50 msec cycle duration at 1Hz. During loading, the leg and calcaneus are held in a fitted, padded splint to prevent translation at the ankle joint. Left limbs are not loaded and serve as internal controls. Animals receive 2700 load cycles daily. This regime causes a stress fracture response in the distal tibial diaphysis after 5-6 weeks of loading. In the preliminary experiments, it was shown that stress fractures in this model rabbits result by repetitive cyclic loading at low stresses. The lesions, which occurred in the distal third of tibial diaphyses, were characterized at the organ level by progressive increases in bone ^{99m}Tc activity, followed later and variably a periosteal reaction (Fig 1). In subsequent studies, we measured tibial diaphyseal strains at the stress fracture site in the range of 1000 μstrain, which is well within normal physiological strain range (see above discussion); strain rates, though increased somewhat over normal, were also within the range reported for normal locomotory activities.

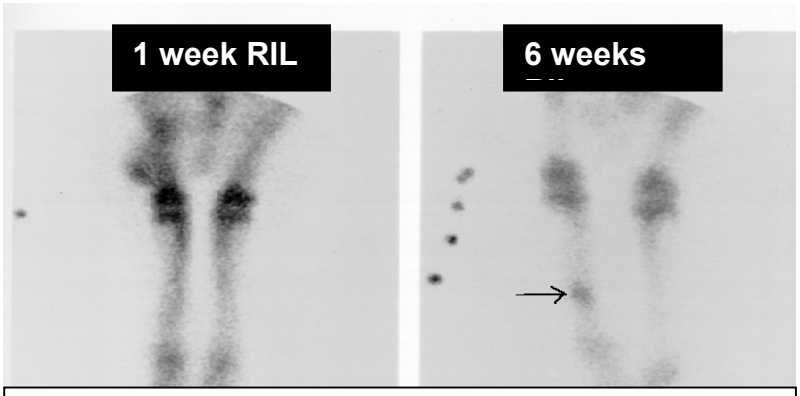

Fig 1: ^{99m}Techetium bone scans from rabbit tibiae subjected to repetitive loading. Arrow shows focal increase in ^{99m}Tc uptake

Experiment 1: Characterization of Remodeling and microdamage

Results: *We found that intracortical remodeling was markedly increased by 6 weeks of loading, with resorption number increased more than 5-fold over control levels (p=0.012, ANOVA followed by post-hoc testing using Fisher's PLSD)*. Data for intracortical resorption activity are summarized in Fig. 2. Resorption occurred primarily in the anterior and posterior tibial cortices, corresponding to the locations of stress fracture and highest strain rate in this model. Bone microdamage was not observed in control bones or after 3 weeks of loading. By 6 weeks of loading, microcracks were observed in diaphyses (Fig. 3). Typically, these were small cracks (mean length = 24 ± 7 μm). In addition, microcracks were observed only in those areas of the cortex that were undergoing intracortical remodeling.

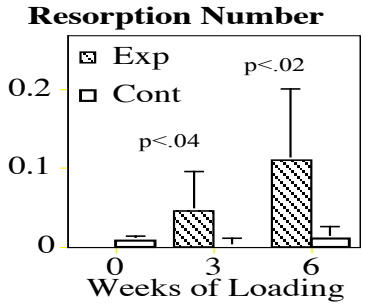

Figure 2: Intracortical resorption activity in distal tibial diaphyses after 3 and 6 week of repetitive loading.

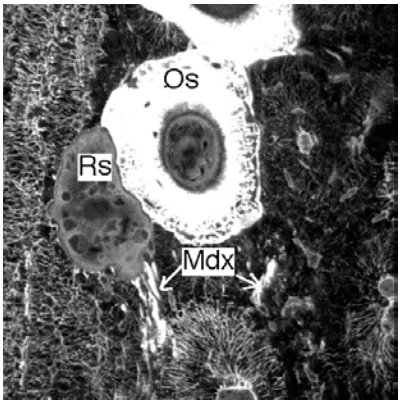

Figure 3: Confocal photo-micrograph of rabbit tibial compact bone at 6 wks of loading, showing intracortical resorption (Rs) and new osteons (Os) in association with bone microdamage (Mdx arrows) (Field width = 400 μm)

Acute in vivo "fatigue" experiments were performed to determine whether microdamage in rabbit tibias accumulates as a direct result of the applied loading regime, in the absence of increased intracortical remodeling. Hindlimbs in anesthetized rabbits were loaded acutely and continuously for the equivalent number of load cycles that limbs would receive after 6 weeks of chronic loading (70,00 load cycles = ~20hrs continuous loading). Animals in these latter experiments were euthanized immediately after completion of the loading so that no new intracortical remodeling was present. These acute loading experiments showed no microdamage with loading alone (Fig 4), *confirming that microdamage accumulation occurred only in the presence of increased bone remodeling.*

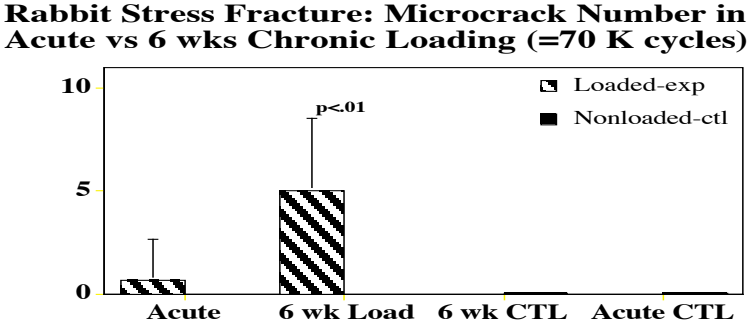

Figure 4: Microcrack content in rabbit distal tibial diaphyses after 6 weeks of daily (chronic) loading and after 70,000 cycles of acute loading

Experiment 2: Effect of Resorption Suppression

Treatment using a bisphosphonate (BIS, Risedronate, Proctor & Gamble Pharmaceutical) was used to test whether remodeling suppression attenuated the severity of stress fracture in this model. Animals were treated using the weight adjusted (0.1 mg/kg given SQ, 5 days/wk) dose used to prevent bone loss postmenopausally. Control animals received saline vehicle by subcutaneous injection.

^{99m}Technetium based bone scans were performed to follow the "clinical" evolution of the stress fracture response. Over the 6 weeks loading experiment, sequential bone scans we performed such that each animal was scanned at baseline (before loading), and then after 3 and 6 weeks of loading (n=92 animals), to allow us to assess the progress of the lesions. The following procedure was used for ^{99m}Technetium injection, scanning, and quantification to control for variability between animals and among groups. Animals were each injected with 3 mCurie of ^{99m}Tc with the isotope was administered IV in the ear vein. Scans were conducted 3 hours later to image the bone phase of ^{99m}Tc using a General Electric STARCAM System with a pinhole collimator and the data archived on optical disk for later analysis. Prior to scanning, rabbits were sedated and the lower extremities placed into one of two positioning devices. The lower limbs were positioned in a holder to allow consistent positioning for A-P and M-L scans. A standardized area (8mm x 8 mm) was used to determine a region of interest at the stress fracture site for the anterior view. This region of interest was of the same dimensions for all animals and provides an average count per pixel of isotope incorporation within the standard area. The same standardized area was also used to determine a background level of isotope incorporation. An average count of isotope incorporation per pixel was obtained within the background area. The average counts per pixel in the stress fracture region of interest were normalized by dividing by the average counts per pixel in the background region (*Average Counts per Pixel Stress Fracture Region of Interest/Average Counts per Pixel Background Region*). Mean value for each time period was compared between the bisphosphonate-injected and saline-injected groups using t-test. Differences among groups over time were assessed using one-way ANOVA.

Results: *Tibiae in animals receiving antiresorptive treatment using bisphosphonate (BIS) showed reduced intensity of the stress fracture response, as indicated by ^{99m}Technetium bone scan*. At 3 weeks, ^{99m}Tc uptake was approximately 10 percent lower in treated animals; this difference was not significant ($p > 0.4$). After 6 weeks of loading, ^{99m}Tc uptake was significantly lower (approximately 50 percent, $p < .05$) in bisphosphonate-treated animals than in non-treated animals. Nevertheless, ^{99m}Tc uptake at 6 week was still significantly ($p < .001$) higher than in non-loaded, bisphosphonate-treated animals. These data are summarized below in Figure 5.

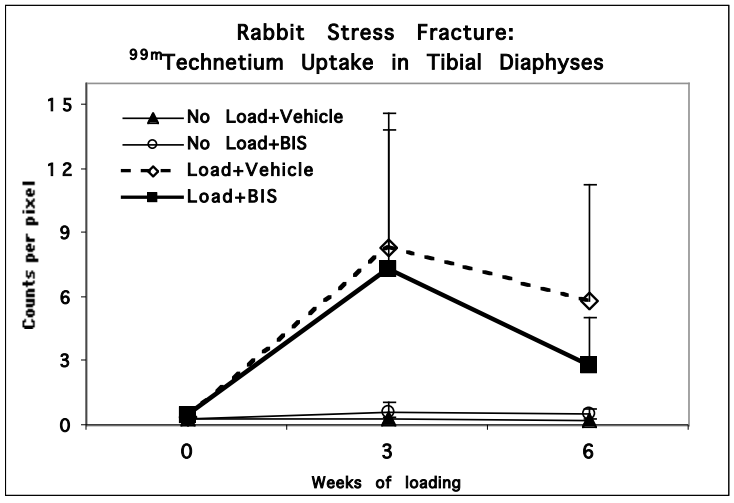

Experiment 3: Bone and Tissue studies:

Tibiae were removed at the time of sacrifice and fixed in 70% ethanol. CT scans of each bone diaphysis were performed to provide a 3-Dimensional "clinical" picture of the stress fracture response. Bones were then embedded in methacrylate resin and sectioned for histomorphometric studies.

Periosteal reactive bone volume – Our early 2-D histological and anatomical studies in this program revealed considerable heterogeneity in the shape of reactive periosteal woven bone (i.e., "fracture" callus) and distribution along the length of the diaphysis, as well as between bones, making measurement from tissue sections problematic. In order to better account for this heterogeneity, we developed a new CT-based approach to measure the 3-D reactive periosteal bone volume for the entire diaphysis.

Method: Prior to histological studies, bones were scanned through the diaphyseal length using a GE clinical CT scanner operated at 0.5 mm voxel resolution. Thresholded diaphyseal cross-sectional images were examined. Reactive (woven) bone on the periosteal surfaces of loaded bones was readily distinguished from the pre-existing cortex. Custom software was developed in MATLAB to allow measurement of reactive bone area and normal bone area from each section. This process was repeated at every millimeter at each level for which woven bone could be observed and summation of the reactive bone area over its longitudinal extent were used to determined volumes.

Fig 6: CT scan taken through the entire reactive region of the tibial diaphysis of an experimentally-loaded rabbit showing periosteal reactive bone after 6 weeks of chronic loading. (Voxel size – 0.5mm x 0.5mm x 0.5 mm).

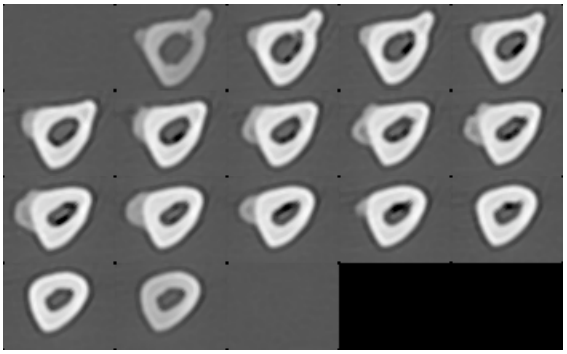

Fig 7: Thresholded (left) and segmented images (right) used to separate cortical bone, reactive mineralized tissue and soft tissue

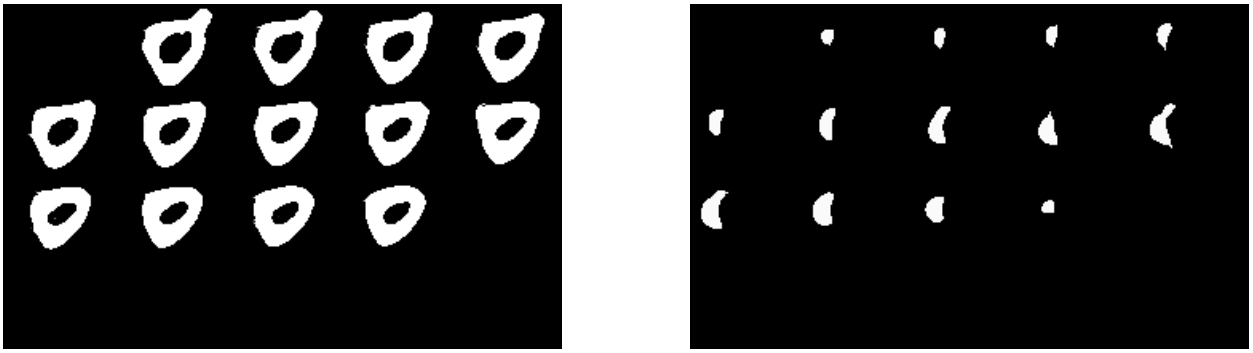

Results: *The volume of reactive bone tissue was significantly ($p<0.05$) correlated to the overall cortical bone porosity, i.e., those bones with the greatest amount of void space due to intracortical resorption showed the*

greatest amount of periosteal reaction (Fig 8). Whether this reflects the fact that more porous bone experiences locally greater strains and hence shows a greater stress fracture response as we hypothesized or perhaps reflects a greater overall reactivity in certain animals could not be determined in this study.

Fig 8

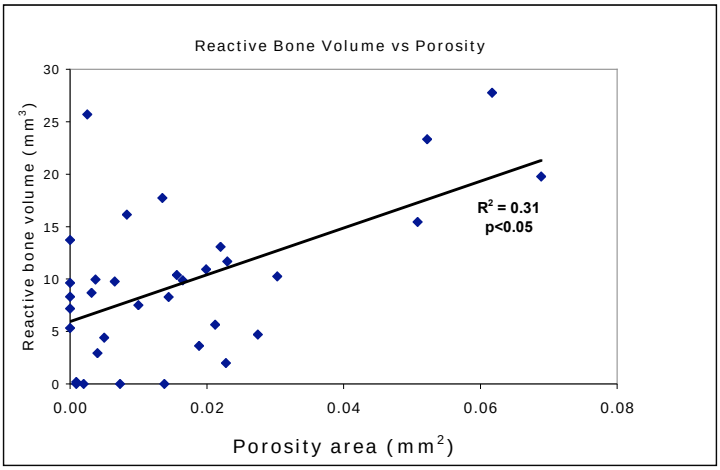

When analyzed on a treatment group basis, BIS treatment resulted in approximately 40 percent less periosteal reactive bone formation after 6 weeks of chronic loading compared to vehicle treated animals (Fig 9, at right). However, these results were not statistically significant (p = 0.09) due to the very high variability among animals (coefficients of variation >100 percent). Thus, *while these trends are consistent with the hypothesis that suppressing resorption will reduce the severity of the periosteal stress reaction in chronic loading, the results are not definitive*

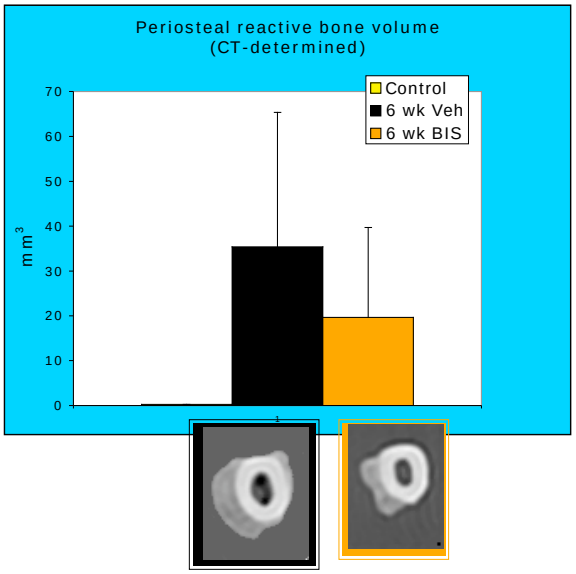

Resorption: After 6 weeks of daily loading, vehicle treated animals showed a nearly 5-fold increase in intracortical resorption (Figure 10A/B). Bisphosphonate (BIS) treatment suppressed this activation of new intracortical remodeling to control levels, but those resorption spaces present in BIS-treated, loaded animals were significantly larger than those in normal bone.

Fig 10 A/B

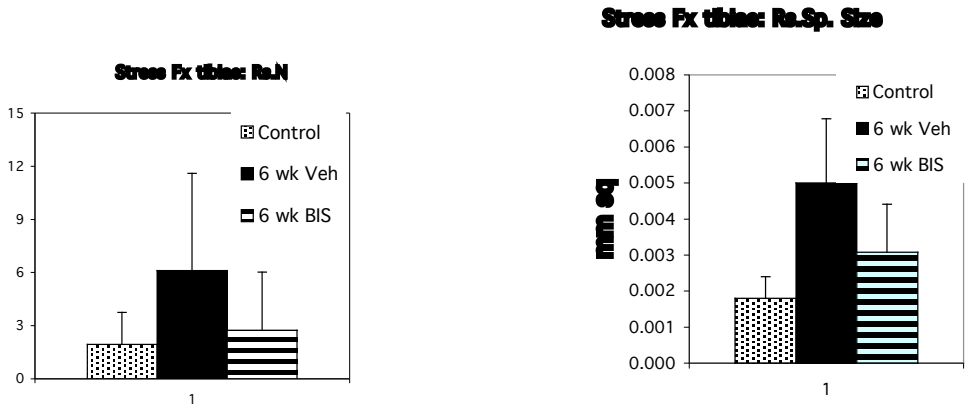

Microdamage: Overall, the amount of microdamage in loaded animals was small (typically less than 0.5 microcracks/cm^2) and highly variable (Coefficient of variation > 100 percent). BIS-treated tibiae showed approximately 50 percent fewer microcracks after 6 weeks of loading than did vehicle treated animals (Figure 11). However, these results were not statistically significant ($p = 0.11$) due to the very high variability among animal.

Fig 11

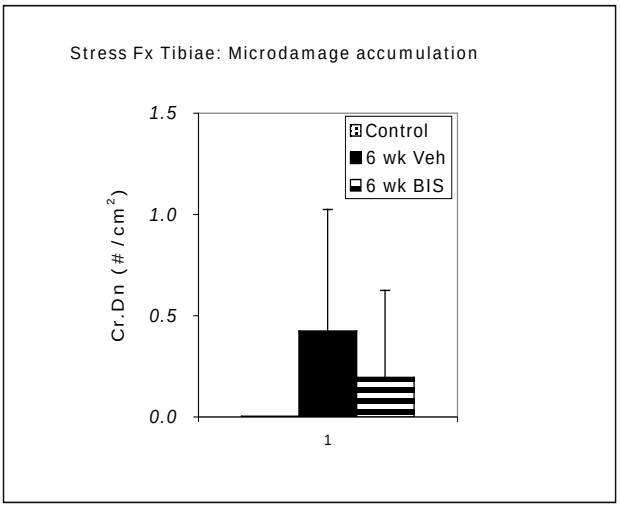

Summary of experiments using rabbit stress fracture model: *While these data are generally consistent with the hypothesis that suppressing resorption will prevent microdamage accumulation, as summarized in Figure 12 below. However, the high degree of variability in this animal model prevents a definitive answer to the question of whether remodeling inhibition suppresses the accumulation of microdamage with loading.*

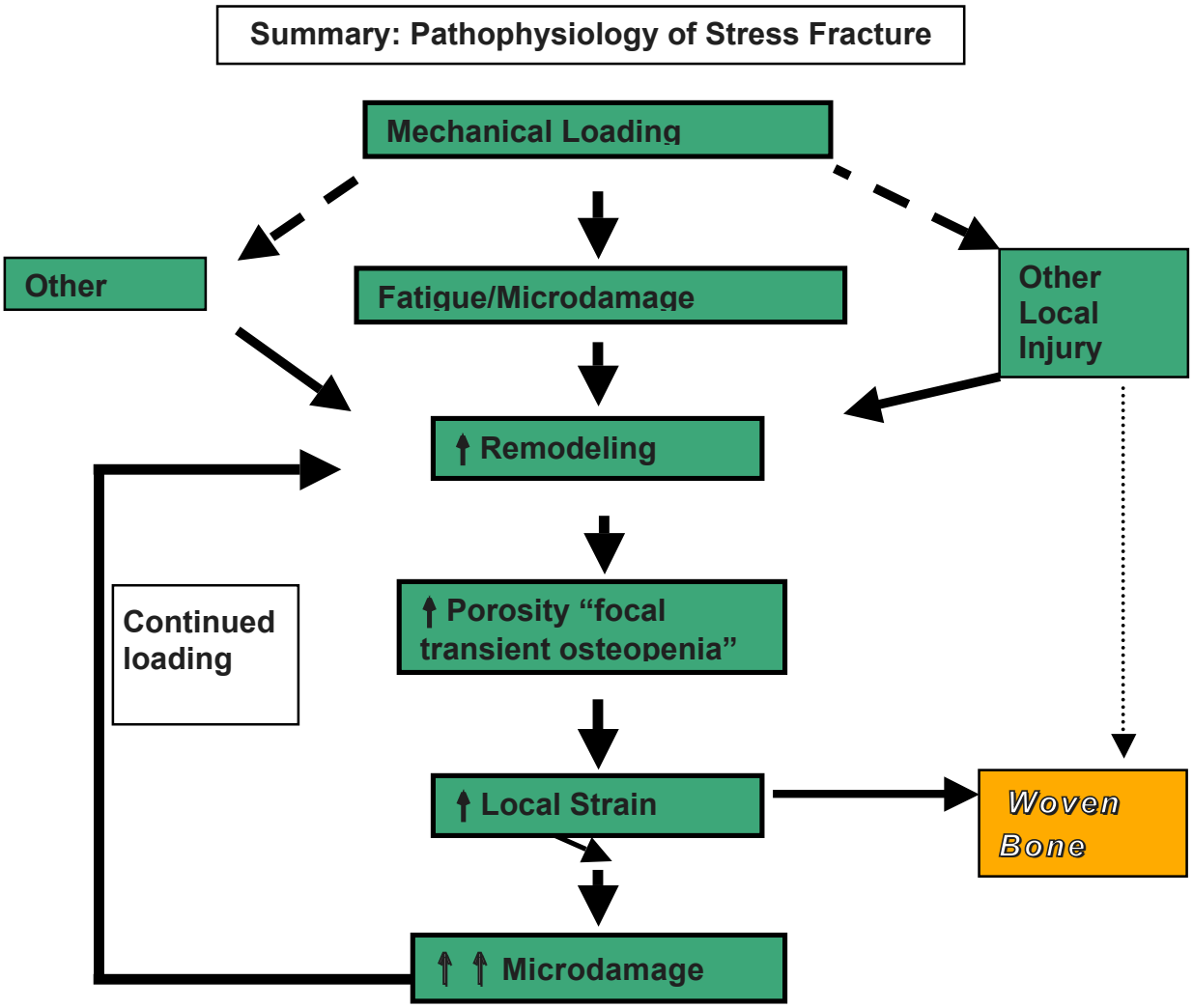

Discussion:

The trends in our data strongly suggest that increased intracortical porosity is associated with increased periosteal stress reaction in chronic loading, and that remodeling suppression can attenuate both the severity of the periosteal stress fracture response (^{99m}Technetium uptake and periosteal reaction) and the accumulation of microdamage in loaded bone. Based on the clinical criterion of ^{99m}Technetium bone scans, bisphosphonate treatment was able to attenuate the development and progression of stress fracture in the rabbit stress fracture model. However, because of the higher than expected variability in the rabbit model, and a hitherto unappreciated soft tissue injury in some of the experimental animals, it was not possible to establish statistical significance for the histological parameters in this model.

Further analyses revealed a curious, but interesting problem in our loading system, which 1) potentially explains the confounding effects of the high variability in this model, and also 2) potentially provide important insights into the pathogenesis of the bone stress reaction in these animals:

1) First, we found that some animals developed a extremely florid woven bone reactions during the chronic loading, and these animals occur in both bisphosphonate and vehicle treated groups. Interestingly, these *animals with the greatest periosteal response appeared to have initially smaller tibial diameters than those that showed less extensive periosteal reactions. This is noteworthy as having a small diaphyseal cross-sectional diameter for body size is well established risk factor for stress fracture in military recruits*.

2) Second, we found that the amount of periosteal reactive tissue in these smaller bones appears to have been large enough in size so as to interfere with the daily loading. Specifically, after several weeks of loading, these initially smaller tibiae enlarged enough in diameter so as to be compressed by the boot-like splint used to hold the limb during loading, thus superimposing a soft tissue injury onto the bone reaction.

Relevant Clinical Studies: Two recent clinical studies have examined the effects of bisphosphosphonate treatment in stress fractures and have yielded completely contradictory results. Milgrom et al (2003) reported that anti-resorptive treatment using risedronate administered to Israeli army soldiers during an intensive training regime did not prevent or alter the frequency and severity of stress fractures based on ^{99m}Technetium bone scans. However, the reliability of this study is difficult to assess as it was found that there was significant noncompliance among subjects during the studies, due to concerns about adverse gastrointestinal side effects of the oral bisphosphonate. A more recent study by Stewart et al (2005) examined the effect bisphosphonate treatment on existing stress fracture in competitive athletes. Pamidronate treatment significantly reduced the severity of stress fractures, with 85% of treated athletes returned to full training within 1 week of treatment, leading these authors to conclude that antiresorptive treatment may play a significant role in stress fracture treatment

Summary:

- Current studies support the hypothesis that increased intracortical porosity is associated with increased periosteal stress reaction in chronic loading.

- Bisphosphonate suppression of bone remodeling was correlated with markedly reduced the amount of woven bone formation (callus) at the periosteal surface in loaded bones. As low BIS treatment like that used here has not been reported to directly suppress bone formation, our results argue that the reduced intracortical porosity within the long bones of treated animals prevented locally elevated bone strain, which in turn prevented the formation of woven bone. However, because of the higher than expected variability in the rabbit model, and a hitherto unappreciated soft tissue injury in some of the experimental animals, statistical significance in this model was marginal.

- These data argue for the need to develop a new animal model to resolve these concerns (see next section), and allow a more definitive test of the question of whether increased intracortical remodeling is a risk factors for adverse reaction of bone to stress.

Development of a New Model for Stress Fracture

To address concerns about high variability, soft tissue involvement in the rabbit model, we have developed a new model using the adult rat skeleton. This model reproduces the features of stress fracture in humans and in horses. In addition, the bone biology of the rat can be readily manipulated to assess the effect of biologically driven remodeling changes (and osteopenias) as well as gender and age issues in the development and reaction to stress fracture. This model is based on end-loading of the ulna in vivo, which produces a bending moment in the ulnar diaphysis. This model represents a new approach to simulating a naturally occurring fatigue fracture in vivo. This model achieves fracture through the development and coalescence of microdamage during controlled, fatigue loading. The loading magnitude per se is hyperphysiological, but it is comparable to that measured in human and horses during very vigorous activities. The loading conditions differ from those occurring during physiological loading, i.e. the load is applied via the flexed carpus and olecranon process. Nonetheless, the distribution of stress and strain along the longitudinal axis of the ulna approximates that occurring physiologically due to the bending moments incurred through axial compression of a curved bone. Furthermore, the fracture configuration is similar to that occurring spontaneously due to fatigue, e.g., as seen in the third metacarpus of racehorses or in the central metatarsal bone of race dogs. Finally, despite being an exogenous loading model, soft tissue surrounding the area of interest is protected from artifactual trauma and damage to the blood supply is minimized.

Ulnae in adult Sprague-Dawley rats were loaded in axial compression using a hydraulically powered Instron Test Machine (Dynamite Instron, Canton, MA), by applying load to the olecranon and the flexed carpus. The mechanical loading device used allows for precise load control to measure the induced displacement on the limb and to automatically stop the test when change in deformation during fatigue reaches a targeted value. Thus, under load control, right ulnae were cyclically loaded to fatigue failure based on increase of bone deformation, which reflects the degree of damage accumulated in the structure). Before the experimental series, strain gauge measurements were carried out to assess the strain occurring on the ulnar surface. A single strain gauge was mounted on the middiaphyseal surface of the medial ulna in previously euthanized rats. The middiaphyseal surface is the site of maximal deformation occurring due to the natural curvature of the bone. This has been confirmed through strain gauge measurements and finite element modeling. Strains of 3500–4000 microstrain resulted from application of 17–18 N consistent with results of a previous study. These strains are consistent with the high strains recorded during vigorous activities in human and racehorses in vivo. Development of damage during fatigue loading. which is reflected as a changes in bone stiffness and whole bone compliance (displacement under loading). The testing machine measures the displacement during the entire loading history and stops the loading when the reference displacement has increased by 35%. During the loading, rats were anesthetized through inhalation; animals received buprenex for two days after loading for post-procedure analgesia. Tissues were examined at 7, 14, 21 and 42 days after fatigue fracture.

Pre-sacrifice in vivo tracer studies were conducted to evaluate perfusion of the vasculature as well as the lacuno-canalicular system at different time points in the healing and remodeling cycle. Each rat was injected via a lateral tail vein with 0.8% Procion Red solution in 0.9% saline. Animals were anaesthetized at the time of injection. Five minutes after injection, animals were euthanized without recovery from anesthesia.

Results: Fatigue fractures were confirmed in eighteen of the 20 loaded ulnae, typically within 12,000-20,000 loading cycles (Fig. 13, left). In all cases the fracture was closed and non-displaced.

Remarkably, no disruption to the periosteum or intramedullary vasculature was observed. Neither soft tissue trauma nor the presence of a hematoma was evident; in fact, fluorescent tracer studies showed no signs of intravascular leakage except by intracortical vessels that were disrupted directly by the fracture line. The fracture was always located in the distal third of the medial ulnar diaphysis.

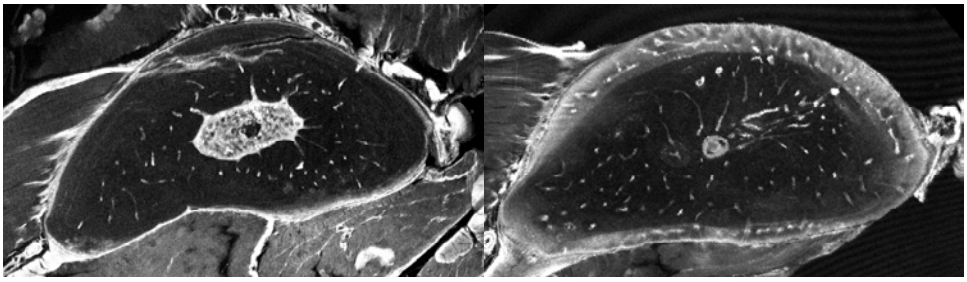

Fig. 13. (Left) Confocal micrograph showing fatigue fracture of medial ulna, representative of those incurred in 90% of cases studied. (Right) 42 days post fracture. In both images, fluorescence indicates presence of Procion Red tracer, an intravital marker.

Fracture healing proceeded by direct bone formation via woven bone proliferation at the periosteal surface, mainly on the medio-lateral side of the injured area. Endochondral ossification was not observed in fractured specimens. Immediately after loading, a fracture line was observed to extend from the mediodorsal to the medioventral surface (Fig. 13, left), with local microdamage coalescing around the fracture line and contained completely within the medial cortex. Seven days after loading, intense periosteal proliferation of woven bone was observed on the medial surface. Woven bone extended between the mediodorsal and medioventral extremities of the fracture. The longer the crack in the cross-section, the larger the increase in surface area due to woven bone reaction (Fig. 14). Microscopic observation revealed initiation of resorption along the fracture site. Fourteen days after loading, resorption cavities could be observed macroscopically at subperiosteal and subendocortical sites abutting the fracture line. Woven bone along the periosteum had consolidated considerably in comparison to the previous time point. Forty two days after loading, the fracture line was only faintly visible in one case. Otherwise, the fracture had remodeled completely. Areas of woven bone were well consolidated.

Fig 14

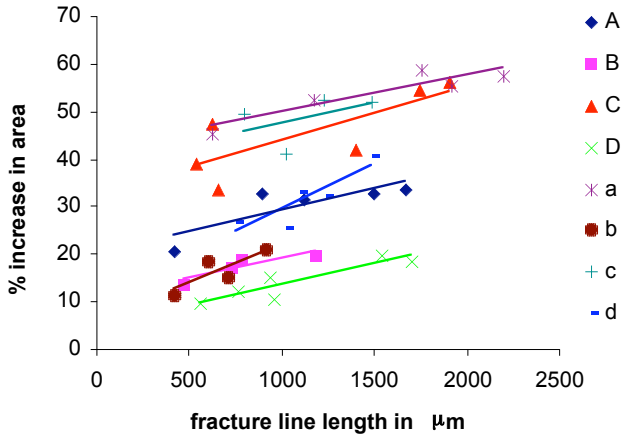

	slope	r^2
A	0.0093	0.685
B	0.0084	0.742
C	0.0115	0.620
D	0.0086	0.838
a	0.0076	0.822
b	0.0165	0.682
c	0.0086	0.217
d	0.0195	0.755
average	0.0130	0.670

Figure 14: Relationship between crack length and increases in bone surface area in the groups observed at 7 and 14 days after fatigue fracture loading. The amount of periosteal woven bone formation increases in proportional to the amount of damage in the bone.

Discussion: This model represents a new approach to simulating a naturally occurring fatigue fracture in vivo. This model achieves fracture through the development and coalescence of microdamage during controlled, fatigue loading. The loading magnitude per se is hyperphysiological, but it is comparable to that measured in human and horses during very vigorous activities. The loading conditions differ from those occurring during physiological loading, i.e. the load is applied via the flexed carpus and olecranon process. Nonetheless, the distribution of stress and strain along the longitudinal axis of the ulna approximates that occurring physiologically due to the bending moments incurred through axial compression of a curved bone. Furthermore, the fracture configuration is similar to that occurring spontaneously due to fatigue, e.g., as seen in the third metacarpus of racehorses or in the central metatarsal bone of race dogs. Finally, despite being an exogenous loading model, soft tissue surrounding the area of interest is protected from artifactual trauma and damage to the blood supply is minimized

Summary:

- A noninvasive long bone fatigue fracture model was developed that lends itself for the study of periosteal woven bone during stress fracture healing and has clear applications for the study of fatigue fracture etiology.

- This model can readily be expanded to look at gender issues, age and to superimpose hormonal and pharmacological manipulations in an animal model where they are well validated.

Bone structural and material properties in stress fracture risk:

Our studies using the rabbit model also found that animals that developed the greatest periosteal response to applied loading had initially smaller tibial diameters than those that showed less extensive periosteal reactions. A number of studies have shown that having a narrow (i.e., more slender) tibia relative to body mass has been shown to be a major predictor of stress fracture risk and fragility in male military recruits and male athletes. We undertook a small-scale study to test the intriguing possibility that slender bones, like those shown in animal models, are composed of more damageable material.

To test this, polar moment of inertia, section modulus, and antero-posterior (AP) and medial-lateral (ML) widths were determined for tibial diaphyses from 17 male cadaver donors, 17-46 years of age. Eight prismatic cortical bone samples were generated from each tibia, and tissue-level mechanical properties including modulus, strength, total energy, post-yield strain, and tissue damageability were measured by four-point bending from monotonic (n = 4/tibia) and fatigue damage accumulation (n = 4/tibia) test methods. Partial correlation coefficients were determined between each geometrical parameter and each tissue-level mechanical property while taking age into consideration.

Results: Significant correlations were observed between tibial morphology and the mechanical properties that characterized tissue brittleness and damageability. Positive correlations were observed between measures of bone size (AP width) and measures of tissue ductility (post-yield strain, total energy), and negative correlations were observed between bone size (moment of inertia, section modulus) and tissue modulus.

Summary:

Tissue-level mechanical properties varied with bone size. Narrower tibias were comprised of tissue that was more brittle and more prone to accumulating microdamage compared with tissue from wider tibias.

KEY RESEARCH ACCOMPLISHMENTS:

1) Rabbit stress fracture experiments: Our results suggest that antiresorptive therapy using a bisphosphonate will reduce the severity of the periosteal stress reaction in an animal model of chronic loading model.

2) New rodent model for stress fractures and healing: Under the aegis of this grant we developed a new model for studying the biology and healing of stress fractures. The resulting fracture is stable and non-displaced and is similar in morphology to that occurring due to fatigue in vivo, e.g., as seen in the third metacarpus of racehorses or in the central tarsal bone of racing dogs. Studies with this new experimental model suggest that healing of stress fractures may differ from other fractures, a finding that may have clinical significance in their treatment. This model can readily be expanded to look at gender issues, age and to superimpose hormonal and pharmacological manipulations.

3) Bone structural and material properties in stress fracture risk: Tissue-level mechanical properties varied with bone size. Narrower tibias were comprised of tissue that was more brittle and more prone to accumulating microdamage compared with tissue from wider tibias.

REPORTABLE OUTCOMES:

1. Publications:

Abstracts

- Yeni Y., M. Grimm, A.M Saad, M.B. Schaffler and D.P. Fyhrie. Microdamage in cortical bone increases attenuation of ultrasonic shear waves. *Trans Orthop. Res. Soc*. 24: 764, 1999
- Tami, A; Schaffler, MB; Nasser, P; Knothe Tate, JL; A Novel, Non-invasive fatigue fracture model of the rat ulna. *Trans. Orthop. Res. Soc*. 27: 335, 2002.

Papers

- Schaffler, M.B. and K.J. Jepsen. Fatigue and repair in bone. *International Journal of Fatigue* 22:839-846, 2000
- Verborgt O., G.J. Gibson and M.B. Schaffler Loss of osteocyte integrity in association with microdamage and bone remodeling after fatigue in vivo. *Journal of Bone and Mineral Research* 15: 60-67, 2000
- Schaffler, M.B. Bone Fatigue and Remodeling in the Development of Stress Fractures. In: D.B. Burr and C. Milgrom, eds., *Stress Fracture*, CRC Press. 2001, pp. 161-182.
- Verborgt O., N.A. Tatton, R.J Majeska and M.B. Schaffler. Differential expression of Bax and Bcl-2 in osteocytes after bone fatigue: Complementary roles in bone remodeling regulation? *Journal Bone and Mineral Research* 17: 907-914, 2002.
- Schaffler MB. Role of bone turnover in microdamage. *Osteoporosis International* 14, Suppl 5:73-80, 2003
- Tami A.E., P. Nasser, M.B Schaffler and M.L. Knothe Tate. Noninvasive fatigue fracture model of the rat ulna. *Journal of Orthopaedic Research* 21: 1018-1023, 2003.
- Tommasini, S.M,. P. Nasser, M.B. Schaffler and K.J Jepsen. The relationship between bone morphology and bone quality in male tibiae: Implications for stress fracture risk. *Journal of Bone and Mineral Research* 20: 1372-1380, 2005.

2. Symposia and major presentations:

- Microdamage and bone remodeling in stress fracture. Presented at the International Bone Fluid Flow Workshop, Amsterdam, The Netherlands, September, 2002.
- Strength, Bone Quality and bone remodeling, Sixth International Symposium on Osteoporosis: Current Trends and Future Directions, National Osteoporosis Foundation, Washington, DC, 2005
- Stress Fractures: Physiology and Prevention. Presented at the Stress Fracture Symposium, American Society for Bone and Mineral Research, Nashville, September, 2005

3. New animal models:

We developed a noninvasive long bone fatigue fracture model based on end-loading of the adult rat ulna in vivo lends itself for the study of periosteal woven bone during stress fracture healing and has obvious applications for the study of fatigue fracture etiology. This model can readily be expanded to look at gender issues, age and to superimpose hormonal and pharmacological manipulations in an animal model where they are well validated. The model is reported in:

Tami A.E., P. Nasser, M.B Schaffler and M.L. Knothe Tate. Noninvasive fatigue fracture model of the rat ulna. *Journal of Orthopaedic Research* 21: 1018-1023, 2003.

4. Trainees:

Post-doctoral fellows

Shijing Qiu, MD, PhD
Oliver Verborgt, MD, PhD
Liyun Wang, PhD

PhD students:

Andrea Tami
Brad Herman
Steven Tomassini

CONCLUSION:

Summarize the results to include the importance and/or implications of the completed research and when necessary, recommend changes on future work to better address the problem. A "so what section" which evaluates the knowledge as a scientific or medical product shall also be included in the conclusion of the report.

Our results suggest that antiresorptive therapy using a bisphosphonate can play a role in reducing the severity of the periosteal stress reaction in an animal model of chronic loading model. These data are consistent with the results of recent clinical studies using bisphosphonate in young athletes with stress fractures, but are contradicted by another study done by the IDF in Israel. Further studies are needed to determine whether antiresorptive therapy can play a role in reducing the severity of the periosteal stress reaction. Moreover, with the next generation of anti-resorptive drugs, such as Cathepsin K inhibitors, already in Phase 3 clinical trial, future studies can be conducted with anti-resorptive drugs that clear very rapidly from the body and from which normal bone remodeling rates will recover within weeks after stopping treatment. This would be much superior to the bisphosphonates, in which the very long biological half life of the resorption suppression has been a continuing source of concern in terms of effects on bone health.

The concept underlying this work on stress fracture pathophysiology, i.e., that increased bone resorption causes focally increased stresses which accelerate the accumulation of bone microdamage, has taken on much wider significance over the last several years. Specifically, there has been extensive discussion in the bone biology community (ASBMR, NOF, NIH) about why anti-resorptive therapies cause a dramatic reduction in the incidence of osteoporotic fractures with a short treatment period, but have no significant effect on bone mineral density. The principle hypothesis around which a consensus has formed is that bone resorption spaces will act as stress concentrations leading to focal failures, and that treating the resorption will lead to a disproportionate gain in fracture risk reduction. Finally, a number of recent studies have shown that bisphosphonate treatment of children with Osteogenesis Imperfecta will dramatically reduced fracture incidence. That reducing resorption in OI will alleviate fractures, despite the presence of an extremely poor quality collagen matrix highlights the potential importance of resorption spaces in exacerbating bone fragility. Thus, the concept that resorption play a major role in bone failures as diverse as stress fractures in the military, OI and fragility fractures in the elderly, has garnered significant recent attention and warrants further study.

REFERENCES:

Milgrom C, Finestone A, Novack V, Pereg D, Goldich Y, Kreiss Y, Zimlichman E, Kaufman S, Liebergall M, Burr D. The effect of prophylactic treatment with risedronate on stress fracture incidence among infantry recruits. *Bone*. 2004, 35(2):418-24

Stewart GW, Brunet ME, Manning MR, Davis FA. Treatment of stress fractures in athletes with intravenous pamidronate. *Clin J Sport Med*. 2005, 15(2):92-4.

APPENDICES

Copies of publications appended

Osteoporos Int (2003) 14 (Suppl 5): S73–S80
DOI 10.1007/s00198-003-1477-1

ORIGINAL ARTICLE

Role of bone turnover in microdamage

Mitchell B. Schaffler

Published online: 29 August 2003

Introduction

Turnover of cells and matrix occurs in a wide spectrum of organs and tissues and is essential to maintenance of tissue integrity. In bone, a major function of osteonal remodeling is to maintain tissue, wherein remodeling serves to remove and replace microscopic regions of compact bone that have reached the end of their functional life. Perhaps the best characterized circumstance in which bone reaches the end of its functional life is when it sustains microdamage due to fatigue. Left undetected and unrepaired, microdamage in bone leads to compromised mechanical properties and bone fragility. Recently, with wide clinical usage of drugs which turn off bone remodeling globally, a number of authors [1, 2] have raised concerns about whether inhibition of bone remodeling will predispose to the accumulation of matrix damage, leading to increased bone fragility. Accordingly, examination of factors that influence detection and repair of microdamage is fundamental to understanding skeletal health and disease.

Fatigue and microdamage in bone

Cyclic loading of bone, as in all materials, leads to failure incrementally through a process known as fatigue. In bone, this incremental failure process corresponds to the accumulation of microstructural level cracks or microdamage. Mechanically, the accumulation of microdamage is correlated to loss of material stiffness, or modulus reduction. Studies from both our laboratory and others show that bone fatigue and microdamage can occur at strain magnitudes comparable to those measured on living bones in the physiological loading environment during vigorous activity in animals and humans. At these modest strain magnitudes, the fatigue life to failure for compact bone is quite long—on the order of millions of loading cycles [3]. In life, this corresponds to approximately 5 to 10 years of use. However, significant amounts of fatigue damage occur *during* loading, damage that weakens the tissue and must be repaired to prevent fracture [3].

Microscopic cracking, or microdamage, in bone is the microstructural consequence of bone fatigue (Fig. 1). In 1960, Harold Frost [4] reported the earliest observations of microdamage in bone. Using human rib samples obtained at autopsy, he found small cracks, with a "linear" morphology, typically on the order of 30 to 100 μm in length. Frost posited that osteonal remodeling functions to remove and replace (repair) these microcracks. Such typical linear microcracks have received much study. They have been produced experimentally by fatigue loading bone in vivo and in vitro. However, linear microcracks appear to occur late in fatigue loading history of bones, after significant modulus degradation has occurred. Thus, there are other levels of matrix failure in bone, which occur early in the fatigue process and also strongly influence its fatigue behavior. Indeed, diffuse matrix damage (sublamellar-level cracking) recently has been shown to be a major characteristic of fatigue in bone [5]. Other types of matrix damage likely exist as well, as bone is a hierarchical, unhomogeneous material with extensive interfaces that potentially allow damage to form at many levels in this composite structure.

Microdamage and bone fragility

Before discussing the potential clinical significance of matrix microdamage, it is useful to review the basic aspects of mechanics that contribute to skeletal mechanical integrity, or the deficiencies therein that give rise to bone fragility. Fragility of bone can be defined in a clinically relevant, straightforward manner as the inability of the tissue to keep pace with normal mechanical demands. Much of the effort for defining bone fragility in aging and osteoporosis has focused on

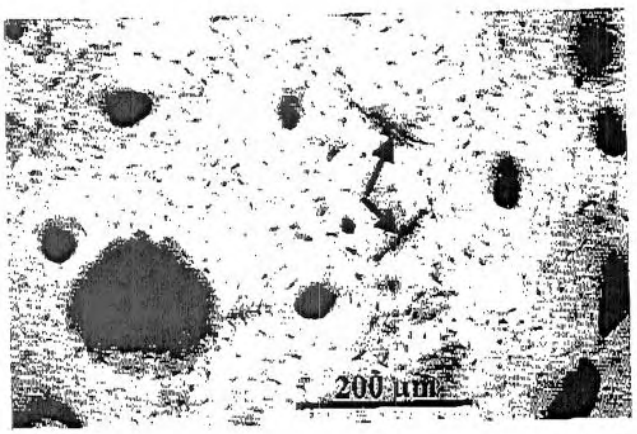

Fig. 1 Photomicrograph of a cross-section of basic fuchsin-stained, human femoral compact bone. *Arrows* show typical microcracks

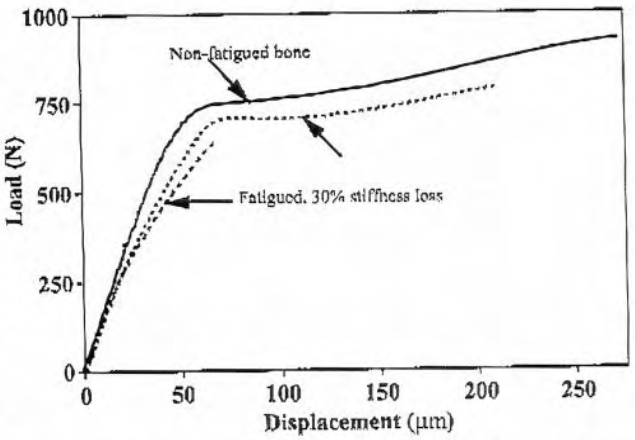

Fig. 2 Residual mechanical properties for human bone specimens at baseline and after fatigue loading. The global mechanical behavior of bone with a lower level of fatigue (15% stiffness loss) is similar to that in nondamaged bone, but with proportionate reductions of stiffness, strength and fracture resistance (work to fracture and postyield deformation). In contrast, bone specimens fatigued to higher fatigue levels showed losses of strength in proportion to stiffness loss, but degradations of work to fracture and postyield deformation were far greater than expected based on the stiffness changes in these specimens. Most striking, however, is that bone specimens fatigued to the higher level of fatigue showed effectively no postyield deformation; they fail immediately upon yield

determining whether bone is strong enough to bear normal loads, a logical extension of the fact that bone density (mass) and strength are well correlated. However, this approach presents an incomplete picture of the effectiveness with which bone resists fracture. Under mechanical loading, bone exhibits a region of elastic (recoverable) deformation, followed by a region of plastic (permanent) deformation; mechanistically, in this plastic or postyield deformation phase, the mineralized matrix cracks and collagen fibers tear, until the point of final complete fracture. Materials can be strong, stiff and tough (long plastic deformation after yield). Materials can also be strong and stiff, but very poor at resisting fracture, and fail in a brittle manner once their yield point has been reached. Examples of such material are glasses and ceramics. The key material properties that describe the fracture resistance of a material include work to fracture, postyield compliance and crack propagation parameters. Fracture resistances are independent of elastic properties or strength, and thus are not indexed at all in bone mass or density measurements. Accordingly, a global definition of bone fragility must take into account bone's fracture resistance as well as its strength determinants.

What are the consequences of different amounts of fatigue damage on the mechanical integrity of compact bone?

Studies show that the declines in fracture resistance for a given amount of fatigue-damaged bone exceed the losses of stiffness and strength, consistent with the consequences of fatigue in many synthetic composite materials as well. However, precise data defining the relationships between the amount of microdamage and degradation of specific mechanical properties do not exist.

It is well established in material sciences that microdamage content (quality and quantity) influences the residual (remaining) mechanical properties of a material. Indeed, in bone, as well as in other composite type materials, the mechanical definition of fatigue is based on stiffness loss. Stiffness loss correlates with loss of strength. However, as bone sustains fatigue and accumulates microdamage, the loss of fracture resistance can be disproportionately large. In the example shown in Fig. 2, low levels of fatigue induced ex vivo in human bone specimens result in proportionate reductions of strength and fracture resistance (work to fracture and postyield deformation); the overall mechanical behavior of bone with low levels of fatigue is similar to that in nondamaged bone. In contrast, bone specimens fatigued to higher fatigue level showed losses of strength in proportion to stiffness loss, but degradation of work to fracture and postyield deformation were far greater than expected based on the stiffness changes in these specimens. Most remarkably, however, is the striking absence of postyield deformation in bone specimens fatigued to the higher level of fatigue; they fail immediately upon yield. Thus, these data reveal that even small amounts of fatigue will compromise the functional-mechanical properties of bone, and show the potentially dramatic functional-mechanical consequences of fatigue in bone. These data also emphasize that the deleterious effects of matrix damage on the fracture resistance of bone may be more important than its effects on diminished stiffness and strength. Further studies are needed to define the threshold levels of microdamage in bone that can significantly impair fracture resistance.

Bone remodeling, microdamage repair and maintenance of tissue integrity

Frost [4, 6] first put the idea forth that remodeling targets microcracks in bone and is necessary to maintain the mechanical integrity of the skeleton. Since that time, considerable data have accrued to support this idea. Microcracks have been shown to be associated with intracortical resorption in overuse and stress fractures in human and dogs. Burr et al. [7] and Mori and Burr [8] showed experimentally that resorption spaces are associated with microcracks in canine compact bone. Bentolila et al. [9] found that when microdamage is produced in rat ulnae by fatigue loading, intracortical remodeling is stimulated in areas where microscopically visible damage occurs and where osteocyte morphology has been changed (Fig. 3). Rats loaded to the same strain magnitude, but which did not exhibit fatigue damage, did not exhibit intracortical remodeling. Since intracortical remodeling does not normally occur in rats, this is convincing evidence that fatigue is the initiating event for remodeling. Most compelling are the recent studies from Burr and coworkers [10, 11, 12]. They have found that in dogs treated with long-term bisphosphonates to suppress remodeling, there is a two- to threefold increase in bone microdamage content and a concomitant impairment of biomechanical properties. Thus, a range of studies during the last decade strongly supports Frost's microdamage-remodeling/repair hypothesis, showing both that microdamage results from normal mechanical use of the skeleton and that remodeling is necessary to prevent its accumulation.

What controls remodeling of microdamage in bone?

It is quite reasonable to presume that osteocytes, the only cells embedded in the bone matrix, would be affected by microdamage in the bone matrix and therefore play a key role in targeted bone remodeling. Osteocytes are extensively distributed throughout the bone matrix. Their canalicular processes completely infiltrate the matrix of bone. They have well-developed cytoskeletons; they are attached to their surrounding matrix through adhesion molecules and to their neighboring cells through gap junctions. Thus, they are strategically well situated to detect or to be affected by disruption of their surrounding matrix.

Several lines of indirect evidence support the hypothesis that osteocytes are needed to detect or respond to matrix-level injury. In several instances where osteocytes are absent from bone, fatigue failures will occur; well-known examples include radiation-induced death of osteocytes and allograft bone. Similar mechanisms also may play a role in bone fragility of avascular necrosis. Absence of osteocytes is associated with hip fracture. Parfitt [1] hypothesized that osteocyte death leads to fatigue microdamage accumulation in bone resulting from decreased ability in bone to detect matrix injury. These data are consistent with the ideas that osteocytes are needed to effect an appropriate biological response to matrix damage and are necessary to maintain the mechanical integrity of the skeleton. The involvement of osteocytes in bone fatigue and remodeling recently was directly shown by Verborgt et al. [13], who found that osteocytes undergo apoptosis (regulated cell death) in bone areas immediately surrounding bone microdamage. These areas of osteocyte apoptosis colocalize exactly with the areas of bone that subsequently undergo later resorption by osteoclasts.

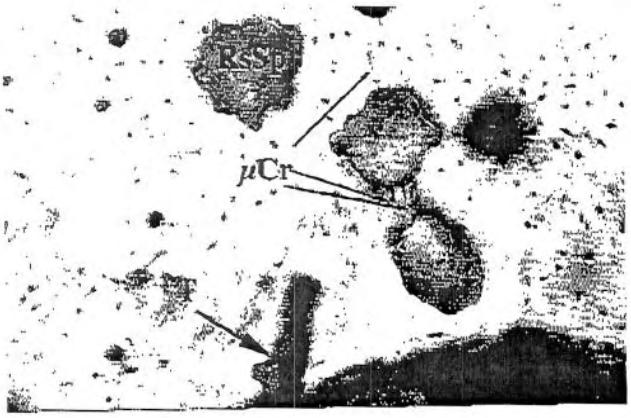

Fig. 3 Intracortical resorption spaces (*RsSp*) in association with fatigue microcracks (μCr) induced in vivo by cyclic loading of rat ulnae

Remodeling and microdamage: what happens when the normal homeostasis is altered?

There are considerable data to support the idea that an appropriate amount of bone remodeling is needed to effectively repair wear and tear microdamage in bone; that is, in healthy bone there is a "homeostatic balance" between wear and tear and intrinsic repair. The next question asks what happens to microdamage accumulation in bone when remodeling is not operating properly.

Can too much remodeling be a problem?

Schaffler, Radin and Burr [14] proposed that elevated intracortical remodeling can accelerate microdamage accumulation. They argued that increases in intracortical porosity, resulting from activation of intracortical remodeling, would have a dramatic effect on decreasing the stiffness of cortical bone. Continued loading of this focal region of osteoporotic bone will result in increased local stresses and strains, leading to rapid bone microdamage accumulation. Martin used a mathematical model to explore this concept in detail in the context of stress fracture development. Using a feedback model to

examine the effects of increasing porosity on the mechanical properties of compact bone, Martin [15] showed that there is a critical porosity, load interaction, microdamage accumulation threshold. Once the threshold for matrix damage is reached, through increased bone porosity and/or through increased local loading, bone becomes mechanically unstable and fails rapidly and catastrophically. Both the Schaffler hypothesis and Martin's model are consistent with a range of recent histopathological observations in early stress fracture. Accordingly, these data suggest that too much remodeling can accelerate bone microdamage accumulation.

Can too little remodeling be a problem?

The converse question, one that is more frequently discussed in context to aging-bone fragility and also to pharmacological treatment of metabolic bone disease, is whether too little bone remodeling leads to the accumulation of bone microdamage. The simple answer to this question is yes—too little remodeling leads to the build-up of bone microdamage. However, the reasons for this remain unresolved.

Analyses of the data pertaining to age-related accumulation of microdamage in bone are instructive in this regard. In 1995, we reported the first observations of increasing in vivo microdamage in aging bone [16]. Subsequent studies in a number of laboratories have shown that microdamage accumulation with aging occurs throughout the appendicular skeleton, in long bone diaphyses, in the cortex of the femoral neck and in the trabeculae of aging femoral heads. It has been argued that ineffective remodeling-repair of normal microdamage (in the aging skeleton) can explain the increasing microdamage content in bone. Alternatively, it has been posited that microdamage accumulation might be a "symptom" of matrix changes in the aging bone matrix (or in the drug-treated skeleton), which predisposes the bone to sustain microdamage.

Recent studies of bone from remodeling-suppressed animals reveal significant increases in bone microdamage in dogs treated with long-term bisphosphonates for 1 to 2 years, supporting the concept that ineffective remodeling-repair can lead to microdamage accumulation [10, 11, 12]. Moreover, the amount of microdamage accumulation was nominally proportional to the amount of remodeling suppression. Dogs treated with alendronate showed both greater remodeling suppression and greater microdamage increases than dogs treated with risedronate.

While at first glance these data suggest that inhibition of bone remodeling using bisphosphonates suppresses the repair of bone microdamage leading to its accumulation, there is a potential confounding factor to this interpretation. With remodeling suppression using bisphosphonates and the resulting low bone turnover, bone matrix mineral content increases at the microscopic level [17]. Such local changes in bone mineral composition are thought to cause bone to become more brittle and damageable [18], although a direct mechanical test of this hypothesis has not been done. Frost [6], Parfitt [1] and our group [16] observed that inadequacies of local remodeling processes in the aging skeleton can lead to a similar end point: bone becomes locally more fragile, and there are likely to be sites at which microdamage occurs. Whether, in fact, local mineral content, in the absence of adequate bone turnover, becomes sufficiently high so as to embrittle bone remains unknown.

Conclusion

In conclusion, existing data indicate that (1) microdamage accumulation impairs the mechanical integrity of bone, more so in terms of its ability to withstand fracture than in terms of reducing its strength, and (2) suppression of bone turnover causes microdamage to build up in vivo. Accordingly, we can ask the question of whether, from the standpoint of microdamage and mechanical integrity of bone, there are theoretical limits to the suppression of bone turnover? Logic dictates that there should be such a limit. However, in our current state of knowledge, we cannot yet define that limit. There remain several key deficiencies in our level of understanding of the processes involved. First, one key piece of needed information is a more complete understanding of how much matrix damage can occur before the mechanical integrity of bone is impaired at a clinically relevant level. Currently, we do not know how much microdamage in bone is too much. Implicit in this issue is the need to differentiate changes in mechanical integrity that are statistically significant in the experimental context from those that are significant and meaningful in the clinical context. Second is the need for more in vivo studies to measure microdamage accumulation in the living skeleton. This latter issue is problematic. Microdamage accumulation occurs in load-bearing bones, and it is not possible at this time to directly monitor matrix damage in patients. The same argument also holds for direct assessment of bone turnover in weight-bearing bones; we cannot do it with our current technologies and are therefore limited to extrapolations about long bone turnover based on direct studies of nonloaded bone biopsy sites, such as the iliac crest. Studies of bone samples from selected hip fractures may provide important insights into whether bisphosphonate-treated patients develop a high bone microdamage burden. Until the advent of new technologies to assess microdamage and bone remodeling in vivo in major load-bearing bones (for example, technologies that are based on functional-biological imaging of bone), the most critical data for microdamage accumulation and bone remodeling will need to come from additional long-term studies in large animals, which use various levels and modalities of remodeling suppression to modulate activation frequency. Such data

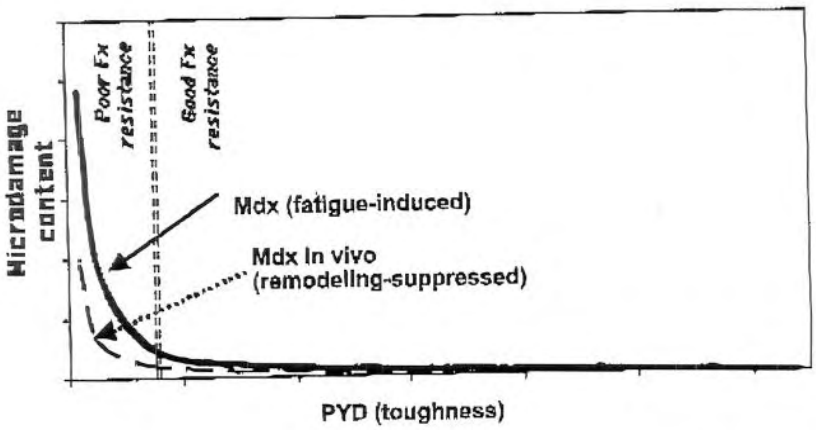

Fig. 4 Theoretical curve showing the expected relationship between microdamage content in bone and residual fracture resistance, as measured from postyield displacement, in fatigue-loaded (*Mdx*, fatigue-induced) bone. The inflection point of this curve is defined as the threshold level distinguishing mechanically good bone [good fracture (*Fx*) resistance] from mechanically impaired bone (poor Fx resistance). This curve provides a basis for estimating the mechanical consequence of in vivo microdamage accumulation, as has been observed with suppression of remodeling (*Mdx*, in vivo: remodeling-suppressed bone). *PYD* postyield depression

for microdamage accumulation in vivo, combined with complementary biomechanical data defining the threshold levels for in vivo bone microdamage accumulation that result in significantly impaired fracture resistance, will allow the development of predictive curves (Fig. 4) to estimate whether suppression of bone turnover will lead to bone fragility.

References

1. Parfitt A. (1993) Bone age, mineral density and fatigue damage. Calcif Tissue Int 53(Suppl):82–7
2. Burr DB, Forwood MR, Fyhrie DP, et al. (1997) Bone microdamage and skeletal fragility in osteoporotic and stress fractures. J Bone Miner Res 12:6–15
3. Schaffler MB, Jepsen KJ. (2000) Fatigue and repair in bone. Int J Fatigue 22:839–46
4. Frost H. (1960) Presence of microscopic cracks *in vivo* in bone. Henry Ford Medical Bulletin 8:27–35
5. Schaffler MB. (2001) Bone fatigue and remodeling in the development of stress fractures. In: Burr DB, Milgrom C, eds. Musculoskeletal Fatigue and Stress Fractures. Boca Raton: CRC Press, 161–82
6. Frost H. (1985) Factors that impair its repair. In: Uhthoff H, ed. Current Concepts in Bone Fragility. Berlin: Springer-Verlag
7. Burr DB, Martin RB, Schaffler MB, Radin EL (1985) Bone remodeling in response to in vivo fatigue microdamage. J Biomech 18:189–200
8. Mori S, Burr DB (1993) Increased intracortical remodeling following fatigue damage. Bone 14:103–9
9. Bentolila V, Boyce TM, Fyhrie DP, et al. (1998) Intracortical remodeling in adult rat long bones after fatigue loading. Bone 23:275–81
10. Mashiba T, Hirano T, Turner CH, et al. (2000) Suppressed bone turnover by bisphosphonates increases microdamage accumulation and reduces some biomechanical properties in dog rib. J Bone Miner Res 15:613–20
11. Mashiba T, Turner CH, Hirano T, et al. (2001) Effects of suppressed bone turnover by bisphosphonates on microdamage accumulation and biomechanical properties in clinically relevant skeletal sites in beagles. Bone 28:524–31
12. Li J, Mashiba T, Burr DB (2001) Bisphosphonate treatment suppresses not only stochastic remodeling but also the targeted repair of microdamage. Calcif Tissue Int 69:281–6
13. Verborgt O, Gibson GJ, Schaffler MB (2000) Loss of osteocyte integrity in association with microdamage and bone remodeling after fatigue in vivo. J Bone Miner Res 15:60–7
14. Schaffler MB, Radin EL, Burr DB (1990) Long-term fatigue behavior of compact bone at low strain magnitude and rate. Bone 11:321–6
15. Martin B (1992) A theory of fatigue damage accumulation and repair in cortical bone. J Orthop Res 10:818–25
16. Schaffler MB, Choi K, Milgrom C (1995) Aging and matrix microdamage accumulation in human compact bone. Bone 17:521–25
17. Meunier PJ, Boivin G (2000) Influence of changes in bone remodeling rate in the degree of mineralization of bone: Therapeutic implications. J Bone Miner Res 15:815–21
18. Jepsen KJ, Pennington DE, Lee YL, Warman M, Nadeau J (2001) Bone brittleness varies with genetic background in A/J and C57BL/6 J inbred mice. J Bone Miner Res 16:1854–62

Discussion

Dr. Currey: I'd like to ask what is the nature of the cracks that you're looking at? I think you show linear cracks in cross-sections. This would indicate to me what you're actually looking at are compressive cracks that go down in a long, straight line. Have you looked at sections at right angles, so the haversian systems are going up and down?

Dr. Burr: In these data, we've not looked at other orientations. In other specimens, we have looked longitudinally. In this case, the cracks basically run down the length of the haversian systems. In fact, they're fairly long, on the order of 200 μm to 300 μm on average.

Dr. Schaffler: Are they lines or planes?

Dr. Burr: They're planes.

Dr. Currey: Do you think they're compression or tension?

Dr. Schaffler: Neither. I think they're internal, interstitial shear in the material. If you apply a uniform load, it's not going to cause the same microstructural strains since the bone has material of different microscopic

stiffnesses. I think that for the linear cracks it gets to a point where either internal friction or whatever causes the damage to initiate gets there, and then material breaks like that internally. We've done a lot of studies on diffuse damage (shown in the confocal photomicrograph). The size order of those cracks is about the same as the crystal aggregates that were described by Green when he deorganified the surface of bone and looked at it with EM. Weiner and Price ground up pieces of bone and ran them through various molecular sieves and found similar results. They got small crystals on the normal crystal-like size, but also had a clustering of aggregates in the range of about 250 nm to 400 nm. That's the size order for those cracks. I think the cracks are a failure between the collagen and the mineral at that size order. But we really don't know what holds the bone together at that level—it's not quite ultrastructure and it's not quite microstructure.

Dr. Ferrari: You pointed out the extraordinary heterogeneity of number of cracks at a given age in a given bone. Which matters most then with regard to fragility, the initiation of cracks or the lack of repair? Maybe we should incorporate some very simple epidemiological data on patients, like the amount of exercise that the people from whom we got those bones were doing at a certain time, or markers of bone turnover to have a rough estimate of remodeling activity. Do we have any study where this heterogeneity has been observed, where we would have markers and epidemiological data to try to pin down what underlies this heterogeneity?

Dr. Burr: I don't know of any, but activity data will be terribly variable and will not tell you much. And I don't have much confidence in marker data. If you were able to look at damage using a bone sample from a biopsy for example, then my suggestion would be to look at turnover rate by labeling ahead of time and also measuring activation frequency. We have actually looked at the relationship between damage accumulation and fracture in femoral heads. We did an autopsy study a few years ago, in which we took femoral heads from women who had fractured the opposite side, i.e., femoral heads from women with a fracture, age-matched women who had not fractured and femoral heads from a younger sample of women. We found that both older groups had significantly more microdamage than the younger group. Within the older groups, the ones that had fractured and the ones that hadn't fractured didn't have any difference in microdamage accumulation. So the relationship between damage accumulation and fracture couldn't be explained based solely on whether there was a fracture present.

Dr. Bilezikian: At the doses of bisphosphonates that we currently use, is there any evidence in human studies for increase in microdamage?

Dr. Burr: We haven't done that study yet, but I would say this: Our study has been criticized because we use such high levels of bisphosphonates, but the amount of suppression that we got is no different than the amount of suppression that women have with lower doses of bisphosphonates. You get 90 to 95% suppression in the iliac crest. What we've shown is that the amount of damage you accumulate is very closely related simply to the amount of suppression that you get. So those studies haven't been done, but I wouldn't expect it to be very different.

Dr. Bouxsein: Do you think it's a function of just reducing turnover or does the actual mechanism of how that's done have an effect? For example, if bisphosphonates and SERMs had equal amount of turnover suppression, would you expect the same effect on microdamage accumulation or different effects because one is directly affecting osteoclast survival and the other presumably not?

Dr. Schaffler: My feeling is that it's strictly related to the amount of remodeling suppression, but we have just started looking at estrogen and SERMs, and there may be some differences.

Dr. Heaney: In the first of the Henry Ford symposium volumes, in a chapter by Lent Johnson, he notes with respect to stress fractures that the fracture occurs after the remodeling starts. So that's a confirmation of your observation.

Dr. Burr: Since that time, there has been at least one other instance in which biopsies have been done on stress fractures by Satosi Mori in Japan, and those pictures show that the remodeling is impressive.

Dr. Schaffler: Reviewing the postmortem data from race horses (if they get a stress fracture it's the end for a thoroughbred horse), Stover and coworkers found elevated remodeling at the contralateral limb at the same site even if they hadn't had the stress fracture occur.

Dr. Heaney: Dr. Burr, you have published a paper with high-dose etidronate in which you didn't find an increase in crack density, but you showed more recent data today. Can you integrate those two studies for me?

Dr. Burr: We used two different dosages of etidronate, 0.5 mg/kg /d and 5 mg/kg/d. The reason we chose these dosages was that we wanted to use a low dosage that wouldn't impair mineralization, and we wanted to use a higher dosage that Larry Flora and others, had found caused spontaneous fractures. We wanted to duplicate that and determine whether the incidence of spontaneous fractures was a microdamage-related or a mineralization phenomenon, and it turns out to be a mineralization phenomenon. In fact, you actually have less microdamage with the high dose of etidronate in those animals, presumably because the bone is more compliant, but they still fracture.

Dr. Heaney: They should be more ductile?

Dr. Burr: Yes, but they don't have much mineral in them.

Dr. Heaney: You can bend them, but that's not the same thing as fracture.

Dr. Burr: Well, high rates of fracture also occur in patients with osteomalacia.

Dr. Heaney: I'm not sure of that.

Dr. Burr: There are some data to suggest that that's true.

Dr. Jepsen: Regarding Dr. Burr's study, why did you attribute the decrease in toughness to microdamage?

Dr. Burr: We know that the reduced toughness is associated with microdamage, but we don't know that microdamage is the cause of the reduced toughness. It could also be the increase in the mean degree of mineralization of the tissue that makes it a bit more brittle. We have now shown that there is also an increased mean degree of mineralization in these dogs.

Dr. Jepsen: One of the things that kept coming up is that microdamage causes fragility, and it's really difficult to say that, because materials that show increased microdamage are also inherently brittle.

Dr. Burr: We did not make that statement in those papers. We never said that it was because of the microdamage. There's an association there, but we absolutely don't know that there's a cause-and-effect relationship.

Dr. Shmookler Reis: If you see an increase in microfracture density with age, it can mean any of three things. One is that the incidence of microfractures is higher in older people. The second is that the remodeling, which would cure them, is impaired. It doesn't have to be less efficient, just slower (it occurs with less frequency and so you can get a higher steady-state level of microfracture). And the third would be that there are some microfractures that are inaccessible to repair. Do we have any idea which of these occurs and is responsible for the difference with age? Is it possible the risk of fracture is considerably greater for either very long or conveniently clustered microfractures and that's what we really should be looking at for this?

Dr. Schaffler: All those factors you identified as potentially leading to damage accumulation with age are possibilities, and they probably all occur to some extent. We don't know which is predominant. We don't know if it's a detection error vis-à-vis the osteocytes or a failure to initiate remodeling. Certainly, there's evidence that older bone may have different damageability and that the damage could have the same mineralization issue that Karl and David were just discussing. In that argument, cracks could be perceived of as a symptom of a sick matrix. Then there's the issue of the loading conditions, which are different in the aging skeleton. It's not necessarily magnitude of load that causes damage, it's repetition of frequencies, and it's also loading rates. If you step off a curb unexpectedly, it's more damaging to your skeleton than if you step off the curb gradually. So it could be the frequency of those accidents that changes with age as well, but we don't have any insight. Eric Radin used to call that "micro-klutziness." It's a term that didn't catch on, but I think it has utility, and that "micro-klutziness" may increase with age as well. As far as the issue of crack number versus crack length interaction, David and I have basically summarized the data on what's known about how cracks interact in a quantitative way to weaken bone. Add to that a bit of data from Peter Ziopis and that summarizes 20 years of intensive research and data collection.

Dr. Jepsen: Typically, people count the number of cracks, so I think that's really going to be critical to some of these issues. I don't think these cracks would be weighted equally; a small crack versus a large crack, cracks in different orientations, and depending on where the crack is actually located within the matrix—are all of these going to have huge effects on the integrity of that tissue? That's not known. How do we count cracks? We just count the numbers. Currently, we don't really weight them.

Dr. Burr: They're weighted by length in some cases. Crack surface density is a combination of number and length, but we don't know how to weigh by orientation. There are lots of subtleties about the measurement techniques that we don't know how to handle.

Dr. Jepsen: The other thing is, a small crack in a brittle matrix is not going to behave the same way as a small crack in a ductile matrix.

Dr. Schaffler: Yes, one could even make the argument that it may be the volume of damage material that you should count (it isn't even the number of cracks) to understand function. It may be that we've approached this with standard histomorphometry tools the same as we've done for trabecular architecture and we've defined a counting paradigm that may not be the appropriate one for defining function.

Dr. Boivin: We have obtained essentially the same results as those reported by David Dempster in collaboration with Klaus Klaushofer. There is no difference between both states, and there is no significant difference with age in the control group. We compared our placebo group with our control group and after the placebo treatment, the degree of mineralization is the same as the control group. We have an increase in mineralization after bisphosphonate treatment if we compare with the placebo and if we compare with the control.

Dr. Turner: We know that reducing turnover has a lot of good effects and this has been reiterated a number of times. If you reduce bone turnover, you can disproportionately affect fracture rates in the spine at the very least. We may know from David's studies in dogs that if you reduce turnover down to 95% or down to 5% of what it was, that you may accumulate microdamage, increase mineralization or maybe create a brittleness issue. So there may be a safe level for reduction of turnover that will maybe repair all the microdamage and still afford antifracture efficacy. I was curious where Dr. Burr got the 50% number for "safe" suppression of remodeling?

Dr. Burr: The reason for the 50% number is because (at least in cortical bone), we found suppressions of 53 to 68%, and we still saw a threefold increase in damage. So I know it's not above 50%. That's why we suspect it's below 50%, but we don't know exactly what it is.

Dr. Bouxsein: Regarding the hypothesis that one of the things we would like to optimize is whole bone toughness, it seems that it is a parameter we're not even sure how to measure. Everything else we're talking about in toughness is on the material level, but what

happens when someone's fracture is a structural failure. Even with your very small decrease in ultimate strength, if it's enough, it is a catastrophic event. How do we bring our material level measurements of microdamage toughness to how they're going to impact whole bone strength or whole bone toughness? I think this is probably what's going to determine fracture risk in the end.

Dr. Jepsen: Just go back to some of the work that was done in the 1950s and 1960s and start breaking some bones and correlating material properties with those whole bone structures and it'll tell you.

Dr. Burr: I don't think that'll tell you. I think what you need to do is fatigue tests. If you're really talking about the toughness issues, then it's got to be a cyclic test.

Dr. Bouxsein: With the proximal femur, when you fall down you don't fracture in a fatigue mode, you fracture in the impact-loading mode.

Dr. Burr: Yes, but you may be predisposed to fracture from the impact. Thus, another interesting thing would be to look at the effect of damage accumulation on impact strength. It is important to try to define the percentage decrease in bone turnover that will be optimal in terms of preventing fracture. We guess that this may be between 30 and 50% suppression of activation frequency.

Dr. Ferrari: Whatever that number is, if it is as low as that, that is probably what we achieve in all the placebo arms of the current trials with just calcium, vitamin D. Yet we know the antifracture efficacy of this treatment is far from optimal. So there is a kind of a paradox coming out here.

Dr. Burr: I agree, we just don't know what the optimal amount of suppression might be for antifracture efficacy.

JOURNAL OF BONE AND MINERAL RESEARCH
Volume 17, Number 5, 2002

Spatial Distribution of Bax and Bcl-2 in Osteocytes After Bone Fatigue: Complementary Roles in Bone Remodeling Regulation?

OLIVIER VERBORGT,[1,2] NADINE A. TATTON,[3] ROBERT J. MAJESKA,[1] and MITCHELL B. SCHAFFLER[1]

ABSTRACT

Osteocyte apoptosis appears to play a key role in the mechanism by which osteoclastic resorption activity targets bone for removal, because osteocyte apoptosis occurs in highly specific association with microdamage and subsequent remodeling after fatigue. However, beyond terminal deoxynucleotidyl transferase (TdT)–mediated deoxyuridine triphosphate (dUTP)–biotin nick end labeling (TUNEL) assay, little is known about the mechanisms controlling osteocyte apoptosis in vivo. In the current studies, expression of Bax, a proapoptotic gene product, and Bcl-2, an antiapoptotic gene product, was determined in osteocytes of fatigued rat bone using immunocytochemical staining and compared with TUNEL staining patterns. Bax and Bcl-2 were evident in osteocytes by 6 h after loading. Moreover, Bax and Bcl-2 in osteocytes were expressed differently as a function of distance from microdamage sites. The peak of Bax expression and TUNEL$^+$ staining in osteocytes was observed immediately at the microcrack locus, which is where bone resorption occurs in this system; in contrast, Bcl-2 expression, the antiapoptotic signal, reached its greatest level at some distance (1–2 mm) from microcracks. These data suggest that near sites of microinjury in bone, those osteocytes that do not undergo apoptosis are prevented from doing so by active protection mechanisms. Moreover, the zone of apoptotic osteocytes around microcracks was effectively "walled in" by a surrounding halo of surviving osteocytes actively expressing Bcl-2. Thus, the expression pattern of apoptosis-inhibiting gene products by osteocytes surrounding the apoptotic osteocyte at microdamage sites also may provide important signals in the guidance of resorption processes that occur in association with osteocyte apoptosis after fatigue. (J Bone Miner Res 2002;17:907–914)

Key words: bone remodeling, osteocytes, apoptosis, Bcl-2, Bax

INTRODUCTION

Induction of regulated osteocyte death, that is, apoptosis, is posited to play a key role in regulating bone-remodeling events in pathological bone turnover,[1] developing bone,[2] estrogen deprivation,[3,4] acute matrix injury,[5] and glucocorticoid-induced osteonecrosis.[6,7] Verborgt et al.[8] showed that osteocyte apoptosis occurs after fatigue-induced bone matrix injury. Moreover, they found that osteocyte apoptosis was not widespread but highly localized to sites of microdamage that are subsequently remodeled.[8] This highly focal localization of osteocyte apoptosis sug-

The authors have no conflict of interest.

[1]Leni and Peter W. May Department of Orthopedics, Mount Sinai School of Medicine, New York, NY, USA.
[2]Department of Orthopedics and Traumatology, University of Antwerp, Antwerp, Belgium.
[3]Department of Neurology, Mount Sinai School of Medicine, New York, NY, USA.

gests that microdamage may affect only osteocytes in the immediate vicinity. Alternatively, it also is possible that osteocytes at some distance from microdamage can protect themselves from matrix injury–induced cell death, thereby exercising an additional level of control in the regulation of osteocyte apoptosis and bone remodeling.

Apoptosis is a highly regulated, intrinsic process involving activation of genes that can promote the death of a cell.[9–12] The *bcl-2* gene family encodes a large number of proteins that participate in programmed cell death. Some members of this family such as Bcl-2 have antiapoptotic protective functions and can prevent the activation of more downstream effector proteins such as the caspase proteases.[13] Other members such as Bax have proapoptotic functions and can antagonize the "protective" actions of Bcl-2.[14,15] The precise roles and mechanism(s) through which the *bcl-2* gene family members inhibit or promote apoptosis is still a matter of active investigation. However, it is known that Bcl-2 family proteins can regulate a voltage-dependent anion channel in the mitochondrial membrane and thus prevent or facilitate the release of proapoptotic signaling molecules such as cytochrome c from the mitochondria.[16]

Although considerable data support the involvement of osteocyte apoptosis in activating and targeting bone resorption, there is scant understanding of the mechanisms controlling osteocyte apoptosis in vivo. Recently, Bcl-2 expression has been reported in newly formed osteocytes in fetal bone but not in other osteocytes.[17] Whether Bcl-2 can be up-regulated and plays any role in osteocyte apoptosis in adult bone is not known. Early controlling factors in the apoptosis cascade in bone have not been studied in situ. In the current studies, we examined whether the regulation of osteocyte apoptosis after fatigue loading is regulated by differences in the expression patterns of Bax and Bcl-2. We examined the expression of Bax and Bcl-2 in fatigued bone, assessing their specific spatial and temporal association with induced fatigue microdamage.

MATERIALS AND METHODS

In vivo fatigue loading

Right ulnas of female adult Sprague–Dawley rats (4–5 months old) were subjected to fatigue loading using the rat ulna fatigue model developed by Bentolila et al.[18] This system applies axial loads to the carpal and olecranon ends of the ulna to generate bending moments in the ulnar diaphyses. It has been shown to activate intracortical remodeling in fatigued ulnas in rats.[18] Under inhalation anesthesia (isoflurane, 0.3–2%), loading was conducted at 4 Hz and performed under load control (maximum load of 20N) and the axial displacement range was monitored using a linear variable differential transducer (LVDT). Loading was performed using a miniservohydraulic testing system (Instron 8841; Instron Corp., Canton, MA, USA) under closed loop control. As in our previous studies, ulnas were fatigued to a single stopping point based on loss of whole bone stiffness, indexed by a 30% increase in ulnar compliance.[18] This stopping point reflects the formation of microdamage in bone but is well in advance of fatigue fracture.[19–23] Left ulnas were not loaded and served as paired internal controls. Before and after loading, animals were allowed unrestricted cage activity and ad libitum access to food and water. Procedures were conducted with approval from the Institutional Animal Care and Animal Use Committee of The Mount Sinai School of Medicine. At necropsy, ulnas were manually dissected free of soft tissue, fixed in formalin, decalcified in formic acid, and embedded in paraffin for histological sectioning. Longitudinal sections of the ulnar diaphysis were cut at a 5-μm thickness and adhered to charged slides.

Overview of experiment

Immunocytochemical studies were performed to determine whether differences in Bax and Bcl-2 expression are involved in the regulation of osteocyte apoptosis in association with microdamage. Specifically, Bax and Bcl-2 were examined (1) to establish unequivocally that osteocytes die by apoptosis, (2) to define the spatial distribution of dead/dying osteocytes in relation to microdamage, and (3) to determine in this context the spatial and temporal expression patterns of Bax and Bcl-2, the archetypical positive and negative regulators of apoptosis.

Localization of osteocyte apoptosis and Bax and Bcl-2 expression: In the first series of studies, we sought to determine how Bax and Bcl-2 are involved in the early regulation of osteocyte apoptosis after fatigue. Localization of Bax and Bcl-2 expression and terminal deoxynucleotidyl transferase (TdT)–mediated deoxyuridine triphosphate (dUTP)–biotin nick end labeling (TUNEL) staining in osteocytes was examined acutely (24 h) after induction of bone fatigue.

Time course of Bax and Bcl-2 regulation: In a second set of analyses, we examined the time course for the expression of Bax and Bcl-2 in osteocytes in response to in vivo fatigue loading to assess whether acute changes in pro- and antiapoptotic events in osteocytes are maintained throughout a 1- to 2-week period, during which the osteoclastic resorption response to osteocyte injury occurs. Previous studies have shown increased $TUNEL^+$, that is, apoptotic, osteocytes by 24 h after fatigue, with no change thereafter up to 10 days.[8] In the current studies, Bax and Bcl-2 were examined at 6 h and 24 h and at 10 days after fatigue loading.

Immunohistochemical detection of Bax/Bcl-2

To detect Bax and Bcl-2 expression in osteocytes after fatigue loading, sections were immunoreacted with antisera against Bax (polyclonal antibody, N-20; Santa Cruz, Carpinteria, CA, USA) and Bcl-2 (monoclonal antibody, C-2; Santa Cruz) using the streptavidin-biotin complex method with the Dako CSA (peroxidase) system (K1500; Dako, Carpinteria, CA, USA). After deparaffinization and rehydration, sections were treated with 3% hydrogen peroxide to block endogenous peroxidase activity. For immunostaining for Bcl-2, sections were pretreated with antigen retrieval solution (Biogenex, San Ramon, CA, USA) for 30

minutes at room temperature. For both primary antibodies, incubations were performed during 30 minutes at room temperature (Bax, 1:500; Bcl-2, 1:1000). Thereafter, sections were treated with sequential 15-minute incubations with biotinylated link antibody, streptavidin-biotin-peroxidase complex, biotinyl tyramide amplification reagent (Perkin Elmer, Boston, MA, USA), and streptavidin-peroxidase. Staining was completed by a 5-minute incubation with 3,3′-diaminobenzidine tetrahydrochloride, which results in a brown-colored precipitate at the antigen site. Between steps, sections were rinsed in three fresh baths of phosphate-buffered saline for 5 minutes each. For negative staining controls, the immunostaining was performed with normal mouse sera (Dako) instead of each primary antibody. Growth plate tissue of growing mice served as positive control for Bax and Bcl-2 expression.

TUNEL staining

To assess directly osteocyte apoptosis in relation to microdamage, TUNEL staining[24–26] to identify DNA fragmentation was performed using the ApopTag system (Intergen, Purchase, NY, USA) as in our previous studies.[8] Deparaffinized sections were placed in phosphate-buffered saline equilibration buffer for 5 minutes and incubated for 60 minutes with TdT/digoxigenin-labeled dUTP at 37°C. The reaction was stopped by immersing the sections with stop/wash buffer at room temperature for 30 minutes. Peroxidase-labeled antidigoxigenin with diaminobenzidine (DAB) staining was used to localize TUNEL-stained cells; fast green was used as a counterstain.[27,28] Rat thymus served as a positive control for apoptotic cells. DNAse-treated control bone was used as a positive control for TUNEL. TdT was not added to negative controls.

Histomorphometry

Localization of osteocyte apoptosis and Bax and Bcl-2 expression: Acute changes in Bax and Bcl-2 expression and TUNEL staining in osteocytes after fatigue were quantified using a histomorphometric approach with differential interference contrast (DIC) light microscopy. To assess the localization of Bax, Bcl-2, and TUNEL staining in osteocytes in fatigued bone, a microcrack was visualized and 15 fields (distance = 3.75 mm) were quantified in longitudinal direction moving away from the microcrack. From Bax and Bcl-2 immunoreacted sections and from TUNEL-stained sections, the osteocyte number densities in lacunae with positive and negative staining were determined. Measurements were performed using point count stereological methods, using a 10 mm × 10 mm eyepiece grid reticule at 40× magnification. In nonloaded control bones, 15 fields were randomly selected and quantified for comparison purposes. All data were collected by a single observer.

Time-course of Bax and Bcl-2 regulation: To assess the expression of Bax and Bcl-2 in osteocytes over time after fatigue loading, specimens were examined at 0 (baseline control), 6, and 24 h and at 10 days after fatigue loading. From Bax- and Bcl-2–stained sections, osteocyte number densities in lacunae with positive and negative staining were determined near microdamage in fatigued bone and in nonloaded control bone.

Statistical analysis

The Kruskal-Wallis analysis of variance (ANOVA) was used to assess expression of Bax and Bcl-2 and TUNEL staining in osteocytes between groups over distance from microdamage with post hoc comparisons performed against control values using Wilcoxon signed-rank test for matched pairs. Equivalent analyses were performed to assess Bax and Bcl-2 expression in osteocytes after fatigue over time. Statistical analyses were performed using the Sigmastat statistical software (version 2.03; SPSS, Inc., Chicago, IL, USA). Data are reported as means ± SD.

RESULTS

Localization of osteocyte apoptosis and Bax and Bcl-2 expression

Intense TUNEL$^+$ staining was found in osteocytes (~25% of total cells) in fatigued bone immediately adjacent to microcracks ($p < 0.001$, compared with control; photomicrographs in Fig. 1, data for distance distribution in Fig. 2). The number of TUNEL$^+$ osteocytes decreased with increasing distance away from microcracks (Fig. 2A). Similarly, Bax expression was increased dramatically in osteocytes in bone immediately adjacent to microcracks, with some 41% of total cells at microcrack loci expressing the Bax protein ($p < 0.001$). The number of osteocytes expressing Bax protein at the crack locus was ~70% higher than the number of TUNEL$^+$ osteocytes. Bax expression also rapidly decreased with increasing distance away from a microcrack. By 2–3 mm away from microcracks, expression of Bax in osteocytes in fatigued bone declined to the same low level in osteocytes in control nonloaded bone (Fig. 2B).

Distribution of Bcl-2 expression in osteocytes was fundamentally different from Bax expression and TUNEL$^+$ staining. Bcl-2 expression was increased moderately in osteocytes immediately around microcracks (23% of total cells at microcrack; $p < 0.001$). However, the population of Bcl-2$^+$ osteocytes peaked at some distance from microcracks, reaching their highest levels (49% of total cells) at 1–2 mm from microdamage foci. Bcl-2 expression in osteocytes decreased to control levels at 3–4 mm away from microcracks (Fig. 2C).

Time course of Bax and Bcl-2 regulation

Figure 3 shows changes over time in the numbers of Bax and Bcl-2$^+$ osteocytes in bone adjacent to microcracks after fatigue loading. At 6 h after fatigue loading, the number of Bax$^+$ osteocytes was increased >10-fold over control values ($^*p < 0.001$), with no further significant changes up to 24 h. By 10 days, numbers of Bax$^+$ cells decreased by approximately one-half ($p < 0.01$, relative to number of Bax$^+$ osteocytes at 24 h). The temporal expression for Bcl-2 in osteocytes was similar to that of Bax. Nonloaded bone showed no significant difference from baseline controls.

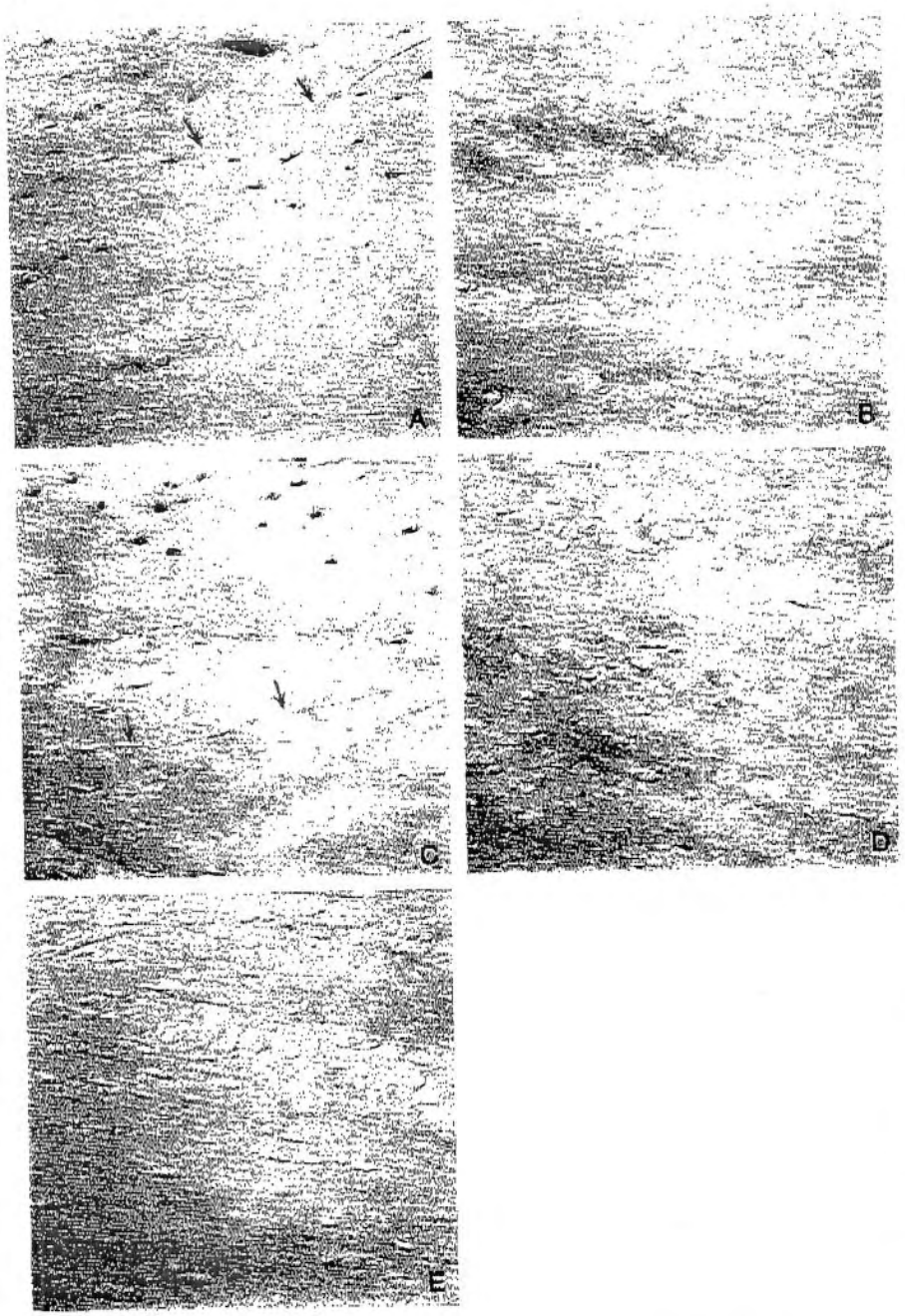

FIG. 1. Photomicrographs showing Bax and Bcl-2 expression in sections of ulnar diaphyses. Brown precipitate in cells indicates immunoreactivity. (A) Bax expression in osteocytes surrounding a microcrack (arrows) in fatigued bone. (B) No Bax expression was seen in osteocytes in fatigued bone away from microcracks. (C) Bcl-2 expression in osteocytes near microdamage (arrows) in fatigued bone. Note high numbers of positive cells at some distance from the microcrack. (D) No Bcl-2 staining was seen in osteocytes in fatigued bone away from microdamage. (E) Bcl-2 immunoreactivity in sections of control nonloaded ulnar diaphyses. (photomicrograph field widths, 880 μm).

DISCUSSION

The current studies show increases of both Bax, a proapoptotic protein, and Bcl-2, an antiapoptotic protein, in osteocytes after fatigue loading. More specifically, analyses of spatial distribution of Bax and Bcl-2 show that the proteins are expressed in fundamentally different patterns in osteocytes as a function of distance from microdamage sites. The proapoptotic signal is highest immediately adjacent to the microcracks, and the antiapoptotic protein reaches its greatest level at some distance from the damage focus. TUNEL studies showed a spatial distribution in relation to microdamage similar to Bax expression in osteocytes, though greater numbers of Bax^+ cells than $TUNEL^+$ cells were a consistent finding at all distances from microdamage. This is an expected consequence after injury. Bax up-regulation occurs at an earlier stage of the apoptotic process than the nuclear degradative changes marked by the TUNEL method.[12,29] The "lifetime" of an apoptotic osteocyte, the duration of the effector stage of apoptosis, or the

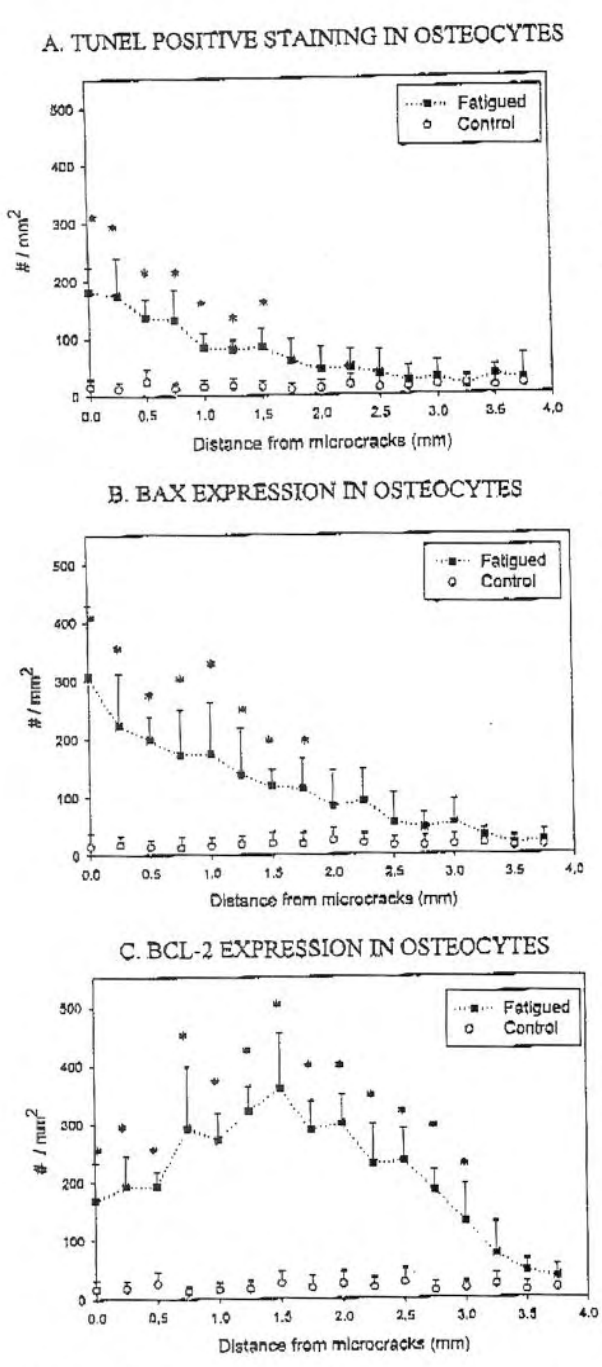

FIG. 2. Distance distribution of (A) TUNEL$^+$ staining, (B) Bax expression, and (C) Bcl-2 expression in osteocytes in relation to microcracks at 24 h after fatigue. Data are shown as osteocyte densities (number of cells/mm^2). (A and B) In bone regions immediately adjacent to microcracks (0 mm), TUNEL$^+$ osteocytes were highly increased over control levels ($^*p < 0.001$). The numbers of TUNEL$^+$ osteocytes decreased with increasing distance away from microcracks. In bone regions away from microcracks (at 2–3 mm away), the number of TUNEL$^+$ osteocytes reached the same low level as seen in non-loaded control bone. Distance distribution of Bax expression in osteocytes in relation to microcracks showed a similar trend as the TUNEL$^+$ staining. (C) Moderate increase of Bcl-2 expression was seen in osteocytes in bone regions immediately adjacent to microcracks ($^*p < 0.001$, relative to control levels). However, in bone regions more remote from microcracks, numbers of Bcl-2$^+$ osteocytes dramatically increased to reach peak values at 1–2 mm away from crack locus. Numbers of Bcl-2$^+$ osteocytes gradually declined to reach control levels at 3–4 mm distant from microcracks. Total osteocyte density was 740 ± 63 (number/mm^2).

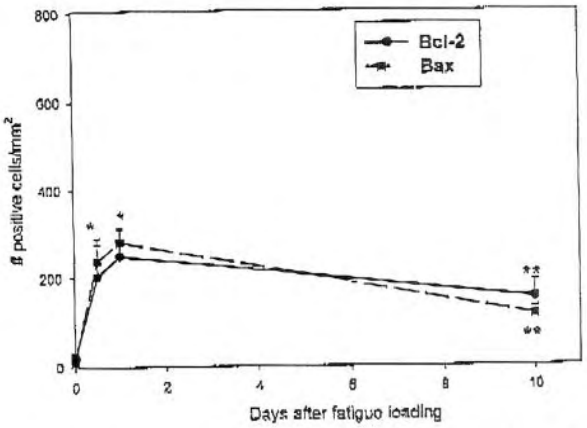

FIG. 3. Changes over time in the numbers of Bax$^+$ and Bcl-2$^+$ osteocytes in bone adjacent to microcracks after fatigue loading. Data are shown as osteocyte densities (number of cells/mm^2). Bax expression was significantly increased at 6 h after fatigue, with no change up to 24 h ($^*p < 0.001$, relative to baseline control). At 10 days, total numbers of Bax$^+$ osteocytes declined by approximately one-half ($^{**}p < 0.01$). Similar trend was seen for Bcl-2 expression in osteocytes near microdamage over time. Total osteocyte density was 740 ± 63 (number/mm^2).

final degradative phase are not known. Therefore, some Bax$^+$ cells present at the earliest time period after mechanical challenge may indicate cells that exhibit nuclear degradative changes only after the time points included in our sampling.[29,30]

Some cell death follows pathways that are mitochondrially dependent.[31,32] A decline in the mitochondrial membrane potential and the release of molecules from the mitochondria such as cytochrome c result in the activation of more downstream caspases. Once activated, these proteases can induce nuclear apoptotic degeneration via DNA fragmentation factor and acinus, which promote endonuclease digestion of DNA and chromatin condensation, respectively.[33,34–37] Our present findings for the involvement of the Bcl-x family of proteins suggest that osteocytes also may select a mitochondrially dependent pathway after microcrack injury, although this must be confirmed with other studies.

Elevated Bcl-2 protein in osteocytes more distant from the microcracks may exert a protective function in these cells, preventing them from entering apoptosis. This may be a response to a very low level of damage. Others have found

that neuronal cultures exposed to subtoxic concentrations of β-amyloid peptide had increased amounts of the antiapoptotic Bcl-x_L protein and messenger RNA (mRNA). Cells that overexpressed Bcl-x_L had increased resistance to apoptosis-inducing concentrations of the β-amyloid peptide.[38] Up-regulation of Bcl-2 and increased cell survival have been observed in tissues with a high rate of apoptosis after sustaining injury.[38–46] In the myocardium, apoptosis occurs during hypoxia and ischemia-reperfusion and occurs most notably in the border zone after infarction.[48–50] In this myocardial injury, Bcl-2 prevents apoptotic cell death in ventricular myocytes in areas of acute infarction.[46] Similar observations have been made in brain ischemia models, in which surviving (nonapoptotic) neurons express Bcl-2 in areas of focal brain ischemia in rats.[39–42] Observations in adult osteoarthritic human cartilage show apoptosis of some chondrocytes with adjacent cells showing up-regulation of Bcl-2.[47] These findings indicate that both acute and chronic injuries, which cause apoptotic cell death, also induce complementary pathways that actively protect cells from impending death.

Previous studies indicate that the levels of Bcl-2 expression in osteocytes in normal adult bone are low.[51–53] However, in human fetal ribs, Stevens et al. found an inverse relationship between osteocyte apoptosis and the distribution of Bcl-2, implying a potential selectivity in cell survival.[17] Wang et al. also suggested that expression of Bcl-2 in chondrocytes and osteocytes near the epiphyseal growth plate protects them until their final maturation.[53] Our findings that Bcl-2 expression is strongly positive in osteocytes in fatigued bone, especially at some distance from microdamage, support the hypothesis that osteocytes may use a similar defense mechanism of cells to escape from impending death induced by matrix injury. Specifically, these data suggest that at the site of microinjury in bone, those osteocytes that do not undergo apoptosis are prevented from doing so by active protection mechanisms. Moreover, the apoptotic region around microcracks was walled-in effectively by a surrounding halo of surviving osteocytes actively expressing Bcl-2. This raises the possibility that targeting and guidance of bone resorption to sites of microdamage may be carried out not only by signals from apoptotic cells near damage sites, but also by signals from surrounding cells expressing apoptosis-inhibiting gene products.

Induction of osteocyte apoptosis after fatigue loading is rapid, with elevation of Bax by 24 h after loading. However, although Bax expression in osteocytes decreased by 10 days after fatigue, Verborgt et al.[8] found that osteocyte TUNEL staining remained elevated even at 10 days after loading. The similarities in early Bax expression and TUNEL staining indicate that induction of osteocyte apoptosis after fatigue is an early event. The continued long-term elevation of TUNEL staining may suggest that the ordered cell disassembly process in vivo is protracted and sustained. Moreover, TUNEL$^+$, that is, apoptotic, debris left in empty lacunae by osteocyte dying over time also likely contributes to the sustained high TUNEL signal observed in bone; this debris may play an important role in the guidance of osteoclastic tunneling within the bone.

Osteocyte apoptosis has been suggested to play an important role in targeting bone remodeling processes in response to a number of stimuli.[1–8,54,55] Osteocyte apoptosis has been shown in association with high bone turnover processes[1,2] after hormonal deprivation[3,4] and in association with glucocorticoid-induced osteonecrosis of the femoral head in humans and mice.[6,7] Previously, we have shown that osteocyte apoptosis occurs in association with areas of microdamaged bone and later on, these identical areas are the location of osteoclastic resorption.[8] Our current studies show complementary pathways in the regulation of osteocyte apoptosis after fatigue by the proto-oncogene products Bax and Bcl-2. By actively expressing Bcl-2, osteocytes can escape from cell death in bone near foci with microdamage and associated osteocyte apoptosis. Moreover, our data suggest that apoptosis protection in osteocytes could play a complimentary role in directing the local osteoclastic activity that occurs in association with microdamage and osteocyte apoptosis. Thus, there appear to be three functional classes of osteocytes in mechanically challenged bone[1]: dying or dead osteocytes,[2] osteocytes affected by the injury but actively protected from death by Bcl-2 expression,[3] and unaffected osteocytes. The actions of each of these cells to trigger and guide bone resorption currently are unknown, but these data suggest a complex osteocyte control system for activation and targeting of osteoclastic activity in bone.

ACKNOWLEDGMENTS

We thank Damien Laudier for guidance in developing the histological and immunocytochemical procedures used in this study. We also thank Philip Nasser for assistance with experimental mechanical loading and instrumentation. This work was supported by a National Institutes of Health (NIH) grant AR41210 and by Department of Defense grant DAMD-17-98-1-8515. O.V. was supported by a fellowship from the University of Antwerp.

REFERENCES

1. Noble BS, Stevens H, Loveridge N, Reeve J 1997 Identification of apoptotic changes in osteocytes in normal and pathological human bone. Bone **20**:273–282.
2. Bronckers ALJJ, Goei W, Luo G, Karsenty G, DeSouza RN, Lyaruu DM, Burger EH 1996 DNA fragmentation during bone formation in neonatal rodent assessed by transferase mediated end labeling. J Bone Miner Res **11**:1281–1291.
3. Tomkinson A, Reeve J, Shaw RW, Noble BS 1997 The death of osteocytes via apoptosis accompanies estrogen withdrawal in human bone. J Clin Endocrinol Metab **82**:3128–3135.
4. Tomkinson A, Gevers EF, Wit JM, Reeve J, Noble BS 1998 The role of estrogen in the control of rat osteocyte apoptosis. J Bone Miner Res **13**:1243–1250.
5. Qiu S-J, Hoshaw SJ, Gibson GJ, Lundin-Cannon KD, Schaffler MB 1997 Osteocyte apoptosis in reaction to matrix damage in compact bone. Trans Orthop Res Soc **22**:89.
6. Weinstein RS, Jilka RL, Parfitt AM, Manolagas SC 1998 Inhibition of osteoblastogenesis and promotion of apoptosis of osteoblasts and osteocytes by glucocorticoids. J Clin Invest **102**:274–282.
7. Weinstein RS, Nicholas RW, Manolagas SC 2000 Apoptosis of osteocytes in glucocorticoid-induced osteonecrosis of the hip. J Clin Endocrinol Metab **85**:2907–2912.

8. Verborgt O, Gibson GJ, Schaffler MB 2000 Loss of osteocyte integrity in association with microdamage and bone remodeling after fatigue in vivo. J Bone Miner Res **15**:60–67.
9. Kerr JFR, Wyllie AH, Currie AR 1972 Apoptosis, a basic biological phenomenon with wide-ranging implications in tissue kinetics. Br J Cancer **26**:239–257.
10. Kerr JFR, Harmon BV 1991 Definition and incidence of apoptosis. In: Tomei LD, Cope FO (eds.) Apoptosis: The Molecular Basis of Cell Death. Cold Springs Harbor Press, Cold Spring Harbor, NY, USA, pp. 5–30.
11. Buja LM, Eigenbrodt ML, Eigenbrodt EH 1993 Apoptosis and necrosis—basic types and mechanisms of cell death. Arch Pathol Lab Med **117**:1208–1214.
12. Hengartner MO 2000 The biochemistry of apoptosis. Nature **407**:770–776.
13. Adams JM, Cory S 1998 The Bcl-2 protein family: Arbiters of cell survival. Science **281**:1322–1326.
14. Hockenbery D, Nunez G, Milliman C, Schreiber RD, Korsmeyer SJ 1990 Bcl-2 is an inner mitochondrial membrane protein that blocks programmed cell death. Nature **348**:334–336.
15. Oltvai ZN, Milliman CL, Korsmeyer SJ 1993 Bcl-2 heterodimerizes in vivo with a conserved homolog, Bax, that accelerates programed cell death. Cell **74**:609–619.
16. Tsujimoto Y, Shimizu S 2000 VDAC regulation by the Bcl-2 family proteins. Cell Death Differ **7**:1174–1181.
17. Stevens HY, Reeve J, Noble BS 2000 Bcl-2, tissue transglutaminase and p53 protein expression in the apoptotic cascade in ribs of premature infants J Anat **196**:181–191.
18. Bentolila V, Boyce TM, Fyhrie DP, Skerry TM, Schaffler MB 1998 Intracortical remodeling in adult rat long bones after fatigue loading. Bone **23**:275–281.
19. Schaffler MB, Burr DB, Radin EL 1989 Mechanical and morphological effects of strain rate on fatigue in compact bone. Bone **10**:207–214.
20. Schaffler MB, Radin EL, Burr DB 1990 Long-term fatigue behavior of compact bone at low strain magnitude and rate. Bone **11**:321–326.
21. Burr DB, Forwood MR, Schaffler MB, Fyhrie DP, Martin RB, Turner CH 1997 Bone microdamage and skeletal fragility in osteoporotic and stress fractures. J Bone Miner Res **12**:6–15.
22. Carter DR, Caler WE, Spengler DM, Frankel VH 1981 Uniaxial fatigue of human cortical bone: The influence of tissue physical characteristics. J Biomechanics **14**:461–470.
23. Carter DR, Caler WE, Spengler DM, Frankel VH 1981 Fatigue behavior of adult cortical bone: The influence of mean strain and strain range. Acta Orthop Scand **52**:481–490.
24. Gavrieli Y, Sherman Y, Ben-Sasson SA 1992 Identification of programmed cell death in situ via specific labeling of nuclear DNA fragments. J Cell Biol **119**:493–501.
25. Kressel M, Groscurth P 1994 Distinction of apoptotic and necrotic cell death by in situ labeling of fragmented DNA. Cell Tissue Res **278**:549–556.
26. Labat-Moleur F, Guillermet C, Lorimier P, Robert C, Lantuejoul S, Brambilla E, Negoescu A 1998 Tunel apoptotic cell detection in tissue sections: Critical evaluation and improvement. J Histochem Cytochem **46**:327–334.
27. Gibson GJ, Koehler WJ, Schaffler MB 1995 Chondrocyte apoptosis in endochondral ossification of chick sterna. Dev Dyn **203**:468–476.
28. Gibson GJ, Lin DL, Schaffler MB, Kimura JH 1995 Endochondral resorption of chick sterna in culture. J Orthoped Res **13**:542–552.
29. Tatton NA 2000 Increased caspase 3 and bax immunoreactivity accompany nuclear GAPDH translocation and neuronal apoptosis in Parkinson's disease Exp Neur **166**:29–43.
30. Darzynkiewicz Z, Traganos F 1998 Measurements of apoptosis. Adv Biochem Eng Biotechnol **62**:34–73.
31. Green DR, Reed JC 1998 Mitochondria and apoptosis. Science **281**:1309–1312.
32. Marzo E, Brenner C, Zamzami N, Jurgensmeier JM, Susin SA, Viera HLA, Prevost MC, Xie Z, Matsuyama S, Reed JC, Kroemer G 1998 Bax and adenine nucleotide translocator cooperate in the mitochondrial control of apoptosis. Science **281**:2027–2031.
33. Liu X, Kim CN, Yang J, Jemmerson R, Wang X 1996 Induction of apoptotic program in cell-free extracts: Requirement for dATP and cytochrome c. Cell **86**:147–157.
34. Sahara S, Aoto M, Eguchi Y, Imamoto N, Yoneda Y, Tsujimoto Y 1999 Acinus is a caspase 3 activated protein required for apoptotic chromatin condensation. Nature **401**:168–173.
35. Thornberry NA, Lazebnik Y 1998 Caspases: Enemies within. Science **281**:1312–1316.
36. Krammer PH 2000 CD95's deadly mission in the immune system Nature **407**:789–795.
37. Schmitz I, Kirchoff S, Krammer PH 2000 Regulation of death receptor-mediated apoptosis pathways. Int J Biochem Cell Biol **32**:1123–1136.
38. Luetjens CM, Lankiewicz S, Bui NT, Krohn AJ, Poppe M, Prehn JH 2001 Up-regulation of Bcl-xL in response to subtoxic beta-amyloid: Role in neuronal resistance against apoptotic and oxidative injury. Neuroscience **102**:139–150.
39. Allsopp TE, Wyatt S, Paterson HF, Davies AM 1993 The proto-oncogene Bcl-2 can selectively rescue neurotrophic factor-dependent neurons from apoptosis. Cell **73**:295–307.
40. Chen J, Graham SH, Chan PH, Lan J, Zhou RL, Simon RP 1995 Bcl-2 is expressed in neurons that survive focal ischemia in the rat. Neuroreport **26**:394–398.
41. Gillardon F, Lenz C, Waschke KF, Krajewski S, Reed JC, Zimmerman M, Kuschinsky W 1996 Altered expression of Bcl-2, Bcl-x, Bax and c-*fos* colocalizes with DNA fragmentation and ischemic cell damage following middle cerebral artery occlusion in rats. Mol Brain Res **40**:254–260.
42. Isenmann S, Stoll G, Schroeter M, Krajewski S, Reed JC, Bahr M 1998 Differential regulation of Bax, Bcl-2 and Bcl-x proteins in focal cortical ischemia in the rat. Brain Path **8**:49–63.
43. Schabitz WR, Sommer C, Zoder W, Kiessling M, Schwaninger M, Schwab S 2000 Intravenous brain-derived neurotrophic factor reduces infarct size and counterregulates Bax and Bcl-2 expression after temporary focal cerebral ischemia. Stroke **31**:2212–2221.
44. Nuydens R, Dispersyn G, Van Den Keiboom G, de Jong M, Connors R, Ramackers F, Borgers M, Geerts H 2000 Bcl-2 protects against apoptosis-related microtubule alterations in neuronal cells. Apoptosis **5**:43–51.
45. Misao J, Hayakawa Y, Ohno M, Kato S, Fujiwara T, Fujiwara H 1996 Expression of bcl-2 protein, an inhibitor of apoptosis, and bax, an accelerator of apoptosis, in ventricular myocytes of human hearts with myocardial infarction. Circulation **94**:1506–1512.
46. Kirschenbaum LA, de Moissac D 1997 The bcl-2 gene product prevents programmed cell death of ventricular myocytes. Circulation **96**:1580–1585.
47. Erlacher L, Maier R, Ullrich R, Kiener H, Aringer M, Menschik M, Graninger W 1995 Differential expression of the proto-oncogene Bcl-2 in normal and osteoarthritic human cartilage. J Rheumatol **22**:926–931.
48. Gottlieb RA, Burleson KO, Kloner RA, Babior BM, Engler RL 1994 Reperfusion injury induces apoptosis in rabbit cardiomyocytes. J Clin Invest **94**:1621–1628.
49. Isner JM, Kearny M, Bortman S, Passeri J 1995 Apoptosis in human atherosclerosis and restenosis. Circulation **91**:2703–2711.
50. Kajstura J, Mansukhani M, Cheng W, Reiss K, Krajewski S, Reed JC, Quaini F, Sonnenblick EH, Anversa P 1996 Programmed cell death and expression of the proto-oncogene

Bcl-2 in myocytes during postnatal maturation of the heart. Exp Cell Res **219**:110–121.
51. Hockenberry D, Zutter M, Hickey W, Nahm M, Korsmeyer SJ 1991 Bcl-2 protein is topographically restricted in tissues characterized by apoptotic cell death. Proc Natl Acad Sci USA **88**:6961–6965.
52. Hatakeyama S, Tomichi N, Ohara-Nemoto Y, Satoh M 2000 The immunohistochemical localization of Fas and Fas ligand in jaw bone and tooth germ of human fetuses. Calcif Tissue Int **66**:330–337.
53. Wang Y, Toury R, Hauchecorne M, Balmain N 1997 Expression of Bcl-2 protein in the epiphyseal plate cartilage and trabecular bone of growing rats. Histochem Cell Biol **108**:45–55.
54. Parfitt AM, Mundy GR, Roodman GD, Hughes DE, Boyce BF 1996 A new model for the regulation of bone resorption with particular reference to the effect of bisphosphonates. J Bone Miner Res **11**:150–159.
55. Plotkin LI, Weinstein RS, Parfitt AM, Roberson PK, Manolagas SC, Bellido T 1999 Prevention of osteocyte and osteoblast apoptosis by bisphosphonates and calcitonin. J Clin Invest **104**:1363–1374.

Address reprint requests to:
Mitchell B. Schaffler, Ph.D.
Leni and Peter W. May Department of Orthopaedics
Box 1188
Mount Sinai School of Medicine
One Gustave L. Levy Place
New York, NY 10029, USA

Received in original form March 20, 2001; in revised form September 28, 2001; accepted October 22, 2001.

JOURNAL OF BONE AND MINERAL RESEARCH
Volume 20, Number 8, 2005
Published online on March 28, 2005; doi: 10.1359/JBMR.050326

Relationship Between Bone Morphology and Bone Quality in Male Tibias: Implications for Stress Fracture Risk

Steven M Tommasini,[1] Philip Nasser,[2] Mitchell B Schaffler,[2] and Karl J Jepsen[2]

ABSTRACT: Biomechanical properties were assessed from the tibias of 17 adult males 17–46 years of age. Tissue-level mechanical properties varied with bone size. Narrower tibias were comprised of tissue that was more brittle and more prone to accumulating damage compared with tissue from wider tibias.

Introduction: A better understanding of the factors contributing to stress fractures is needed to identify new prevention strategies that will reduce fracture incidence. Having a narrow (i.e., more slender) tibia relative to body mass has been shown to be a major predictor of stress fracture risk and fragility in male military recruits and male athletes. The intriguing possibility that slender bones, like those shown in animal models, may be composed of more damageable material has not been considered in the human skeleton.
Materials and Methods: Polar moment of inertia, section modulus, and antero-posterior (AP) and medial-lateral (ML) widths were determined for tibial diaphyses from 17 male donors 17–46 years of age. A slenderness index was defined as the inverse ratio of the section modulus to tibia length and body weight. Eight prismatic cortical bone samples were generated from each tibia, and tissue-level mechanical properties including modulus, strength, total energy, postyield strain, and tissue damageability were measured by four-point bending from monotonic (n = 4/tibia) and damage accumulation (n = 4/tibia) test methods. Partial correlation coefficients were determined between each geometrical parameter and each tissue-level mechanical property while taking age into consideration.
Results: Significant correlations were observed between tibial morphology and the mechanical properties that characterized tissue brittleness and damageability. Positive correlations were observed between measures of bone size (AP width) and measures of tissue ductility (postyield strain, total energy), and negative correlations were observed between bone size (moment of inertia, section modulus) and tissue modulus.
Conclusions: The correlation analysis suggested that bone morphology could be used as a predictor of tissue fragility and stress fracture risk. The average mechanical properties of cortical tissue varied as a function of the overall size of the bone. Therefore, under extreme loading conditions (e.g., military training), variation in bone quality parameters related to damageability may be a contributing factor to the increased risk of stress fracture for individuals with more slender bones.
J Bone Miner Res 2005;20:1372–1380. Published online on March 28, 2005; doi: 10.1359/JBMR.050326

Key words: bone biomechanics, stress fracture, bone quality, bone morphology, strength, damage, brittleness

INTRODUCTION

STRESS FRACTURES ARE overuse injuries of bone that are common among elite runners and military recruits.[1–3] Before injury, affected bones are typically normal with no acute injury. Morbidity from stress fractures ranges from minor pain to serious lifetime disability for the individual.[4] Stress fractures have been reported in the ribs, hip, spine, and metatarsals,[3,5] but vigorous weight-bearing activities, such as running and jogging, commonly lead to stress fractures of the lower extremities, especially the tibia.[3] During basic training, 1–5% of U.S. male military recruits sustain a stress fracture.[2] However, this incidence is two to five times higher in female recruits.[6] Stress fractures lead to loss of manpower, valuable loss of training time, expense of medical care, and discharge of affected soldiers.[7] A better understanding of the factors contributing to stress fractures is needed to identify new prevention strategies that will reduce fracture incidence.

A number of risk factors for stress fracture have been identified including physical fitness, external hip rotation, body height and weight, age, race, gender, muscle mass, motivation, footwear, smoking, and family history of osteoporosis.[1,4,8–10] One of the best predictors of stress fracture risk is bone geometry. Specifically, having a narrow (i.e., more slender) tibia relative to body mass has been shown to

The authors have no conflict of interest.

[1]New York Center for Biomedical Engineering, CUNY Graduate School, Department of Biomedical Engineering, City College of New York, New York, New York, USA; [2]Leni & Peter W. May Department of Orthopaedics, Mount Sinai School of Medicine, New York, New York, USA.

be a major predictor of stress fracture risk and fragility in male military recruits[1,2,11] and male athletes.[12] A stress fracture is thought to be a consequence of transiently reduced tissue strength arising from increased resorptive activity (i.e., increased porosity) that acts to repair damage induced by vigorous physical activity.[13] Thus, stress fractures may be pronounced in individuals with more slender bones because smaller bone size is thought to lead to higher tissue-level stresses and thus increased damage accumulation.[1,2] However, this postulate is based on the assumption that all bones are constructed in equivalent manners, and the contribution of variable tissue-level mechanical properties to stress fracture incidence has not been explored.

An examination of inbred mouse strains may help explain why bone size is a risk factor for stress fractures in the human skeleton. A comparison of adult A/J and C57BL/6J inbred mouse strains revealed that the bone slenderness was inversely related to mineral content (as measured by ash content) and, by correlation, tissue modulus and strength.[14] Mineral content has been shown to be positively correlated with tissue stiffness and strength.[15] These results suggested that bone morphology and mineral content were coordinately regulated so whole bone stiffness appropriately matched the mechanical demands imposed by weight bearing. However, the downside of regulating mineral content to match bone size was that mineral content was also negatively correlated with tissue ductility.[14,15] We postulate that a similar reciprocal relationship between bone size and bone quality exists in the human skeleton. The intriguing possibility that slender bones, like those shown in animal models, may be composed of more damageable material has not yet been considered in the human skeleton.

The goal of this study was to determine whether tissue-level mechanical properties vary with bone size in the human skeleton. This was tested by assessing the biomechanical properties of tibias from young adult males. Understanding why bone morphology is a risk factor for stress fractures should lead to better identification of those at risk and, ultimately, to early diagnosis, treatment, and modification of training regimens.

MATERIALS AND METHODS

Sample population

Tibias of 17 male donors (15 white, 1 Hispanic, 1 black) 32.9 ± 10.4 years of age (range, 17–46 years) were acquired from the Musculoskeletal Transplant Foundation (Edison, NJ, USA). Donor body weight and height were obtained from the source. Only donors with no known skeletal pathology were included in the study. The tibias were freshly harvested, wrapped in wet gauze, and stored in plastic bags at −40°C.

Whole bone morphology

Tibia length (L) was measured as the average distance between the distal articular center (the middle of the talar trochlear facet) and the two proximal articular centers (medial and lateral condyles)[16] using a large-capacity slide caliper with an accuracy of ±2.54 mm (Mantex Precision; Haglöf, Madison, MS, USA). Tibia width was measured in the antero-posterior (AP) and medial-lateral (ML) directions at 10% intervals from 30–70% of the total tibia length using a 300-mm vernier caliper with an accuracy of ±0.02 mm (Fowler Company, Newton, MA, USA).

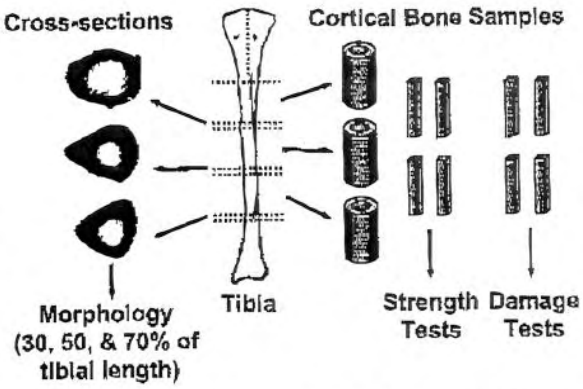

FIG. 1. Schematic of how whole tibias were sectioned to produce the 3-mm-thick sections used for cross-sectional morphology and cortical bone samples for biomechanical testing from three diaphyseal cylindrical sections (monotonic, n = 4/tibia; damage accumulation, n = 4/tibia).

Cross-sectional morphology was determined from 3-mm-thick middiaphyseal cross-sections cut at 30%, 50%, and 70% of the total tibia length (Fig. 1) using a diamond coated metallurgical saw (Model 660; South Bay Technology, San Clemente, CA, USA). A calibrated image of each cross-section was obtained using a digital camera at a 0.024 mm/pixel resolution. Image analysis software (IMAQ Vision Builder 6.0; National Instruments, Austin, TX, USA) was used to threshold each image and quantify cortical area (CtAr), the moments of inertia about the AP (I_{AP}) and ML (I_{ML}) axes, the polar moment of inertia ($J = I_{AP} + I_{ML}$), and the section modulus in the AP (J/APwidth/2) and ML (J/MLwidth/2) directions. Moment of inertia and section modulus were assessed because these geometric measures are related to the bending and torsional stiffness of intact tibias. A slenderness index (S) was calculated in the AP and ML directions as the ratio of the AP and ML section modulus values, respectively, to tibia length and body weight[17]:

$$S = 1/[[J/(\text{width}/2)]/(L \times BW)] \quad (1)$$

where L = tibia length (mm) and BW = body weight (kg). The section modulus has been shown to scale linearly with body mass.[17] The inverse ratio was used so that a tibia with a large slenderness value is one that is thinner or gracile for the weight and height of an individual. A small slenderness value reflects a stocky or robust tibia. All morphological traits were averaged over the three cross-sections for each tibia.

Bone sample generation

Cortical bone samples were prepared from the diaphysis of each tibia for biomechanical testing (Fig. 1). The three diaphyseal cylindrical sections were rough-cut into antero-

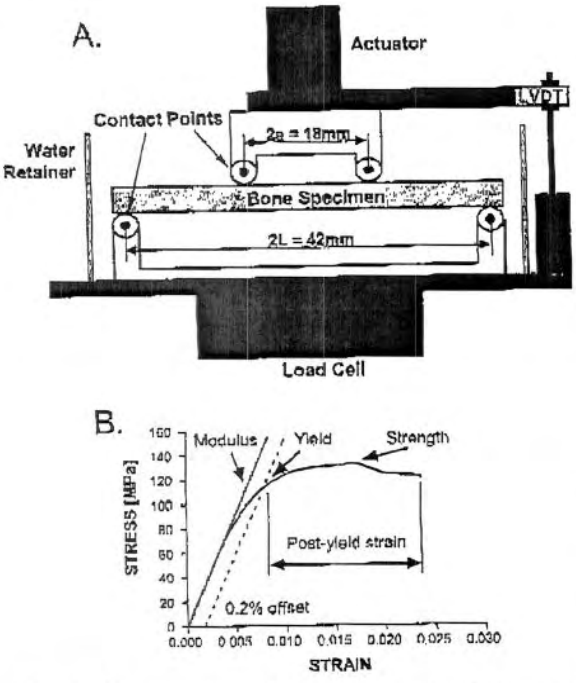

FIG. 2. (A) Schematic of the four-point bending device shows how cortical bone samples were tested. The span between the upper contact points is 2a = 18 mm, and the span between the lower contact points is 2L = 42 mm. (B) Typical stress-strain curve from the four-point bending monotonic tests shows how modulus, strength, postyield strain, and total energy were calculated.

lateral, antero-medial, and posterior regions. From each of these regions, one to three prismatic beams were cut using a diamond-coated metallurgical saw (Isomet; Buehler, Lake Bluff, IL, USA). The beams were machined to regular test samples using an automated CNC milling machine under constant irrigation (Modela MDX-20; Roland DGA, Irvine, CA, USA). Sample width (circumferential direction) was machined to 5 mm and length (longitudinal direction) was machined to 55 mm for all samples. Sample height (radial direction) was 2.5 mm except for four tibias with thin cortices, which were machined to 2.2 mm. A total of eight samples were generated from each tibia and randomly distributed to monotonic (n = 4) and damage accumulation (n = 4) test groups. All samples were stored at −40°C in gauze saturated with PBS with added calcium[18] and placed individually in airtight bags.

Monotonic failure properties

Tissue-level mechanical properties were assessed by loading four cortical bone samples from each tibia to failure in four-point bending at 0.05 mm/s (Fig. 2A) using a servo-hydraulic materials testing system (Instron model 8872; Instron, Canton, MA, USA). Specimens were submerged in a PBS solution with added calcium[18] and maintained at 37°C throughout all tests. Load and deflection were converted to stress and strain using the following equations, which take yielding into consideration[19]:

$$\sigma = 2[2M + \phi(dM/d\phi)]/bh^2 \quad (2)$$

$$\varepsilon = h\phi/2a = \tfrac{1}{2}h\Delta[(L - a)/(2a^3/3 - a^2L + L^3/3)] \quad (3)$$

where σ and ε are the stress and strain at the outer surface of the beam, M = applied moment, b = specimen width, h = specimen height, a = ½ the span between the upper two load points = 9 mm, L = ½ the span between the two lower load points = 21 mm, ϕ = angle of inclination = a/ρ, and d/dϕ is the derivative with respect to ϕ. The angle of inclination was written in terms of the measured deflection (Δ) by estimating the curvature (ρ) using standard beam equations. Mechanical properties were calculated from the stress-strain curves, and these included modulus, strength, total energy, and postyield strain (Fig. 2B). Modulus was calculated from a linear regression of the initial portion of the stress-strain curve. Yield was determined using the 0.2% offset method. Postyield strain was defined as the strain at failure minus the strain at yield. All properties were averaged over the four samples tested for each tibia.

Damage accumulation tests

Tissue damageability was assessed using a protocol designed to induce and accumulate cracks in cortical bone specimens. The accumulation of damage leads to measurable degradation of mechanical properties.[20] Therefore, the degradation of mechanical properties can be used as an index of matrix damage. Four cortical bone samples from each tibia were subjected to a fifteen cycle damage accumulation protocol (Fig. 3A) similar to that described previously.[21] For this protocol, "diagnostic" cycles (1, 3, 5, 7, 9, 11, 13, and 15) were interposed between "damage" cycles (2, 4, 6, 8, 10, 12, and 14). For the diagnostic cycles, the specimens were loaded in four-point bending at 0.5 mm/s to 50% of the average displacement at yield (determined from the monotonic tests), held for 60 s, and unloaded at 0.5 mm/s. Preliminary studies indicated that this load level provided information on tissue-level mechanical properties without inducing additional damage. For the damage cycles, the specimens were loaded at 0.5 mm/s to 50%, 75%, 100%, 125%, 150%, 175%, and 200% of displacement at yield, respectively, held for 60 s, and unloaded at 0.5 mm/s. A 5-minute recovery period followed each damage cycle. Displacement at yield was used as a reference in the damage cycles because this parameter showed little variation among the test samples when subjected to monotonic four-point bending. The displacement at yield was 1.0 mm for the samples with a height of 2.5 mm and 1.07 mm for the samples with a height of 2.2 mm.

A mechanical measure of the amount of damage that accumulated within the test sample was quantified from the magnitude of stiffness degradation. For each diagnostic cycle, stiffness was calculated from a linear regression of the initial portion of the load-deformation curve. Specimen stiffness decreased nonuniformly with each cycle revealing increasing amounts of damage induced within each cycle and an overall damage accumulation by the end of the protocol (Fig. 3B). At the end of the test sequence, the overall

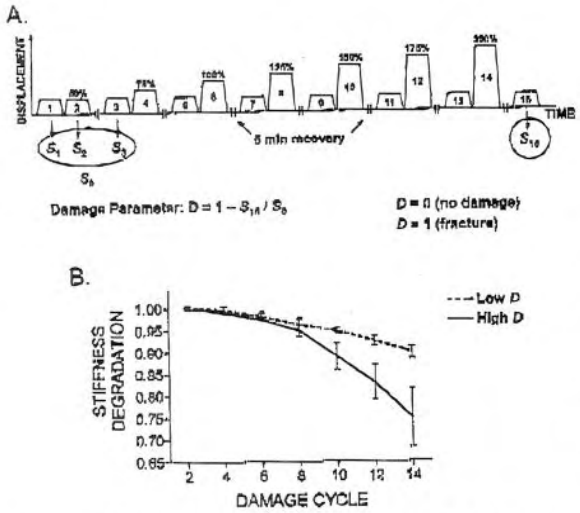

FIG. 3. (A) A 15-cycle loading protocol was used to induce damage within machined cortical bone specimens and to measure resultant stiffness degradation. Damage was induced during cycles 2, 4, 6, 8, 10, 12, and 14 by conducting relaxation tests at increasing levels of applied displacement (expressed as a percentage of the displacement at yield). Diagnostic cycles were interposed between damaging cycles. Each damage cycle was preceded by a diagnostic cycle at 50% of displacement at yield. A 5-minute recovery period was introduced after the damage cycles to relieve residual internal stresses. (B) The change in stiffness calculated between sequential diagnostic tests was plotted vs. cycle number for the damage tests. The dashed curve represents a specimen showing little stiffness degradation (i.e., little damage accumulation). The solid line represents a specimen showing large stiffness degradation (i.e., more damage accumulation).

damage parameter, D, was calculated by comparing the stiffness of the first and last diagnostic tests such that:

$$D = 1 - S_{15}/S_0, \quad (4)$$

where S_{15} is the stiffness of the last diagnostic cycle and S_0 is the average stiffness of the first two diagnostic cycles (S_1, S_3) and the first damage cycle (S_2).

Statistical analysis

All data were regressed against age using linear regression analysis to identify the properties that varied significantly with age (GraphPad Prism, San Diego, CA, USA). To determine whether bone morphology was related to tissue level material properties, partial correlation coefficients were determined between each geometrical parameter (e.g., I_{AP}, I_{ML}, J, S) and each tissue level mechanical property (modulus, strength, total energy, postyield strain, damageability) while taking age into consideration (Minitab, State College, PA, USA).[22]

RESULTS

The sample population showed broad ranges of body size, body stature, and bone morphology values (Table 1). Modulus and strength showed little variation among individuals (CV = 9.73% and 4.62%, respectively). However,

TABLE 1. VARIATION IN PROPERTIES AMONG YOUNG ADULT MALE TIBIAS

Property	*Mean ± SD*	*Range*
Age (years)	32.9 ± 10.4	17–46
Body weight (kg)	83.8 ± 25.1	57.2–158.8
Body height (cm)	177.7 ± 4.3	170.2–182.9
Body mass index (kg/m^2)	26.7 ± 8.0	17.1–51.7
Tibia length (cm)	38.1 ± 1.9	34.4–40.4
Cortical area (mm^2)	355.9 ± 55.2	268.3–511.1
AP width (mm)	31.2 ± 2.5	28.4–36.9
ML width (mm)	24.3 ± 2.3	19.9–30.6
AP moment of inertia (mm^4)	34,390 ± 10,149	19,466–60,698
ML moment of inertia (mm^4)	17,250 ± 5,945	8,246–34,734
Polar moment of inertia (mm^4)	51,640 ± 15,886	27,713–95,432
AP section modulus (mm^3)	3,279 ± 819	1,925–5,172
ML section modulus (mm^3)	4,188 ± 907	2,785–6,237
AP slenderness (1/mm^2/kg)	9.9 ± 2.0	6.5–13.4
ML slenderness (1/mm^2/kg)	7.7 ± 1.5	5.4–10.2
Modulus (GPa)	17.0 ± 1.7	13.4–19.0
Strength (MPa)	130.7 ± 6.1	120.8–144.5
Total energy (MPa)	3.3 ± 0.9	2.3–5.6
Postyield strain	0.026 ± 0.006	0.016–0.039
Damage parameter (D)	0.165 ± 0.038	0.103–0.253

AP, antero-posterior direction; ML, medial-lateral direction.

postyield strain (CV = 24.0%), total energy (CV = 26.4%), and the damage parameter (CV = 23.0%) all showed large variability among the samples. Morphological measures such as AP width, section modulus, and the polar moment of inertia, J (Fig. 4), increased linearly with body weight ($R^2 = 0.59$, $p < 0.003$) and body mass index (BMI; $R^2 = 0.57$, $p < 0.004$), but were independent of body height ($R^2 = 0.01$, $p < 0.7$). These relationships did not change when the body weight values were corrected for age (data not shown). Body height was uncorrelated with body weight ($R^2 = 0.01$, $p < 0.8$), indicating that the sample population consisted of individuals with similar heights but widely varying body weights.

Significant age-related changes were observed for the tissue-level mechanical properties and the size of the tibia. A significant, positive correlation was observed between tibia slenderness in the AP ($R^2 = 0.31$, $p < 0.02$) and ML ($R^2 = 0.24$, $p < 0.05$) directions and age. However, I_{AP}, I_{ML}, and J did not vary with age, suggesting that the variation in slenderness with age was due largely to higher body weight and BMI ($R^2 = 0.29$–0.32, $p < 0.03$) values for the older individuals. Although tissue modulus did not vary significantly with age, tissue strength ($R^2 = 0.53$, $p < 0.001$), postyield strain ($R^2 = 0.44$, $p < 0.004$), and total energy ($R^2 = 0.32$, $p < 0.002$) were significantly lower for the older individuals. Furthermore, a significant, negative correlation was observed between the damage parameter and age ($R^2 = 0.41$, $p < 0.006$). This data suggested that, whereas the tibia became more slender relative to body size with age, the cortical tissue became progressively less strong and less ductile (i.e., more brittle) with age.

The correlation analysis showed significant correlations between tibial morphology and the mechanical properties that characterized tissue brittleness and damageability (Table 2). The relationships among tissue-level mechanical

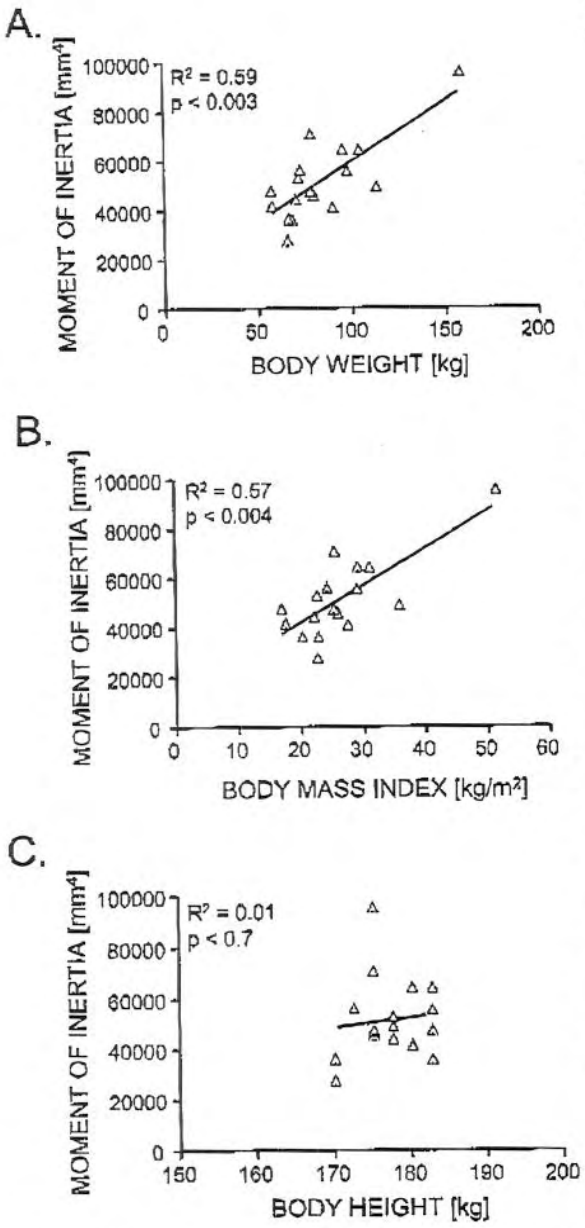

FIG. 4. The average cross-sectional polar moment of inertia of the tibia from males increased with (A) body weight and (B) body mass index but not with (C) body height. Removing the outlier changed the R^2 values to 0.24 ($p < 0.05$) for A and 0.20 ($p < 0.09$) for B.

properties and cross-sectional morphology were linear. Postyield strain and total energy increased significantly with AP width (Figs. 5A and 5B). Modulus decreased with I_{AP} ($p < 0.07$), J ($p < 0.08$), AP section modulus ($p < 0.05$), and ML section modulus (Figs. 5C–5F). Tissue damageability increased with tibia slenderness in the AP ($p < 0.05$; Fig. 6) and ML ($p < 0.09$) directions. These correlations, which were independent of age, indicated that a narrower bone was comprised of tissue that failed in a more brittle manner and accumulated more damage.

DISCUSSION

The results of this study revealed that the tissue-level mechanical properties of cortical bone varied with the size of the tibia. Positive correlations were observed between measures of bone size (AP width) and measures of tissue ductility (postyield strain, total energy), and negative correlations were observed between bone size (moment of inertia, section modulus) and tissue modulus. Many of these correlations were significant. The lack of significant correlation with all measures of bone size can be attributed largely to the complex shape of the tibia. The tibia has a triangular cross-section and, consequently, measures of width correlated significantly with mechanically relevant traits like cortical area and moment of inertia but explained only 50–80% of the variability in these measures (data not shown). These correlations would be greater if the cross-section had a circular shape. The variability in these correlations was sufficiently large that neither the linear (width) traits nor the integrated traits like area and moment of inertia correlated significantly with a particular tissue-level mechanical property simultaneously. Nevertheless, the data indicated that bones with smaller width were comprised of stiffer and less ductile (i.e., more brittle) material compared with larger, more robust bones. The correlation between tissue ductility and bone size may help explain why male military recruits[1,2,11] and male athletes[12] with narrow bones show a higher incidence of stress fractures compared with individuals with wide bones.

The development of the slenderness index[17] was for a "normal" range in height and weight and is probably not useful beyond this range. However, the morphological variation observed in our sample population was consistent with that reported for military recruits[1,2] and runners,[12] and height and weight were consistent with recent national averages.[2,3] As expected, bone size varied with body weight,[17] but did not vary with height (Fig. 4).[24] Thus, narrow bones came from less heavy individuals who were of similar height as those with wide tibias. Weight varied more than height for our sample population similar to that observed for the aged-matched national data. Furthermore, the variability in weight, specifically inclusion of one outlier (Fig. 4), did not affect the results (i.e., the heaviest person did not have an unusual slenderness value). Thus, the bones used in this study seem to be an appropriate size relative to body type.

The variation in long bone slenderness has been attributed to genetic and environmental factors influencing growth and development[2,5] and has been implicated as a risk factor for osteoporotic fracture.[26] To be relevant for military recruits, the sample population should have ranged in age between 18 and 25 years. However, for the age range in this study, the tissue-level mechanical properties varied linearly with age and were easily corrected using a linear regression method.[22] Consequently, the correlation analysis presented here provides relevant insight into the relationship observed between bone size and stress fracture risk

TABLE 2. PARTIAL CORRELATION COEFFICIENTS TAKING AGE INTO CONSIDERATION

	Modulus	*Strength*	*Total energy*	*PY strain*	*Damageability*
Cortical area	−0.24	0.03	0.37	0.40	−0.23
	(0.35)	(0.90)	(0.14)	(0.11)	(0.37)
AP width	−0.09	−0.03	**0.57**	**0.70**	−0.16
	(0.74)	(0.90)	**(0.02)**	**(0.002)**	(0.55)
ML width	−0.32	−0.22	0.34	0.41	−0.19
	(0.21)	(0.39)	(0.18)	(0.11)	(0.45)
AP moment of inertia	**−0.45**	−0.10	0.25	0.32	−0.27
	(0.07)	(0.70)	(0.34)	(0.21)	(0.29)
ML moment of inertia	−0.39	−0.18	0.22	0.28	−0.25
	(0.12)	(0.50)	(0.39)	(0.28)	(0.32)
Polar moment of inertia	**−0.43**	−0.13	0.24	0.31	−0.27
	(0.08)	(0.61)	(0.35)	(0.23)	(0.30)
AP section modulus	**−0.50**	−0.13	0.10	0.14	−0.30
	(0.04)	(0.62)	(0.70)	(0.60)	(0.25)
ML section modulus	**−0.47**	−0.05	0.18	0.23	−0.33
	(0.06)	(0.84)	(0.49)	(0.38)	(0.20)
Ap slenderness	0.36	0.10	0.09	0.03	**0.48**
	(0.15)	(0.69)	(0.72)	(0.92)	**(0.05)**
ML slenderness	0.23	−0.01	0.04	−0.05	0.41
	(0.39)	(0.96)	(0.89)	(0.84)	(0.10)

Pearson correlation coefficients are shown with p values in parentheses. Significant correlations are shown in bold. Abbreviations are as shown in Table 1.

for young adult males. Further studies are needed to determine if this relationship holds over a wider (older) age range.

The data provide a new paradigm that may explain how variation in bone slenderness contributes to stress fracture risk. Individuals with narrow tibias were previously thought to show increased fatigue damage during intense training because the smaller bone size would lead to an overload situation (i.e., higher tissue level stresses).[1,2,12] This interpretation was based on the assumption that tissue mechanical properties did not vary among individuals. However, the current results indicated that tissue-level mechanical properties do vary among individuals. Specifically, the data suggest that there are at least two important tissue-level mechanical property variations that need to be considered to understand why bone size is a risk factor for stress fractures. Narrower tibias were comprised of tissue that was more brittle (low total energy) and was prone to accumulate more damage compared with tissue from wider tibia. Having tissue that is more or less damageable may be inconsequential during day-to-day activities. However, tissue-level mechanical properties like total energy and ductility become particularly important in defining the response of bone to an extreme loading condition, such as that expected during military training or during a fall. Total energy defines the amount of energy required to break a bone (important during a fall) and ductility and damageability define the amount of damage accumulated under overload or repetitive loading (important during military training). Furthermore, tissue stresses would be expected to remain higher for narrow tibias loaded in bending or torsion. Moment of inertia is related to the external diameter raised to the fourth power. Because whole bone stiffness and strength are correlated with moment of inertia,[17,27] a bone with a large external diameter should also show large overall stiffness and strength values. However, the ~30% variation in tissue modulus (Table 1) did not fully compensate for the ~100% variation in the moment of inertia or the section modulus (Table 1).[27] Thus, in situ damage accumulation may elicit a biological response (remodeling) that, coupled with the higher tissue stresses, exacerbates the fatigue process.[13,28] Consequently, individuals with narrow tibia may be at higher risk of stress fractures because of higher in vivo tissue stresses (overloading) coupled with tissue that is more prone to accumulating damage.

The data may also help explain why age is another risk factor for stress fractures.[7,29] Bone strength, postyield strain, and total energy decreased over the 17- to 46-year-old age range. This was consistent with previous studies[30–32] and indicated that cortical bone becomes less ductile (i.e., more brittle) and weaker with age and that these changes began early in life. This age-related decline in strength and ductility is thought to be a result of increased mineralization and remodeling.[33,34] Thus, even in the young adult age range, the amount of damage accumulated under vigorous loading regimens would be expected to increase with age. This variation in tissue ductility may increase the susceptibility of stress fracture risk for recruits that enter into military training at an older age.

These results, and those of others, indicated that not all cortical tissue was constructed in the same manner. The mechanical properties of cortical tissue vary with age,[30–32,35] across species,[35] among bones of the same individual,[36] and among anatomical sites within the same bone.[37,38] Here we showed that the average mechanical properties of cortical tissue also varied as a function of the overall size of the bone. This coupling between bone morphology and tissue-level mechanical properties has been attributed to an adaptive response of bone.[14,35,39] In this study, smaller tibia bone size was coupled with an increase

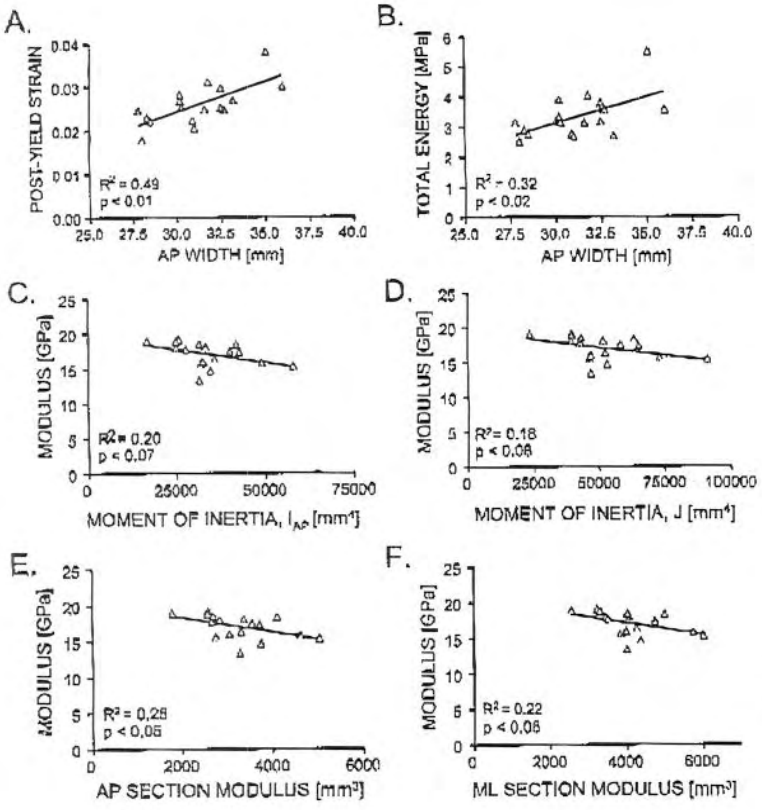

FIG. 5. (A) Postyield strain and (B) total energy correlated with AP width. Modulus decreased with (C) I_{AP}, (D) J, (E) AP section modulus, and (F) ML section modulus. Data were age-corrected based on a linear regression method.[22]

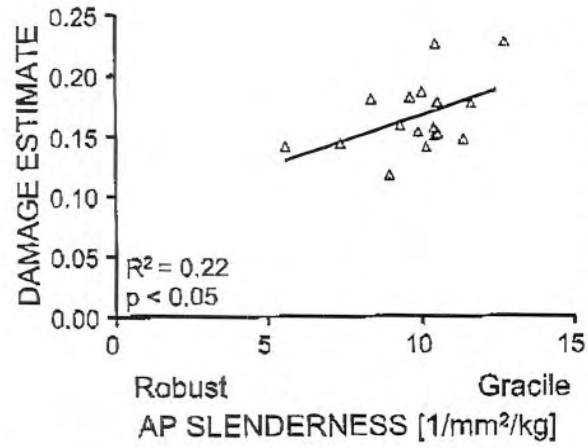

FIG. 6. Damageability correlated with AP slenderness suggesting that tibias that were more slender relative to body size and stature were comprised of tissue that accumulated more damage. Data were age-corrected based on a linear regression method.[22]

in tissue modulus. The goal of this adaptive response is to ensure that morphology and quality together meet mechanical demands. This coupling was observed when comparing bones subjected to widely varying mechanical demands from different species[35] and has also been used to explain the maturation of bone during growth.[40–43] Our current results suggested that this coupling might also exist for a particular bone (tibia) within the same species (human). Additional studies are needed to determine if similar relationships between morphology and quality exist for other long bones (femur, humerus, radius).

The relationship between morphology and tissue-level mechanical properties observed in the human skeleton was consistent with that observed for the mouse skeleton.[14] In both the mouse and human skeletons, genetic heterogeneity leads to variability in adult bone morphology and tissue level mechanical properties. A comparison of femurs from A/J and C57/BL6 (B6) inbred strains showed that A/J femurs were more slender than B6 as a result of the two strains having similar bone lengths, but A/J having a significantly smaller cross-sectional size and shape.[14] Despite the difference in bone size, the two strains showed similar whole bone stiffness values. The variability in bone slenderness was inversely related to mineral content, suggesting that bone morphology and mineral content were coordinately regulated so whole bone stiffness appropriately matched the mechanical demands imposed by weight bearing. However, as a result of regulating mineral content to match bone size, A/J femurs failed in a brittle manner and showed poor fatigue properties. In the human skeleton, smaller bones were stiffer and less ductile. Thus, a reciprocal relationship was observed between bone stiffness and ductility for both skeleton systems. This reciprocal relationship has been extensively reported for cortical bone,[15] and

it is thought to be a result of the nature of the compositional and structural factors that can be modulated on a biological level.[44–47] Although variation in mineral content may have explained the differences in brittleness for the mouse skeleton, we expect that the human skeleton will be more complex and that the variation in tissue-level mechanical properties will be a consequence of variable composition (mineral, collagen, water) as well as microarchitecture (lamellae, osteon size, porosity).

The calculated bending modulus and strength values, which were determined from machined bone samples and were thus quantified in a manner that was independent of bone size, were consistent with bone tensile properties,[30] as expected. Test samples were randomly selected to obtain representative mean values for each tibia and the variation in mechanical properties within each tibia was similar to the variability observed across tibias. Thus, we believe that the mean values reported here represent the generalized tissue-level mechanical behavior for each tibia.

Compared with back-calculating tissue-level mechanical properties from whole bone failure tests, the current method of measuring tissue-level mechanical properties directly from machined samples provided a broader range of mechanical properties that were needed to better understand why bone size is a risk factor for stress fractures. The mechanical properties included measures of ductility (i.e., postyield strain, total energy) as well as an independent measure of damageability (i.e., the damage parameter). These properties were chosen because they were relevant for understanding the material response of bones subjected to the vigorous, repetitive loading associated with military training and running. Postyield strain and total energy represent measures of tissue ductility and were assessed to discriminate between ductile and brittle failure modes. Materials that fail in a brittle manner show low postyield strain and total energy values. Variation in the ductility of cortical bone arises from differences in the initiation, accumulation, propagation, and coalescence of damage in the form of microcracks.[48,49] Variation in the damage parameter reflected differences in the amount of damage accumulated within the tissue and/or differences in the way damage degraded tissue stiffness. The damage parameter correlated negatively with postyield strain and total energy (R^2 = 0.22–0.25, $p < 0.05$) indicating that cortical tissue that failed in a brittle manner also tended to have higher tissue damageability or, accumulate more damage. Although the ex vivo bending tests do not necessarily reflect the in vivo loads imposed on the tibia,[17,50–52] the bending loads were expected to induce a combination of tensile, compressive, and shear damage[53] that may be sufficiently complex to represent a generalized variation in bone quality among human tibias.

The results of this study provide new insight into why bone size is a risk factor for stress fractures. Stress fractures are believed to be a consequence of excess damage accumulation following intense, repetitive activities. Biological processes that attempt to repair the damage may further weaken the tissue because the increased resorption results in increased tissue porosity.[54] However, the actual contribution of biological repair processes to stress fracture risk remains unclear.[55] Damage, in the form of microcracks, is the expected sequelae of repetitive loading following normal, daily activities.[56] Intense loading conditions, such as those associated with military training and long distance running, are expected to further increase in situ damage accumulation and degrade tissue-level mechanical properties.[13] Therefore, under extreme loading conditions (e.g., military training), variation in bone quality, specifically tissue damageability, may be a contributing factor to the increased risk of stress fracture for individuals with more slender bones. The current data suggested that bone morphology could be used as a predictor of tissue fragility and stress fracture risk in the absence of available noninvasive imaging techniques that accurately measure bone damageability.

ACKNOWLEDGMENTS

The authors thank the U.S. Department of Defense (DAMD17-01-1-0806; DAMD17-98-1-8515) and the Musculoskeletal Transplant Foundation for their support of this research.

REFERENCES

1. Milgrom C, Giladi M, Simkin A, Rand N, Kedem R, Kashtan H, Stein M, Gomori M 1989 The area moment of inertia of the tibia: A risk factor for stress fractures. J Biomech 22:1243–1248.
2. Beck TJ, Ruff CB, Mourtada FA, Shaffer RA, Maxwell-Williams K, Kao GL, Sartoris DJ, Brodine S 1996 Dual-energy X-ray absorptiometry derived structural geometry for stress fracture prediction in male U.S. Marine Corps recruits. J Bone Miner Res 11:645–653.
3. Milgrom C, Giladi M, Stein M, Kashtan H, Margulies JY, Chisin R, Steinberg R, Aharonson Z 1985 Stress fractures in military recruits. A prospective study showing an unusually high incidence. J Bone Joint Surg Br 67:732–735.
4. Lappe JM, Stegman MR, Recker RR 2001 The impact of lifestyle factors on stress fractures in female Army recruits. Osteoporos Int 12:35–42.
5. Milgrom C, Finestone A, Sharkey N, Hamel A, Mandes V, Burr D, Arndt A, Ekenman I 2002 Metatarsal strains are sufficient to cause fatigue fracture during cyclic overloading. Foot Ankle Int 23:230–235.
6. Friedl KE, Nuovo JA, Patience TH, Dettori JR 1992 Factors associated with stress fracture in young army women: Indications for further research. Mil Med 157:334–338.
7. Brudvig TJ, Gudger TD, Obermeyer L 1983 Stress fractures in 295 trainees: A one-year study of incidence as related to age, sex, and race. Mil Med 148:666–667.
8. Bennell K, Matheson G, Meeuwisse W, Brukner P 1999 Risk factors for stress fractures. Sports Med 28:91–122.
9. Jones BH, Thacker SB, Gilchrist J, Kimsey CD Jr, Sosin DM 2002 Prevention of lower extremity stress fractures in athletes and soldiers: A systematic review. Epidemiol Rev 24:228–247.
10. Giladi M, Milgrom C, Simkin A, Danon Y 1991 Stress fractures. Identifiable risk factors. Am J Sports Med 19:647–652.
11. Giladi M, Milgrom C, Simkin A, Stein M, Kashtan H, Margulies J, Rand N, Chisin R, Steinberg R, Aharonson Z 1987 Stress fractures and tibial bone width. A risk factor. J Bone Joint Surg Br 69:326–329.
12. Crossley K, Bennell KL, Wrigley T, Oakes BW 1999 Ground reaction forces, bone characteristics, and tibial stress fracture in male runners. Med Sci Sports Exerc 31:1088–1093.
13. Mori S, Burr DB 1993 Increased intracortical remodeling following fatigue damage. Bone 14:103–109.

14. Jepsen KJ, Pennington DE, Lee YL, Warman M, Nadeau J 2001 Bone brittleness varies with genetic background in A/J and C57BL/6J inbred mice. J Bone Miner Res 16:1854–1862.
15. Currey JD 1984 Effects of differences in mineralization on the mechanical properties of bone. Philos Trans R Soc Lond B Biol Sci 304:509–518.
16. Ruff CB 2000 Body size, body shape, and long bone strength in modern humans. J Hum Evol 38:269–290.
17. Selker F, Carter DR 1989 Scaling of long bone fracture strength with animal mass. J Biomech 22:1175–1183.
18. Gustafson MB, Martin RB, Gibson V, Storms DH, Stover SM, Gibeling J, Griffin L 1996 Calcium buffering is required to maintain bone stiffness in saline solution. J Biomech 29:1191–1194.
19. Nádai A 1950 Theory of Flow and Fracture of Solids. Engineering Societies Monographs. McGraw-Hill, New York, New York, USA.
20. Lemaitre J 1992 A Course on Damage Mechanics. Springer-Verlag, Berlin, New York.
21. Jepsen KJ, Davy DT 1997 Comparison of damage accumulation measures in human cortical bone. J Biomech 30:891–894.
22. Di Masso RJ, Font MT, Capozza RF, Detarsio G, Sosa F, Ferretti JL 1997 Long-bone biomechanics in mice selected for body conformation. Bone 20:539–545.
23. Ogden CL, Fryar CD, Carroll MD, Flegal KM 2004 Mean body weight, height, and body mass index, United States 1960-2002. Adv Data 347:1–17.
24. Miller GJ, Purkey WW Jr 1980 The geometric properties of paired human tibiae. J Biomech 13:1–8.
25. Christian JC, Yu PL, Slemenda CW, Johnston CC Jr 1989 Heritability of bone mass: A longitudinal study in aging male twins. Am J Hum Genet 44:429–433.
26. Kiel DP, Hannan MT, Broe KE, Felson DT, Cupples LA 2001 Can metacarpal cortical area predict the occurrence of hip fracture in women and men over 3 decades of follow-up? Results from the Framingham Osteoporosis Study. J Bone Miner Res 16:2260–2266.
27. van der Meulen MC, Jepsen KJ, Mikic B 2001 Understanding bone strength: Size isn't everything. Bone 29:101–104.
28. Burr DB, Forwood MR, Fyhrie DP, Martin RB, Schaffler MB, Turner CH 1997 Bone microdamage and skeletal fragility in osteoporotic and stress fractures. J Bone Miner Res 12:6–15.
29. Shaffer RA, Brodine SK, Almeida SA, Williams KM, Ronaghy S 1999 Use of simple measures of physical activity to predict stress fractures in young men undergoing a rigorous physical training program. Am J Epidemiol 149:236–242.
30. Burstein AH, Reilly DT, Martens M 1976 Aging of bone tissue: Mechanical properties. J Bone Joint Surg Am 58:82–86.
31. McCalden RW, McGeough JA, Barker MB, Court-Brown CM 1993 Age-related changes in the tensile properties of cortical bone. The relative importance of changes in porosity, mineralization, and microstructure. J Bone Joint Surg Am 75:1193–1205.
32. Currey JD, Butler G 1975 The mechanical properties of bone tissue in children. J Bone Joint Surg Am 57:810–814.
33. Evans FG 1976 Age changes in mechanical properties and histology of human compact bone. Yearb Phys Anthropol 20:1361–1372.
34. Currey JD, Brear K, Zioupos P 1996 The effects of ageing and changes in mineral content in degrading the toughness of human femora. J Biomech 29:257–260.
35. Currey JD 1979 Mechanical properties of bone tissues with greatly differing functions. J Biomech 12:313–319.
36. Papadimitriou HM, Swartz SM, Kunz TH 1996 Ontogenetic and anatomic variation in mineralization of the wing skeleton of the Mexican free-tailed bat, *Tadarida brasiliensis*. J Zool 240:411–426.
37. Riggs CM, Vaughan LC, Evans GP, Lanyon LE, Boyde A 1993 Mechanical implications of collagen fibre orientation in cortical bone of the equine radius. Anat Embryol (Berl) 187:239–248.
38. Skedros JG, Dayton MR, Sybrowsky CL, Bloebaum RD, Bachus KN 2003 Are uniform regional safety factors an objective of adaptive modeling/remodeling in cortical bone? J Exp Biol 206:2431–2439.
39. Ferretti JL, Capozza RF, Mondelo N, Zanchetta JR 1993 Interrelationships between densitometric, geometric, and mechanical properties of rat femora: Inferences concerning mechanical regulation of bone modeling. J Bone Miner Res 8:1389–1396.
40. Ferretti JL, Cointry GR, Capozza RF, Frost HM 2003 Bone mass, bone strength, muscle-bone interactions, osteopenias and osteoporoses. Mech Ageing Dev 124:269–279.
41. Heinrich RE 1999 Ontogenetic changes in mineralization and bone geometry in the femur of muskoxen (Ovibos moschatus). J Zool 247:215–223.
42. Brear K, Currey JD, Pond CM 1990 Ontogenetic changes in the mechanical properties of the femur of the polar bear Ursus maritimus. J Zool 222:49–58.
43. Carrier D, Leon LR 1990 Skeletal growth and function in the California gull (*Larus californicus*). J Zool 222:375–389.
44. Martin RB, Boardman DL 1993 The effects of collagen fiber orientation, porosity, density, and mineralization on bovine cortical bone bending properties. J Biomech 26:1047–1054.
45. Portigliatti Barbos M, Bianco P, Ascenzi A, Boyde A 1984 Collagen orientation in compact bone: II. Distribution of lamellae in the whole of the human femoral shaft with reference to its mechanical properties. Metab Bone Dis Relat Res 5:309–315.
46. Skedros JG, Sybrowsky CL, Parry TR, Bloebaum RD 2003 Regional differences in cortical bone organization and microdamage prevalence in Rocky Mountain mule deer. Anat Rec 274A:837–850.
47. Skedros JG, Hunt KJ 2004 Does the degree of laminarity correlate with site-specific differences in collagen fibre orientation in primary bone? An evaluation in the turkey ulna diaphysis. J Anat 205:121–134.
48. Jepsen KJ, Davy DT, Akkus O 2001 Observations of damage in bone. In: Cowin SC (ed.) Bone Mechanics Handbook, 2nd ed. CRC Press, Boca Raton, FL, USA, pp. 17.1–17.18.
49. Currey JD, Brear K 1992 Fractal analysis of compact bone and antler fracture surfaces. Biomimetics 1:103–118.
50. Ruff CB 1984 Allometry between length and cross-sectional dimensions of the femur and tibia in Homo sapiens sapiens. Am J Phys Anthropol 65:347–358.
51. Lanyon LE, Hampson WG, Goodship AE, Shah JS 1975 Bone deformation recorded in vivo from strain gauges attached to the human tibial shaft. Acta Orthop Scand 46:256–268.
52. Burr DB, Milgrom C, Fyhrie D, Forwood M, Nyska M, Finestone A, Hoshaw S, Saiag E, Simkin A 1996 In vivo measurement of human tibial strains during vigorous activity. Bone 18:405–410.
53. Boyce TM, Fyhrie DP, Glotkowski MC, Radin EL, Schaffler MB 1998 Damage type and strain mode associations in human compact bone bending fatigue. J Orthop Res 16:322–329.
54. Schaffler MB, Burr DB 1988 Stiffness of compact bone: Effects of porosity and density. J Biomech 21:13–16.
55. Milgrom C, Finestone A, Novack V, Pereg D, Goldich Y, Kreiss Y, Zimlichman E, Kaufman S, Liebergall M, Burr D 2004 The effect of prophylactic treatment with risedronate on stress fracture incidence among infantry recruits. Bone 35:418–424.
56. Schaffler MB, Radin EL, Burr DB 1990 Long-term fatigue behavior of compact bone at low strain magnitude and rate. Bone 11:321–326.

Address reprint requests to:
Karl J Jepsen, PhD
Department of Orthopaedics
Mount Sinai School of Medicine
Box 1188, One Gustave L. Levy Place
New York, NY 10029, USA
E-mail: karl.jepsen@mssm.edu

Received in original form November 12, 2004; revised form March 16, 2005; accepted March 28, 2005.

ELSEVIER

Journal of Orthopaedic Research 21 (2003) 1018–1024

Journal of Orthopaedic Research

www.elsevier.com/locate/orthres

Noninvasive fatigue fracture model of the rat ulna

A.E. Tami [a,b], P. Nasser [c], M.B. Schaffler [c], M.L. Knothe Tate [a,*]

[a] *The Departments of Biomedical Engineering and Orthopaedic Surgery, Orthopaedic Research Center, ND 20 Lerner Research Institute, The Cleveland Clinic Foundation, 9500 Euclid Avenue, Cleveland, OH 44195, USA*

[b] *Institute of Biomedical Engineering, University and Swiss Federal Institute of Technology, 8092 Zurich, Switzerland*

[c] *Leni and Peter May Department of Orthopaedics, The Mount Sinai School of Medicine, New York, NY 10029, USA*

Abstract

Fatigue damage occurs in response to repeated cyclic loading and has been observed in situ in cortical bone of humans and other animals. When microcracks accumulate and coalesce, failure ensues and is referred to as fatigue fracture. Experimental study of fatigue fracture healing is inherently difficult due to the lack of noninvasive models. In this study, we hypothesized that repeated cyclic loading of the rat ulna results in a fatigue fracture. The aim of the study was to develop a noninvasive long bone fatigue fracture model that induces failure through accumulation and coalescence of microdamage and replicates the morphology of a clinical fracture. Using modified end-load bending, right ulnae of adult Sprague–Dawley rats were cyclically loaded in vivo to fatigue failure based on increased bone compliance, which reflects changes in bone stiffness due to microdamage. Preterminal tracer studies with 0.8% Procion Red solution were conducted according to protocols described previously to evaluate perfusion of the vasculature as well as the lacunocanalicular system at different time points during healing. Eighteen of the 20 animals loaded sustained a fatigue fracture of the medial ulna, i.e. through the compressive cortex. In all cases, the fracture was closed and non-displaced. No disruption to the periosteum or intramedullary vasculature was observed. The loading regime did not produce soft tissue trauma; in addition, no haematoma was observed in association with application of load. Healing proceeded via proliferative woven bone formation, followed by consolidation within 42 days postfracture. In sum, a noninvasive long bone fatigue fracture model was developed that lends itself for the study of internal remodeling of periosteal woven bone during fracture healing and has obvious applications for the study of fatigue fracture etiology.

Keywords: Noninvasive fracture model; Fatigue loading; Fracture healing; Remodeling; End-load bending; Bone

Introduction

Fatigue fracture is a common injury spontaneously occurring in bones subjected to cyclic stress. It has been observed frequently in situ in rib and long bone cortices of humans [10,20,32,38] in the tarsal bones of racing dogs [33], and in the third metacarpal bone of racehorses [34]. The etiology of fatigue fracture has been attributed to classic material fatigue [1] as well as weakening of bone due to remodeling of areas subjected to ischemia and reperfusion injury [35]. Fracture or failure in fatigue is the culmination of microdamage accrual within the tissue. It has been suggested [7] and recent experimental data show that not only overt fracture but also microdamage to bone [4,7,9,22,27,28,39,45] triggers osteoclastic resorption, initiating the remodeling cycle. However, no published studies have addressed intrinsic differences between the fracture repair response and the remodeling response to repair microdamage in bone.

From a materials perspective, bone is analogous to a composite, showing a gradual and progressive loss of stiffness under fatigue (Fig. 1) [9,14,23,39]. Repetitive loading of bone tissue results in microdamage and correlates with a degradation of mechanical properties. These changes in material properties during the course of fatigue life are described by three progressive phases of fatigue, the first of which is characterized by rapid degradation in modulus. In the second stage of fatigue, the rate of change in stiffness quickly stabilizes to a constant level. The third phase is defined by catastrophic failure, i.e. end of fatigue life. Fatigue behavior depends on loading parameters including strain rate, strain magnitude and cycle number. In addition, tensile and compressive stresses generate different fracture patterns

* Corresponding author.
E-mail address: tatem@bme.ri.ccf.org (M.L. Knothe Tate).

0736-0266/$ - see front matter © 2003 Orthopaedic Research Society. Published by Elsevier Ltd. All rights reserved.
doi:10.1016/S0736-0266(03)00099-8

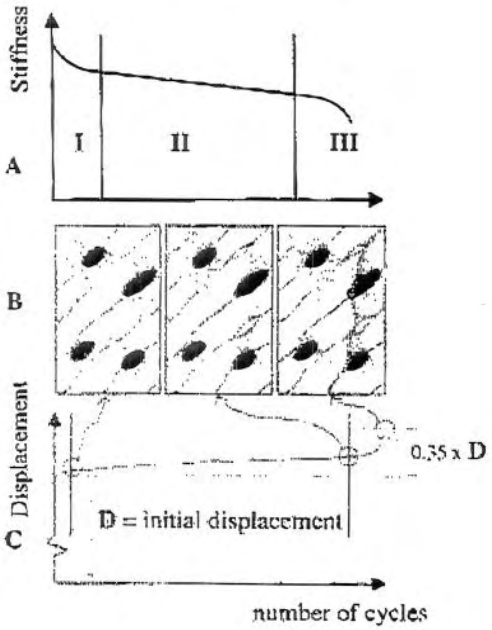

Fig. 1. Schematic diagram depicting the stages of fatigue (A), in terms of damage to bone (B, schematic) and changes in compliance (C) [39,43,44,47]. (A) The first phase is characterized by rapid modulus degradation. Thereafter, the rate of changes in stiffness stabilizes rapidly and remains constant during the second phase. At the onset of the third phase, the specimen catastrophically fails. (B) Development of damage during fatigue loading. Diffuse damage associated with intralamellar structural discontinuities within the matrix combined with microcracks formed by interlamellar debonding may coalesce, forming macrocracks and culminating in catastrophic failure. (C) The testing machine measures the displacement during the entire loading history and stops the loading when the reference displacement has increased by 35%.

under fatigue loading [14]. Strain rate affects viscoelastic behavior of bone [23,24]. Finally, in the course of fatigue loading, the range of strain to which the specimen is subjected is inversely proportional to the cycle number until failure [11–13].

Despite the wealth of literature on fatigue damage and fatigue behavior of bone, the etiology of fatigue failure in vivo is not yet understood. Theoretical models aid in understanding the interactions between loading, damage, internal remodeling and the occurrence of fatigue fractures [3,28,30]. A number of fracture models exist to replicate traumatic fracture and healing response to surgical intervention; all involve some degree of invasiveness to system physiology, e.g., wound healing after osteotomy and soft tissue trauma following impact fracture, thus, producing undesired artifacts [2,5,17,19, 21,29,36,37,40]. To date, the only published in vivo study addressing fatigue fracture is a rabbit impact model developed by Burr et al. [8] in which a qualitative assessment of the fracture was described. To our knowledge, no previous studies have addressed the failure of bone in vivo under cyclic loads. We hypothesize that through repeated cyclic application of loads that have been used in previous experiments to induce fatigue microdamage [4,45], it is possible to produce a fatigue fracture in vivo. Hence, the goal of this study was to develop an in vivo, noninvasive long bone fatigue fracture model that (i) induces fracture through continuous accumulation and coalescence of microdamage during a single bout of cyclic loading, (ii) replicates the morphology of a clinical fatigue fracture, and (iii) allows for histological monitoring of the healing response.

Methods

Animal model

Right ulnae of 30 adult (6–9 months) female Sprague–Dawley rats (retired breeders, 265 ± 55 g) were subjected to loading in vivo through modified end-load bending (loading described in more detail below). All procedures were carried out with the approval from IACUC. Rats were anaesthetized using isoflurane inhalation (1–3%) during the period of loading, for a maximum duration of 3 h. During loading body temperature was maintained at 36–37 °C using a heating pad. Before and after loading the rats were allowed unrestricted cage activity and unlimited access to food and water.

Loading regime

The rat ulna was loaded in axial compression using a hydraulically powered Instron Test Machine (Dynamite Instron, Canton, MA), by applying load to the olecranon and the flexed carpus. This device allowed for precise load control to measure the induced displacement on the limb and to automatically stop the test when change in deformation during fatigue reaches a targeted value. Thus, under load control, right ulnae were cyclically loaded to fatigue failure based on increase of bone deformation, which reflects the degree of damage accumulated in the structure (Fig. 1). Before the experimental series, strain gauge measurements were carried out to assess the strain occurring on the ulnar surface. A single strain gauge was mounted on the middiaphyseal surface of the medial ulna in previously euthanized rats. The middiaphyseal surface is the site of maximal deformation occurring due to the natural curvature of the bone. This has been confirmed through strain gauge measurements [42] and finite element modeling [41]. The limb was preconditioned the same way as in the fatigue experiments (refer to next paragraph) and then loaded with a monotonic triangular load with a peak force of 27 N. Strains of 3500–4000 μstrain resulted from application of 17–18 N consistent with results of a previous study [42].

The fatigue loading sequence involved two steps including preconditioning (static and dynamic) and fatigue fracture loading. Preconditioning served as a means to reduce effects of soft tissue compliance, so that the measurable changes in actuator displacement mainly reflect the progressive degradation of structural bone properties due to damage. Moreover, preconditioning helps in estimating the maximal force to be applied during the subsequent fatigue fracture loading. During static preconditioning the ulna was loaded for 5 min with a compressive force of 6 N. Immediately thereafter, dynamic preconditioning was performed with a sinusoidal waveform, cycling between 2 and 10 N, with a mean compressive load of 6 N and an amplitude of 4 N for 1 min, i.e., 240 cycles. Then, after preconditioning, ulnae were subjected initially to a mean cyclic load of 8 N magnitude and an amplitude of 6 N (Fig. 2). This load corresponds to two standard deviations below the force required to impart a compressive deformation of 4000 μstrain on the medial side, as measured using strain gauges. If necessary, the load was increased gradually in 1 N steps to achieve an initial displacement amplitude (based on the system displacement control) between 0.250 and 0.350 mm, according to previously described protocols [4,45] and strain gauge measurements. Peak load never exceeded 20 N. The value of the initial displacement was always measured at the hundredth cycle of the fatigue loading sequence, i.e. during the first phase of fatigue (Fig. 1). That

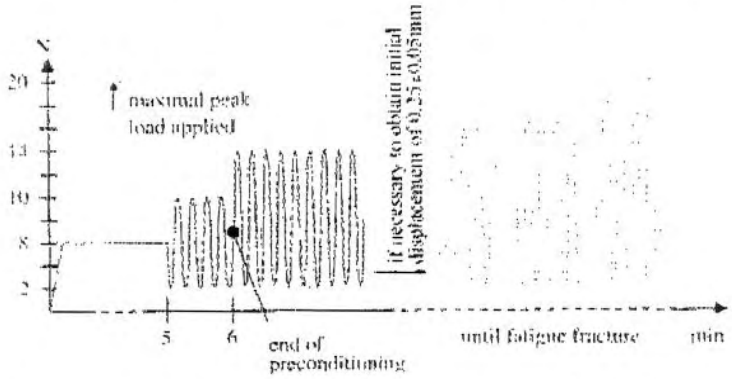

Fig. 2. Experimental loading. The load was increased gradually in 1 N steps up to a peak load of 20 N (i.e., mean load 11 N with 9 N amplitude) to achieve an initial displacement amplitude, based on the system displacement control, of approximately 0.30 ± 0.05 mm during the first 100 cycles.

value was then used as a reference to monitor the change in deformation during fatigue loading and to calculate the end displacement targeted to induce fatigue fracture. After having adjusted the load to achieve the targeted deformation during phase I (Fig. 1), the displacement amplitude rapidly entered into phase II of fatigue behavior. This region was characterized by a much smaller rate of change in compliance, i.e., a stabilization of displacement to a threshold level. The experiment was continued until the rate of change in displacement increased rapidly, indicating the end of fatigue life (phase III); loading was stopped at 35% increase in ulnar compliance compared to the reference cycle measured at the beginning of the fatigue loading sequence.

Intravital marker perfusion

The rats were divided into six groups of five animals each (Table 1). Preterminal tracer studies were conducted according to protocols described previously [26] to evaluate perfusion of the vasculature as well as the lacunocanalicular system at different time points in the healing and remodeling cycle. Each rat was injected via a lateral tail vein with 0.8% Procion Red solution in 0.9% saline. Animals were anaesthetized at the time of injection. Five minutes after injection, animals were euthanized without recovery from anesthesia. Five rats (group 2, Table 1) were injected immediately after loading. Three other groups of five rats each (group 3, 4 and 5) were loaded and then injected at respectively 7, 14 and 42 days thereafter. Two more groups (1 and 6) served as controls that were not loaded but were injected with the tracer immediately and 42 days after 30 min of anaesthesia.

Histological observations

Both the loaded (right) and non-loaded (left) limbs were harvested and manually dissected free of soft tissue, fixed in ethanol (40%), dehydrated in ethylene glycol (100%), cleared with petroleum ether, and finally infiltrated in PMMA. Cross-sections of the embedded, undecalcified bones were cut serially every 500 μm using a diamond saw microtome (SP 1600, Leica, Nussloch, Germany), polished to 80–100 μm, and mounted for microscopic analysis. Specimens were observed qualitatively using bright field microscopy.

For tracer studies, the specimens were observed with a confocal microscope (TCS SP2, Leica, Heidelberg, Germany) with excitation/emission spectra set to 568/580–624 nm. For detailed morphological studies of tracer perfusion during fracture healing, observations were made using 40× (nA 1.25, plan Apochromat) and 63× (nA 1.32, plan Apochromat) magnification oil-immersion objectives. The location of the fracture was noted, damage was characterized in terms of linear microcracks versus diffuse damage, resorption spaces and woven bone response were documented. Perfusion of the tracer was noted through the vascular and periosteocytic fluid spaces in bone. Moreover, the healing process was assessed with respect to time. For each fluorescent image taken, transmission images in DIC mode were taken to document bone morphology. For the specimen injected 7 and 14 days after loading (group 3 resp. group 4) the contour of woven bone as well as the fracture line were traced on the digitized sequential cross-sections in which the crack was visible. The surface area of woven bone and the length of the crack on each cross-section were measured using OpenLab® (Improvision Inc., Lexington, MA).

Results

Fatigue fractures were confirmed in eighteen of the 20 loaded ulnae. The fracture, in the medial ulnar cortex, occurred within 12,000 loading cycles (Fig. 3, left). In all cases the fracture was closed and non-displaced. No disruption to the periosteum or intramedullary vasculature was observed. Neither soft tissue trauma nor the presence of a haematoma was evident; in fact,

Table 1
Preterminal tracer study

Groups	Rat with fracture	Protocol
1	–	No loading, t_i = immediately after anesthesia (baseline control 1)
2	5 (100%)	$t_i = t_{fx}$
3	4 (80%)	t_i = 7 days post t_{fx} (onset of intracortical resorption)
4	4 (80%)	t_i = 14 days post t_{fx} (completion of resorption phase)
5	5 (100%)	t_i = 42 days post t_{fx} (completion of remodeling cycle)
6	–	No loading: t_i = 42 days postanesthesia (baseline control 2)

t_i = time point of injection.
t_{fx} = time point of fracture (end of fatigue loading).

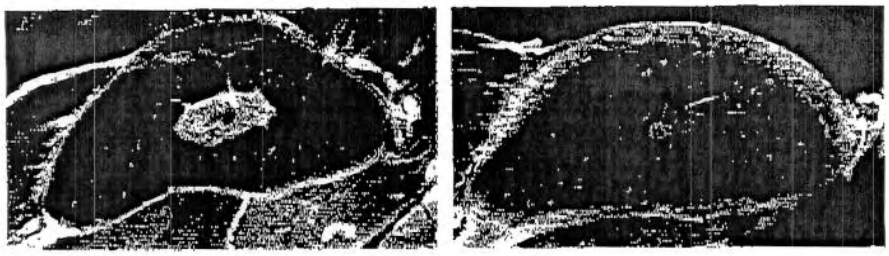

Fig. 3. (Left) Confocal micrograph showing fatigue fracture of medial ulna, representative of those incurred in 90% of cases studied. (Right) 42 days postfracture. In both images, fluorescence indicates presence of Procion Red tracer, an intravital marker.

fluorescent tracer studies showed no signs of intravascular leakage except by intracortical vessels which were disrupted directly by the fracture line. The fracture was always located in the distal third of the medial ulnar diaphysis. The fracture line extended between the midcortex and the periosteum, from the mediodorsal to the medioventral surface (Fig. 4). After digitizing sequential cross-sections of a specimen showing a fracture line, it was possible to trace the contours of periosteum, endosteum and of the fracture. By creating a surface mesh between the collected contours, we reconstructed a three-dimensional model of the fractured volume. The 3D reconstruction revealed an oblique fracture surface, spanning between the endosteum and periosteum and corresponding to a plane of high shear stress arising from compressive loading (45° from the longitudinal axis). The axial crack distance comprised 2.5–3.5 mm.

Fracture healing proceeded by direct bone formation via woven bone proliferation at the periosteal surface, mainly on the medio-lateral side of the injured area. Endochondral ossification was not observed in fractured specimens imaged using laser scanning confocal microscopy with protocols designed to excite collagen autofluorescence and Procion Red excitation [25]. Immediately after loading, a fracture line was observed to extend from the mediodorsal to the medioventral surface (Fig. 3, left), with local microdamage coalescing around the fracture line and contained completely within the medial cortex. Seven days after loading, intense periosteal proliferation of woven bone was observed on the medial surface (Figs. 3 and 4). Woven bone extended between the mediodorsal and medioventral extremities of the fracture. The longer the crack in the cross-section, the larger the increase in surface area due to woven bone reaction (Fig. 5). Microscopic observation revealed initiation of resorption along the fracture site. Fourteen days after loading, resorption cavities could be observed macroscopically at subperiosteal and subendocortical sites abutting the fracture line. Woven bone along the periosteum had consolidated considerably in comparison to the previous time point. Forty two days after loading, the fracture line was only faintly visible in one case. Otherwise, the fracture had remodeled completely. Areas of woven bone were well consolidated.

Discussion

Based on the results of this study, repeated cyclic loading of the ulna in compression through the third phase of fatigue culminated in a repeatable and nondisplaced fracture through the distal aspect of the diaphyseal cortex. Lack of extravasation of the dye from periosteum and vasculature suggested that fatigue fracture did not disrupt those structures. Based on the fa-

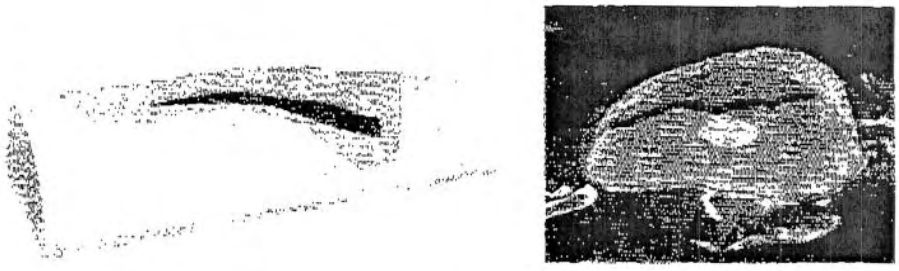

Fig. 4. Three-dimensional reconstruction of the ulnar section containing the fracture. The cross-sections containing a fracture line were digitized. Thereafter, the contours of periosteum (gray) and woven bone (green) as well as the fracture line (brown) were traced on each digitized cross-section. Finally, a three dimensional reconstruction with surface mesh was generated which connected the contours of sequential cross-sections. Complete woven bone reaction surrounding the fracture (left); single section showing periosteum, fracture line, and woven bone surface (right).

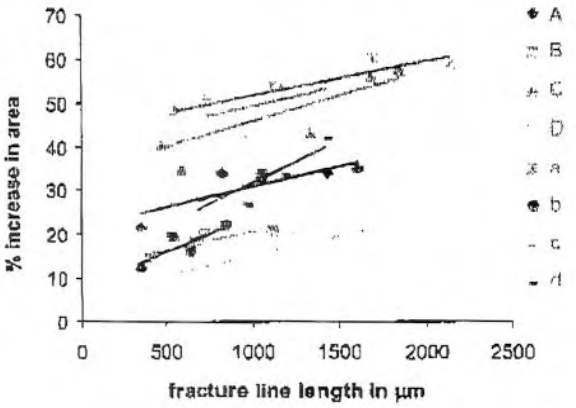

	slope	r^2
A	0.0093	0.685
B	0.0084	0.742
C	0.0115	0.620
D	0.0086	0.838
a	0.0076	0.822
b	0.0165	0.682
c	0.0086	0.217
d	0.0195	0.755
average	0.0130	0.670

Fig. 5. Relationship between crack length and increase in bone surface area in the groups observed 7 (a–d) and 14 (A–D) days after loading. The periosteal woven bone formation increases proportional to crack length.

tigue fracture model of the rat ulna developed within the context of this study, controlled, in vivo cyclic fatigue loading can be utilized to apply microdamage to the rat ulna to the point of fatigue failure, confirming our hypothesis. The resulting fracture traverses the compressive cortex, which heals by means of woven bone formation following the path of intramembranous ossification.

The model is highly reproducible and internally consistent; 18 of 20 loaded rat ulnae sustained a non-displaced, closed fracture of the medial cortex, corresponding to a 90% success rate. Damage to soft tissues and to the blood supply was minimal. Half an hour after recovering from anesthesia, the rats ambulated on all four limbs. Neither extraperiosteal/intramedullary bleeding, nor formation of haematoma was evident immediately after loading or during the healing phase thereafter. The loading history, i.e. the change in displacement, respectively, stiffness as a function of increasing cycle number, exhibited the three phases of fatigue behavior typical for composite structures such as bone [31]. The initial modulus degradation was followed by a longer period during which the stiffness changed very slowly; this is typical composite behavior that limits the degradation of material properties while allowing for creep effects, finally resulting in a continuously increasing displacement. Finally, in the third phase of the fatigue process, damage accumulation and coalescence lead to a rapid decline in stiffness until the structure ultimately fails. The loading history taken during the course of this experiment showed all the three phases of fatigue, with fracture occurring very rapidly in phase three. Hence, the observed fractures most likely derived from a combination of microdamage development, coalescence and accumulation through the fatigue life of the tissue. Fracture did not result from a single overload of the structure, but from a repeated, non-critical (i.e. peak stress below ultimate strength) load. Although this model replicates a classical material fatigue fracture well, it does not replicate a physiological bone fatigue fracture perfectly, because failure is induced in a single loading bout. This makes the model an acute fatigue fracture model, and physiological fatigue fractures may occur either acutely or over time. Hence, the model may be analogous, albeit in an extreme form, to the fatigue fracture incurred by distance runners and military recruits, whereby there is a mismatch between the rate of damage production and coalescence and the rate of bone repair processes.

Based on histological observation, the fractures healed through proliferation of woven bone. Within 7 days, massive woven bone was observed histologically in the medial aspect and surrounding the fracture. This immediate tissue response has been suggested [16] to stabilize and strengthen the structure rapidly by bridging the damaged area and increasing the cross-sectional area, thereby increasing the second moment of inertia. Experimental observation in the following weeks showed a gradual consolidation of the new tissue and repair of the fracture gap through remodeling.

The in vivo fatigue fracture model described here represents a heretofore unexplored approach to mimicking natural bone failure through cyclic loading. Previously published fracture models used techniques to induce failure in a single load; those include application of three-point-bending [19,29,36], torsional [40] and impact loads (by means of a blunt guillotine) [5,17,21]. Surgical osteotomy has also been used as a surrogate for acute fracture [2,37]. Fatigue loading has been used previously to induce microdamage and to study its repair [4,6,13–15,18,22,30,39,42,45,46]. The response of bone to repeated cyclical loading was examined previously in an impact model [8] inducing fatigue fracture. The fracture model presented here is based on a previously developed compressive loading model for the rat ulna [4], with the aim of producing fatigue fracture [22,23,45]. Strain gauge measurements conducted in the development of this fracture model corroborate data reported by Torrance et al. using the same loading configuration [42] in which compressive strains as high as 4350 µstrain were reported medial to the neutral axis and tensile strains up to 2900 µstrain were reported

lateral to the neutral axis under a 20 N peak load. In the fracture model reported here, maximal strains of 3500–4000 μstrain were measured on the medial side of the cortex under application of 18 N peak cyclic loads. This area corresponds to the area of highest strains reported previously [42] and coincides with the location of the fracture. The fracture morphology, i.e. the oblique fracture surface, typifies a fatigue failure arising in an area of compact bone subjected to longitudinal compressive stresses [14].

The fracture occurred on the compressive side [42] which may at first appear contrary to observations that bone is more fatigue resistant under compression [9,13,31]. However, due to the natural shape of the bone, axial loads, such as those applied in the model described here, engender compressive strains in the ulnar cross-section that are higher than the respective tensile strains due to the superposition of axial and bending modes [42]. Thus, it is likely that the number of cycles to failure for the resulting tensile strains is higher than that for compressive strains.

This model represents a new approach to simulating a naturally occurring fatigue fracture in vivo. This model achieves fracture through the development and coalescence of microdamage during controlled, fatigue loading. The loading magnitude per se is hyperphysiological, but it was shown in previous experiments [4,45] that it is adequate to induce and simulate fatigue damage in a rat model. The loading conditions differ from those occurring during physiological loading, i.e. the load is applied via the flexed carpus and olecranon process. Nonetheless, the distribution of stress and strain along the longitudinal axis of the ulna approximates that occurring physiologically due to the bending moments incurred through axial compression of a curved bone. Furthermore, the fracture configuration is similar to that occurring spontaneously due to fatigue, e.g., as seen in the third metacarpus of racehorses [34] or in the central tarsal bone of race dogs [33]. Finally, despite being an exogenous loading model, soft tissue surrounding the area of interest is protected from artifactual trauma and damage to the blood supply is minimized.

In conclusion, based on the noninvasive long bone fatigue fracture model described in this study, application of repeated cyclic loads with a magnitude below the ultimate strength, can be used to produce a fatigue fracture in vivo. The fatigue behavior observed in this study was consistent with that observed in previous studies on compact bone tissue, and the resulting fracture corresponded to spontaneously occurring failures observed clinically [14]. Supported by tracer methods and reconstruction of the fracture morphology in three dimensions, the model presented here lends itself for the study of internal remodeling of periosteal woven bone during fracture healing, and has obvious applications for the study of fatigue fracture etiology.

Acknowledgements

The experimental aspects of this project were carried out by AT during MKT's sabbatical in New York. Microscopy, modeling, and analysis were conducted at the Lerner Research Institute in Cleveland. The work was supported by funding from the Institute of Biomedical Engineering under the auspices of the Swiss Federal Institute of Technology and University of Zürich (AT), the AO/ASIF Research Institute (AT) and the Swiss National Science Foundation (Grant no. 823A-056609, MKT). Parts of the study were also supported by NIH (AR41210), the U.S. Army (DAMD 17-98-1-8515) and NASA (JGBEC NCC3-1000). The authors kindly acknowledge Damien Laudier, and Prof. Peter Niederer for their support during the course of the experimental work. Parts of the study were also supported by NIH (Grant AR41210) and US Army (Grant DAMD17-98-1-8515).

References

[1] Anderson TL. Fracture mechanics: fundamentals and applications. Boca Raton, FL, USA: CRC Press; 1991.
[2] Baumgart R, Kettler M, Zeiler C, Weiss S, Schweiberer L. Indications and technique of bone cutting. Chirurg 1998;69:1188–96.
[3] Beaupre GS, Orr TE, Carter DR. An approach for time-dependent bone modeling and remodeling-application: a preliminary remodeling simulation. J Orthop Res 1990;8:662–70.
[4] Bentolila V, Boyce TM, Fyhrie DP, Drumb R, Skerry TM, Schaffler MB. Intracortical remodeling in adult rat long bones after fatigue loading. Bone 1998;23:275–81.
[5] Bonnarens F, Einhorn TA. Production of a standard closed fracture in laboratory animal bone. J Orthop Res 1984;2:97–101.
[6] Burr DB, Forwood MR, Fyhrie DP, Martin RB, Schaffler MB, Turner CH. Bone microdamage and skeletal fragility in osteoporotic and stress fractures. J Bone Miner Res 1997;12:6–15.
[7] Burr DB, Martin RB, Schaffler MB, Radin EL. Bone remodeling in response to in vivo fatigue microdamage. J Biomech 1985;18:189–200.
[8] Burr DB, Milgrom C, Boyd RD, Higgins WL, Robin G, Radin EL. Experimental stress fractures of the tibia. Biological and mechanical aetiology in rabbits. J Bone Joint Surg Br 1990;72:370–5.
[9] Burr DB, Turner CH, Naick P, Forwood MR, Ambrosius W, Hasan MS, et al. Does microdamage accumulation affect the mechanical properties of bone? J Biomech 1998;31:337–45.
[10] Burrows HJ. Fatigue infraction of the middle of the tibia in ballet dancers. J Bone Joint Surg 1956;38B:83.
[11] Caler WE, Carter DR. Bone creep-fatigue damage accumulation. J Biomech 1989;22:625–35.
[12] Carter DR, Caler WE. Cycle-dependent and time-dependent bone fracture with repeated loading. J Biomech Eng 1983;105:166–70.
[13] Carter DR, Hayes WC. Compact bone fatigue damage—I. Residual strength and stiffness. J Biomech 1977;10:325–37.
[14] Carter DR, Hayes WC. Compact bone fatigue damage: a microscopic examination. Clin Orthop 1977;265–74.
[15] Currey JD. Strain rate and mineral content in fracture models of bone. J Orthop Res 1988;6:32–8.

[16] Einhorn TA. Clinically applied models of bone regeneration in tissue engineering research. Clin Orthop 1999:S59–67.
[17] Einhorn TA, Simon G, Devlin VJ, Warman J, Sidhu SP. Vigorita VJ. The osteogenic response to distant skeletal injury. J Bone Joint Surg Am 1990;72:1374–8.
[18] Frost HM. A brief review for orthopedic surgeons: fatigue damage (microdamage) in bone (its determinants and clinical implications). J Orthop Sci 1998;3:272–81.
[19] Fujita M, Matsui N, Tsunoda M, Saura R. Establishment of a non-union model using muscle interposition without osteotomy in rats. Kobe J Med Sci 1998;44:217–33.
[20] Gilbert RS, Johnson HA. Stress fractures in military recruits; a review of twelve years' experience. Milit Med 1966;131:716.
[21] Hiltunen A, Vuorio E, Aro HT. A standardized experimental fracture in the mouse tibia. J Orthop Res 1993;11:305–12.
[22] Hsieh YF, Silva MJ. In vivo fatigue loading of the rat ulna induces both bone formation and resorption and leads to time-related changes in bone mechanical properties and density. J Orthop Res 2002;20:764–71.
[23] Hsieh YF, Wang T, Turner CH. Viscoelastic response of the rat loading model: implications for studies of strain-adaptive bone formation. Bone 1999;25:379–82.
[24] Jepsen KJ, Davy DT. Comparison of damage accumulation measures in human cortical bone. J Biomech 1997;30:891–4.
[25] Knothe Tate ML, Bauer T, Schaffler MB, Currey JD. Live-dead assay for osteocytes in unstained, undemineralized bone samples. Trans ORS 2002;506.
[26] Knothe Tate ML, Niederer P, Knothe U. In vivo tracer transport through the lacunocanalicular system of rat bone in an environment devoid of mechanical loading. Bone 1998;22: 107–17.
[27] Knothe Tate ML, Schaffler MB. Loss of osteocyte integrity colocalizes with bone resorption following disuse. Trans ORS 2002;37.
[28] Knothe Tate ML, Steck R, Forwood MR, Niederer P. In vivo demonstration of load-induced flow in the rat tibia and its potential implications for processes associated with functional adaptation. J Exp Bio 2000;203(18):2737–45.
[29] Macdonald W, Skirving AP, Scull ER. A device for producing experimental fractures. Acta Orthop Scand 1988;59:542–4.
[30] Martin B. Mathematical model for repair of fatigue damage and stress fracture in osteonal bone. J Orthop Res 1995;13: 309–16.
[31] Martin B, Burr DB, Sharkey NA. Skeletal tissue mechanics. New York: Springer-Verlag; 1998.
[32] McBryde Jr AM. Stress fractures in athletes. J Sports Med 1975;3:212–7.
[33] Muir P, Johnson KA, Ruaux-Mason CP. In vivo matrix microdamage in a naturally occurring canine fatigue fracture. Bone 1999;25:571–6.
[34] Nunamaker DM, Butterweck DM, Provost MT. Fatigue fractures in thoroughbred racehorses: relationships with age, peak bone strain, and training. J Orthop Res 1990;8:604–11.
[35] Otter MW, Qin YX, Rubin CT, McLeod KJ. Does bone perfusion/reperfusion initiate bone remodeling and the stress fracture syndrome? Med Hypotheses 1999;53:363–8.
[36] Park SH, Cassim A, Llinas A, McKellop HA, Sarmiento A. Technique for producing controlled closed fractures in a rabbit model. J Orthop Res 1994;12:732–6.
[37] Park SH, O'Connor K, Sung R, McKellop H, Sarmiento A. Comparison of healing process in open osteotomy model and closed fracture model. J Orthop Trauma 1999;13:114–20.
[38] Schaffler MB. In: Burr DB, Milgrom C, editors. Musculoskeletal fatigue and stress fractures. New York: CRC Press; 2001. p. 161–82.
[39] Schaffler MB, Radin EL, Burr DB. Mechanical and morphological effects of strain rate on fatigue of compact bone. Bone 1989;10:207–14.
[40] Seibold R, Schlegel U, Cordey J. A method for inducing standardized spiral fractures of the tibia in the animal experiment. Unfallchirurg 1995;98:376–8.
[41] Tami AE, Nasser P, Verborgt O, Schaffler MB, Knothe Tate ML. The role of interstitial fluid flow in the remodeling response to fatigue loading. J Bone Miner Res 2002;17:2030–7.
[42] Torrance AG, Mosley JR, Suswillo RF, Lanyon LE. Noninvasive loading of the rat ulna in vivo induces a strain-related modeling response uncomplicated by trauma or periostal pressure. Calcif Tissue Int 1994;54:241–7.
[43] Vashishth D, Behiri JC, Bonfield W. Crack growth resistance in cortical bone: concept of microcrack toughening. J Biomech 1997;30:763–9.
[44] Vashishth D, Tanner KE, Bonfield W. Contribution, development and morphology of microcracking in cortical bone during crack propagation. J Biomech 2000;33:1169–74.
[45] Verborgt O, Gibson GJ, Schaffler MB. Loss of osteocyte integrity in association with microdamage and bone remodeling after fatigue in vivo. J Bone Miner Res 2000;15:60–7.
[46] Zioupos P. Accumulation of in-vivo fatigue microdamage and its relation to biomechanical properties in ageing human cortical bone. J Microsc 2001;201:270–8.
[47] Zioupos P, Currey JD, Sedman AJ. An examination of the micromechanics of failure of bone and antlerby acoustic emission tests and laser scanning confocal microscopy. Med Eng Phys 1994;16(3):203–12.

CHAPTER 11

Bone Fatigue and Remodeling in the Development of Stress Fractures

Mitchell B. Schaffler

CONTENTS

INTRODUCTION

Stress fractures result from repetitive loading and occur commonly among physically active individuals. Stress fractures are not associated with a specific history of trauma. Rather, they are frequently reported in soldiers, ballet dancers, joggers, and other individuals who have increased their levels of repetitive-type physical activities.[4,28,30,52,55,74-76,78,81] As such, they have been often regarded as a mechanical fatigue-driven process. Stress fractures are ranked between the second and eighth most common running injury, with incidences reported between 4 and 14%.[48,59] Rates of occurrence of stress fracture in the U.S. military were reported by Jones et al.[59] to be in the range of less than 4%. However, recent studies by Hise et al.[52] found that stress

0-8493-0317-6/01/$0.00+$.50

In: Stress Fractures
DB Burr & C Milgrom, eds
CRC Press, 2001

fracture incidence among female soldiers in basic training was considerably higher, at nearly 8%. In other military training environments, such as the Israeli army, the incidence of stress fracture among soldiers has been reported as high as 31 percent.[74,75]

Clinically, stress fractures present as bone tenderness, often with radiographic evidence of a periosteal callus; less frequently observed is occurrence of an actual fracture line.[30,81,109] Typically, stress fractures occur after four to six weeks of increased activity. This is estimated to correspond to about 100,000 load use cycles.[24,30] In recent years, diagnosis of stress fracture has shifted from radiology to bone scintigraphy using ^{99m}technetium (^{99m}Tc).[46,74-76,91,109,114,115]

There are two hypotheses regarding the cause of stress fractures. One hypothesis holds that stress fractures are the result of development, accumulation, and growth of microcracks within the bone.[20-25,29,35,80] In this view, stress fractures are considered a purely mechanical damage occurrence, i.e., fatigue failure of the skeleton. An alternative hypothesis models stress fracture as a positive feedback mechanism: increased mechanical usage stimulates bone turnover, which results in focally increased bone remodeling space (porosity) and decreased bone mass. With continued loading of this focally, transiently osteopenic bone, local stresses are markedly elevated, leading to accelerated damage and failure. Fracture is the result of continued repetitive loading superimposed on the decreased bone mass caused by more and larger resorption spaces.[30,58,68,97,98]

DOES BONE FATIGUE WITHIN THE NORMAL RANGE OF PHYSIOLOGICAL STRAINS AND CYCLES?

Bone can fracture with relatively few loading cycles when cyclic stresses or strains are large. Carter and Caler[20,21] showed that bone can fail in fatigue in as few as 1000 to 100,000 loading cycles at strain ranges of 5000 to 10,000 microstrain (0.5 to 1 percent deformation). However, *in vivo* bone strain studies indicate that habitual peak physiological strain ranges in living animals are considerably lower, typically less than 1500 microstrain in tension and 2500 microstrain in compression.[62,92,93] Very high bone strains (in the range of 4000 to 5000 microstrain) in muscularly fatigued, growing racehorses have been reported by Nunamaker et al.[80] However, other studies have not observed comparably high strain levels in race horses.[93,94] Recently, Burr and co-workers[18,44,53] applied strain gages to the tibial shafts in Israeli soldiers during intensive training regimes and found that repetitive strains did not exceed 2000 microstrain for any voluntary activity, no matter how extreme the regimen. They also observed that after extreme muscular fatigue, strain magnitudes did not change but strain rates increased significantly.[44] In summary, these data indicate that maximum bone strains *in vivo* during vigorous activities, in humans and in animals, are in the range of about 2000-2500 microstrain.

HOW DOES BONE BEHAVE WHEN FATIGUE-LOADED AT LOWER, MORE PHYSIOLOGICAL STRAINS?

At physiological strains in the range of 1500 to 2500 microstrain, the *predicted fatigue life to failure* of compact bone (defined as fracture) is extremely long — up

to 10 million load cycles. However, Schaffler et al.[97,98] showed that during cyclic loading at such low strains as encountered in habitual loading, bone sustains a significant amount of fatigue damage. This fatigue is evidenced by up to 10% stiffness (modulus) loss in bone test specimens over the first few hundred thousand cycles of loading. A number of other studies have since reported similar observations for fatigue in bovine, canine, equine, and human bone.[17,47,85,100] The mechanical loss of material stiffness, or modulus reduction, during fatigue is correlated to the accumulation of microdamage. All of these studies found that the fatigue process begins early in the loading history, with most of the modulus degradation occurring within several hundred thousand cycles of loading. Stiffness loss then stabilizes for the duration of the experimental loading period and does not progress to failure for up to several million load cycles (Figure 1). Thus, at the levels of stress and strain which are habitually developed *in vivo*, the fatigue life to failure for compact bone is extremely long — 1 to 10 million load cycles, which corresponds to approximately five to ten years of use in life. However, significant amounts of fatigue damage occur throughout the loading history. This damage must be repaired in order to avoid failure of skeletal elements. It should also be noted that strain rate, or the rate at

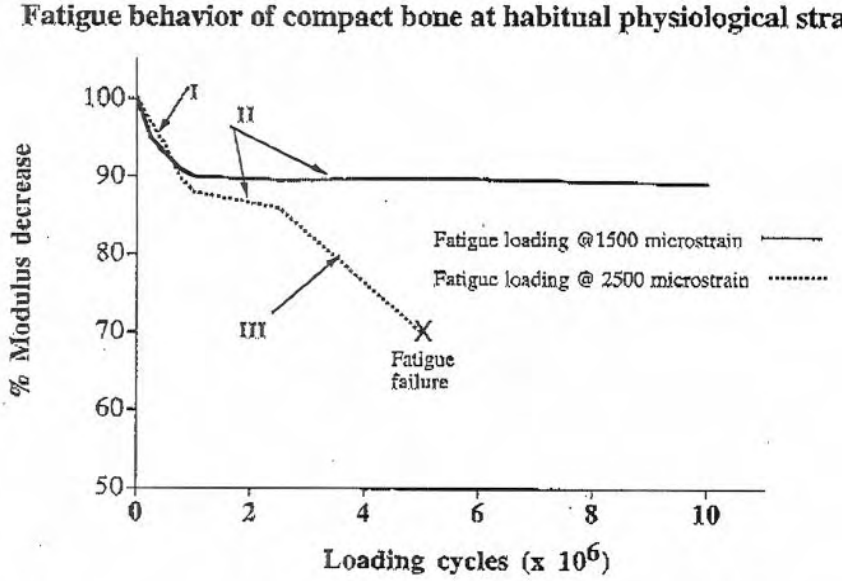

Figure 1 Summary of fatigue behavior of compact bone loaded at two strain levels characteristic of the physiologic loading environment. At the lower strain, characteristic of rapid walking, bone sustains damage and loses stiffness (shown as percentage decrease from the initial elastic modulus) early in its loading history (phase I). Stiffness loss then slows and remains stable (phase II) for up to 10 million cycles. At 2500 microstrain, the strain level characteristic of normal running, bone shows a similar early degradation of modulus (I). Damage accumulation then slows and remains stable for 1 to 2 million cycles (II). At this higher strain, however, modulus degradation will resume and progress to fatigue failure (phase III) after several million cycles of loading.

which peak strains are generated in bone, has a significant effect on damage accumulation. In laboratory fatigue tests, loading at strain rates characteristic of running were more damaging to bone than loading at lower rates, regardless of the magnitude of strain or load.[97]

The key point of these data is that bone readily sustains fatigue damage at modest stresses or strains. An analogous temporal pattern of fatigue behavior occurs in many fiber–reinforced composite materials.[1,89] Under low stress or strain cyclic loading conditions, stiffness loss occurs early in the loading history, corresponding structurally to the initiation of new cracks and voids in the material. Stiffness loss then slows until very late in the loading history, when it again resumes and progresses rapidly to failure. This three-phase failure behavior for low stress/strain cyclic loading failure of composite materials, and apparently compact bone as well, stands in contradistinction to the earlier idea that compact bone can be characterized as a material that has a linear, progressive loss of stiffness leading to failure. Thus, at the low stress/strain levels at which bone is habitually loaded, bone sustains fatigue damage quickly, but that damage does not readily progress to failure.

FATIGUE MICRODAMAGE IN COMPACT BONE

Loss of stiffness with fatigue loading is direct mechanical evidence for the existence of damage within the matrix in composite material such as bone.[1,8,22,85,97,98,100] However, given that bone is a comparatively brittle, inhomogeneous material, it has been problematic to visualize matrix damage and validate that matrix cracking is not an artifact of microscopic preparation techniques.

Frost[40] reported the first observations of microdamage (small, 30 to 100 μm-long cracks) in human rib samples obtained at autopsy. He suggested that such microcracks result from fatigue *in vivo*. Frost's simple and elegant approach for visualizing microscopic damage in bone is still central to bone fatigue and matrix damage research some 40 years after its original description.[11,17,47,101,104] Large blocks of bone tissue were stained in a dye (basic fuchsin) which binds non-specifically to open bone surfaces prior to histological sectioning. Microcracks existing in the bone prior to sectioning were stained; new cracks introduced during sectioning for microscopic observation remained unstained and could therefore be readily distinguished as artifact. This bulk staining approach has been updated to include fluorescent and heavy metal dyes, allowing studies using confocal microscopy and electron microscopy.[64,99,103]

Bone microcracks, of the typical linear morphology first described by Frost (Figure 2), have been produced experimentally by applying physiological levels of stress or strain cyclically to devitalized bone samples[17,19,97,98,100] and *in vivo* as well.[5,15,77,108] Moreover, bone is a hierarchical, inhomogeneous material, and cracks can potentially form at any level in its microstructural organization. Thus, it is clear that there can be other levels of matrix failure in bone which occur early in the fatigue process and strongly influence its fatigue behavior. In experiments from our laboratory,[100] human compact bone samples were fatigued to increasing amounts of damage, as evidenced by modulus degradation. Typical linear-type microcracks (Figure 3a) were observed rarely in specimens at lower fatigue level (15% modulus

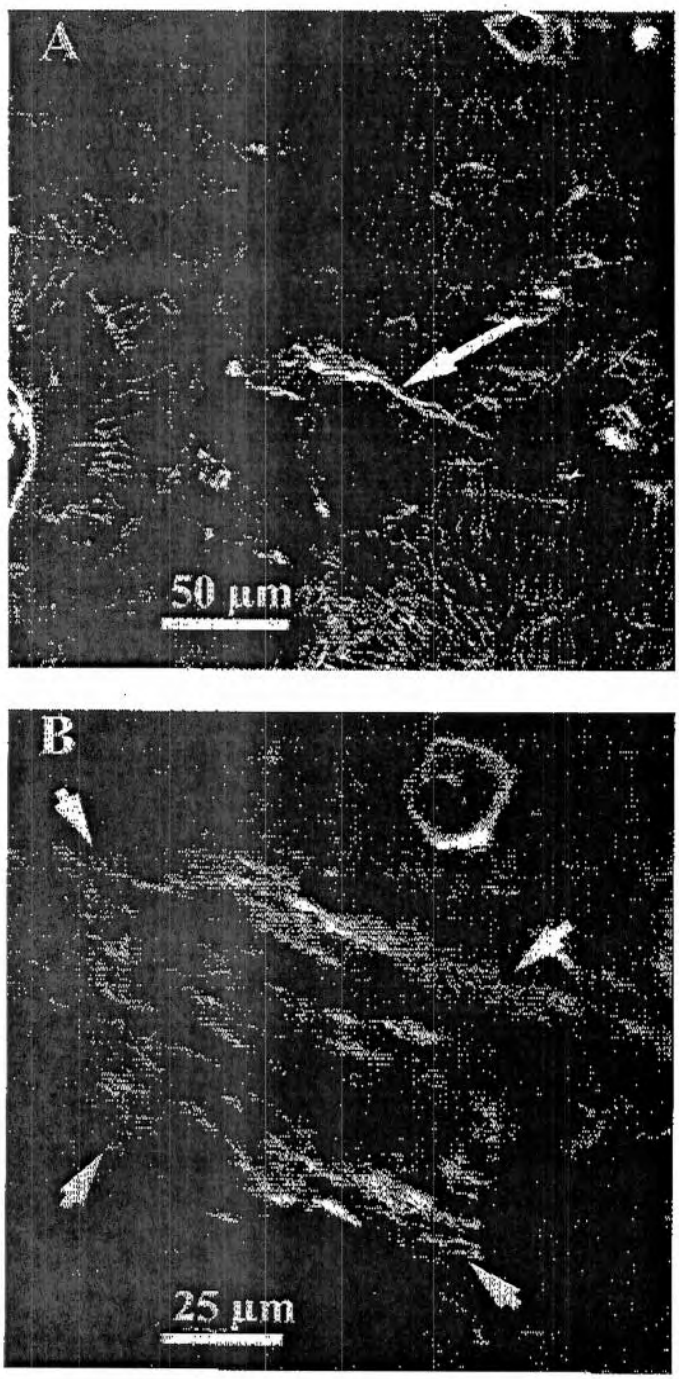

Figure 2 Confocal photomicrographs of microdamage in human bone samples. Upper panel (A) shows a linear microcrack (arrow) typical of that first described by Frost.[40] Lower panel (B) shows a higher magnification view of a region of diffuse matrix damage, comprised of large numbers of very small microcracks.

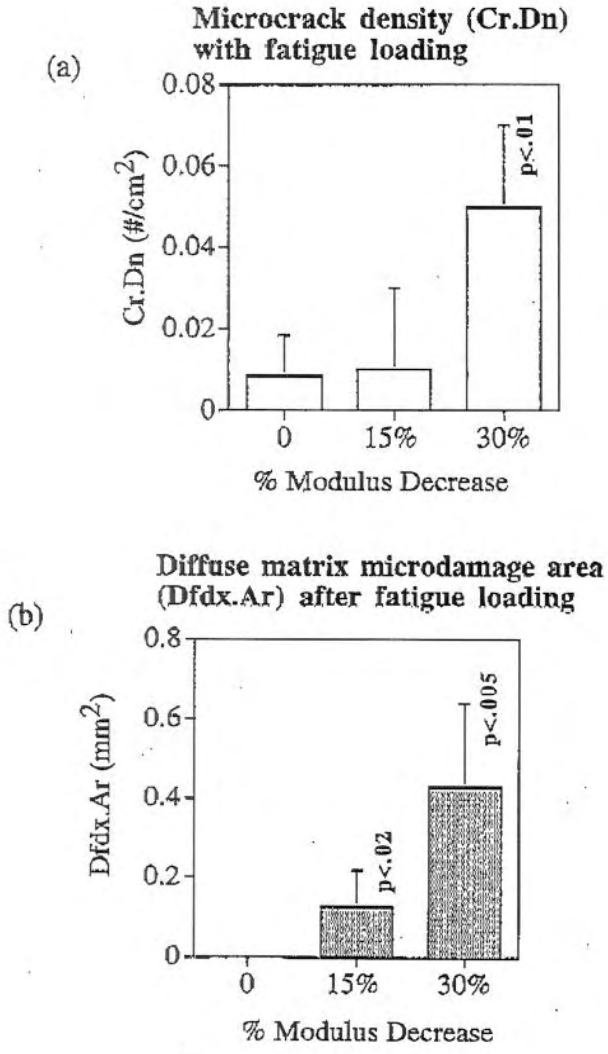

Figure 3 Linear microcrack density (Cr.Dn) and diffuse damage content (Dfdx.Ar) in human bone specimens experimentally loaded to increasing levels of fatigue. a. For linear microcracks, increased Cr.Dn occurs after a 30% modulus decrease. b. In contrast, diffuse damage content increases in direct relation to increasing amounts of fatigue in these samples.

loss) but were observed routinely at higher levels of fatigue (30% modulus degradation). In studies of whole bone fatigue in canine long bones, Burr et al.[9] also reported that linear microcracks were not observed until 15% stiffness loss. However, in fatigue-loaded human bone specimens, patches of diffuse basic fuchsin staining of the bone matrix were observed at all fatigue levels, indicating a fatigue-induced change in bone matrix permeability to the stain. The amount of this diffuse staining increased in direct relation to increasing specimen fatigue levels (Figure 3b).

Confocal microscopy showed these patches of diffuse basic fuchsin staining in fatigued bone to be comprised of very fine matrix cracking at the sub-lamellar level (<5 μm) size order in bone. (Figure 2). Occasional foci of dye uptake were observed within regions of identifiable matrix microcracking, for which no cracks could be resolved using confocal microscopy. As the maximum lateral resolution of confocal microscopy is ~200 nanometers, these foci indicate that some damage occurs at even finer levels of bone matrix structure. Zioupos and Currey,[113] in their recent studies of fracture toughening mechanisms in bone, reported similar early mechanisms of matrix failure. The principal bone matrix structures at the level of organization of these very small cracks in bone are hydroxyapatite crystals and their aggregates, suggesting that early matrix failure in bone might occur principally at the level of these structures.

In summary, compact bone undergoes fatigue and sustains matrix-level damage as a result of cyclic loading at the magnitudes of stress or strain that can be generated with habitual physiological activities. However, at these same stresses/strains, fatigue does not progress to failure within a time frame consistent with the development of stress fractures *in vivo*. These data suggest that other mechanisms must be involved in the development of so-called fatigue or stress fractures *in vivo*.

Studies show that different amounts of fatigue in compact bone lead to different amounts of microdamage, but also to different qualities of the damage present (i.e., diffuse matrix microdamage early in fatigue; typical microcracking later in fatigue). It is well established in materials science that microdamage content (quality and quantity) compromises the residual (remaining) mechanical properties of a material. Diminished residual properties in bone after fatigue were first demonstrated by Carter and Hayes.[22] In order to assess how different amounts and types of damage with different levels of bone fatigue alter functional-mechanical properties, Boyce et al.[8] examined the residual properties of human compact bone after fatigue, using matched contralateral femurs to those used in fatigue experiments described in the preceding section. After completion of fatigue loading, specimens were tested monotonically to failure. Residual properties of ultimate stress (strength), ultimate strain, and work to fracture were measured from stress-strain curves. Among specimens loaded to the lower level of fatigue (15% modulus decrease), residual stress, strain, and work to fracture were reduced in general proportion to the amount of modulus degradation. In contrast, bone specimens fatigued to greater levels (30% modulus decrease) showed losses of ultimate strength and work to fracture far greater than expected based on the stiffness changes in these specimens (67 and 76% reductions, respectively). Most striking, however, is that bone specimens fatigued to the higher level of fatigue showed effectively no post-yield deformation (Figure 4). In other words, the accumulation of fatigue damage caused a disproportionate loss of the ability of bone to withstand a catastrophic fracture.

REMODELING AND REPAIR OF MICRODAMAGE IN BONE

Unlike synthetic engineering materials, bone is capable of detecting and repairing fatigue damage at the microscopic level. Numerous investigators have suggested that

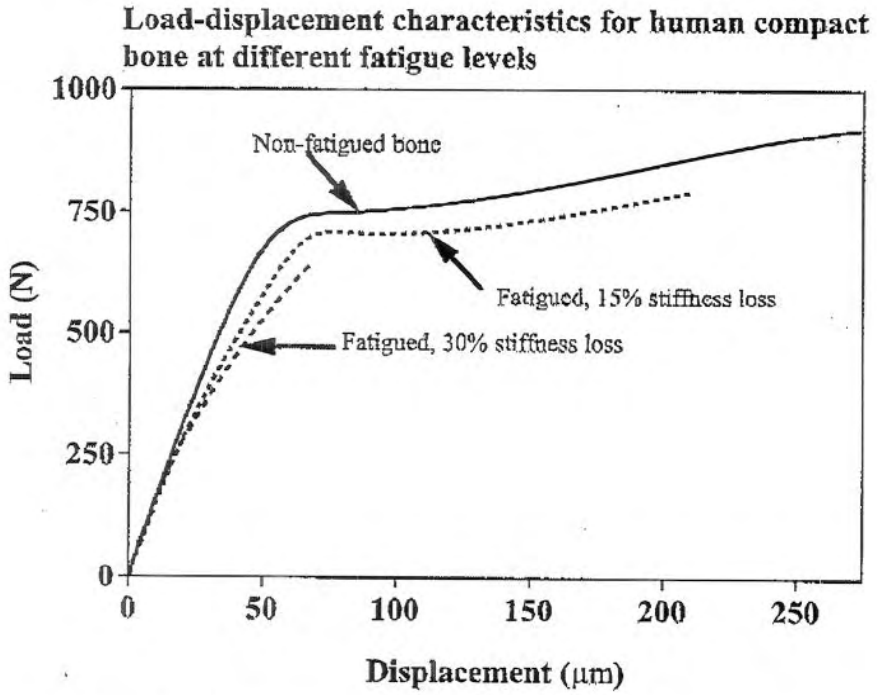

Figure 4 Residual mechanical properties for bone specimens after different amounts of fatigue. Non-fatigued bone shows well-defined elastic, yield, and plastic regions of the loading curve. At a modest level of fatigue (15% modulus decrease), the bone mechanical properties are reduced in close proportion to the induced fatigue level. At the higher fatigue level (30% modulus loss), bone stiffness and strength are reduced proportionally. However, the load-displacement curve no longer shows a yield point or any post-yield region. These data show that higher levels of fatigue cause a disproportionate loss of bone's fracture toughness, or the ability of bone to withstand fracture.

a primary function of osteonal remodeling in the adult skeleton is reparative: remodeling serves to remove and replace fatigue-damaged regions of compact bone.[5,15,19,40-42,68,69,77,84,97,98,101] Specifically, repair of matrix microdamage occurs through a microscopic "drill and fill" process, in which osteoclasts tunnel into bone and remove damaged regions. Osteoblasts then concentrically fill in the resorption space, forming a completed osteon. The remodeling repair response is summarized schematically in Figure 5. How bone remodeling units (tunneling osteoclast followed by osteoblasts) target damaged areas of bone is not understood. Osteocytes, the resident cells buried within the mineralized matrix of bone, appear to play a critical role in this process. Indeed, despite the widely held concept that bone remodeling functions in the repair of microdamage, empirical data demonstrating this basic physiological mechanism are scant, owing to the difficulty and complexity of performing such studies.

Burr, Martin, Schaffler, and Radin,[15] and Mori and Burr[77] showed experimentally that bone resorption spaces are associated with remodeling of linear microcracks in experimentally loaded canine compact bone. Recently, Bentolila et al.[5] reported an

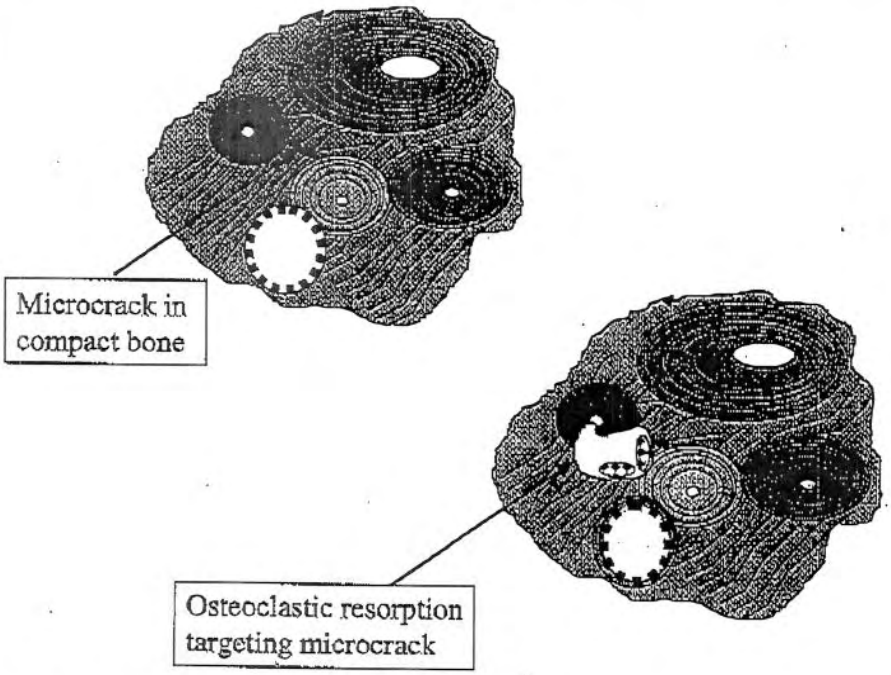

Figure 5 Schematic diagram showing microdamage in compact bone and targeted removal of the damage by osteoclastic resorption.

in vivo fatigue model based on end-load ulnar bending in adult rats, in which bone fatigue levels can be monitored as changes in whole bone stiffness. After fatigue loading, bone remodeling was activated and was observed in association with both linear microcracks and areas of diffuse matrix damage. Remodeling was effective in removing both damage types from the bone. Recent studies by Mashiba and coworkers[70] have taken a different approach to examining the relationship between microdamage and remodeling in normal bone physiology. They found that inhibiting bone remodeling in normally active dogs, using two types of bisphosphonate,[2,3] leads to a significant increase in bone microdamage content in the axial skeleton (ribs and vertebral bodies) as well as in long bones (femurs). These experiments show very convincingly that without an active remodeling-repair system, microdamage will accumulate in skeletal tissues as a result of normal, mechanically nominal levels of mechanical usage.

The cellular mechanisms by which groups of osteoclasts target regions of bone for resorption are unknown. However, it is reasonable to presume that osteocytes, the only cells embedded in the bone matrix, would be involved. Osteocytes and their elongated cell processes (in their lacunae and canaliculi, respectively) are widely and extensively distributed throughout the bone matrix. These cells are attached to their surrounding bone matrix with numerous attachment molecules, and to their neighboring cells through electrical connections known as gap junctions.[31,32] Osteocytes are highly responsive to mechanical loading.[63,103] Matrix disruption from

microdamage can be expected to directly injure osteocytes, disrupt their attachments to bone matrix, interrupt their communication through canalicular cellular and fluid flow processes, or alter their metabolic exchange. When osteocytes are lost from bone, complete fatigue fracture occurs. Examples include radiation-induced death of osteocytes,[72] allograft bone[6] and avascular necrosis.[60] Dunstan et al.[33] showed that the absence of osteocytes is associated with hip fracture. Osteocytes are focally lost in areas of microcrack accumulation in aging human bone.[86]

The involvement of osteocytes in bone fatigue and remodeling was recently demonstrated by Verborgt et al.[108] using the rat *in vivo* fatigue model. They found that with fatigue *in vivo*, osteocytes surrounding microcracks are injured and undergo an ordered cell disintegration process following a genetically regulated program, i.e., apoptosis. Regulated cell death is the ubiquitous biological process by which cells break down at the end of their functional life,[10,61,106] with the resulting cell breakdown products targeted by phagocytic cells. Osteoclasts belong to the phagocytic cell lineage. Osteocyte apoptosis has been observed in other metabolic situations associated with bone resorption.[9,79,106] Thus, osteocytes, and in particular the events surrounding their death, appear to provide a key part of the signaling process by which osteoclasts target microdamaged bone for removal and focal repair.

Left undetected and unrepaired, the accumulation of microdamage in bone leads to compromised mechanical properties and bone fragility. Damaged bone has significantly reduced mechanical properties in terms of strength and stiffness, and especially fracture toughness. Even small amounts of ultrastructurally based microdamage associated with early fatigue will compromise the functional-mechanical properties of bone. Fatigue damage has both mechanical and biological consequences. Stress fractures are the obvious application of the damage and repair concept in bone. However, bone microdamage, repair, and fragility are also implicated in bone aging, bone implant failure, and fractures associated with long-term usage of drugs that suppress bone remodeling physiology.[19,37,54,101] Suppressing remodeling may allow damage accumulation that will have deleterious mechanical consequences.

HOW DOES STRESS FRACTURE OCCUR?

There are two hypotheses regarding the causes of stress fractures. One hypothesis holds that stress fractures are the result of the accumulation and growth of microcracks within the bone. In this view, stress fractures are considered a purely mechanical damage occurrence, i.e., fatigue failure of the skeleton. However, fatigue to fracture as the primary mechanical causation for stress fractures is not supported by the experimental data (reviewed above). Alternatively, stress fracture has also been variously described as being primarily a biological process in which bone remodeling processes and periosteal reaction constitute the key features. However, there is little direct data on the pathophysiology of stress fractures. Attempts to understand the stress fracture process from human clinical studies have met with only limited success because of the inability to study bone tissue mechanisms directly. Mechanistic studies have not been performed in animals because of lack of a suitable experimental system until recently.

Of the few studies of human stress fracture tissues, those of Johnson and co-workers,[58] from the Armed Forces Institute of Pathology, stand out as the most critical in gaining insight into the physiology of stress fracture processes (also see Morris and Blickenstaff[78] for detailed discussion of Johnson's work). They obtained biopsies of stress fracture lesions from military recruits. Johnson observed woven bone reactions in numerous samples. Perhaps most significantly, however, focally increased intracortical remodeling was observed at stress fracture sites even in the absence of any woven bone response. Johnson's studies were based on histopathological biopsies of the lesions, taken at single time points, and therefore did not systematically examine the underlying development or physiology of the stress fracture lesions. Nevertheless, these data indicate that increased intracortical remodeling is one of the earliest and most prominent features in human stress fracture.

The association of remodeling and damage is supported by the stress fracture biopsy study presented by Mori in Chapter 10. Photomicrographs of the biopsy show accumulation of both diffuse damage and multiple linear microcracks in the region where the stress fracture occurred. Moreover, the bone surrounding the damaged regions is highly porous because of the presence of numerous active resorption cavities which are actively removing the damaged bone. These observations show that extensive microdamage is associated with the stress fracture and that bone mounts a repair reaction that will ultimately remove this damage.

Milgrom and co-workers in Israel[74,75] examined the time course of development of stress fractures among military recruits using serial ^{99m}Tc bone scans. They found that scintigraphic activity in bones destined for stress fracture increased significantly well before the existence of any increase in observable periosteal reaction. Early increased ^{99m}Tc uptake provides intriguing, albeit indirect evidence that increased bone turnover processes may be a significant early component in the development of stress fractures.

Recently, Stover and colleagues[104] reported histopathological data from racehorses with stress fracture that suggests that increased remodeling precedes the occurrence of microdamage in stress fracture. They obtained paired long bones from horses that had suffered complete (catastrophic) stress fractures of one limb. Cortical bones adjacent to the fracture sites showed elevated intracortical porosity. Most remarkable, however, is that comparable increases of intracortical porosity were also present at the same locations of the contralateral non-fractured long bones. Based on these findings, the authors suggested that increased intracortical porosity might be a necessary prerequisite to the development of stress fracture. As these were single time point studies, questions about the exact role of this increased bone turnover in the pathogenesis of stress fracture were not addressed.

Li et al.[66] reported experimental serial histological observations on the development of stress fractures in an animal model (Chapter 14). They produced stress fracture in rabbits by a chronic repetitive activity model. Animals were forced to jump and run in their cages for several hours per day for two months. Li et al. found that initial intracortical remodeling of the tibial diaphysis was the earliest observable change in the stress fracture sequence, with increased vascularity and osteoclastic resorption evident within the first week of repetitive loading. Periosteal reaction was not evident until the onset of intracortical resorption.

In our laboratory, we have developed an experimental animal model for stress fractures in rabbits, using repetitive impulsive loading of hindlimbs (Chapter 14).[12,16,102] Microfractures of trabecular bone and remodeling of the subchondral bone are a well established consequence of the repetitive impulsive loading model.[36,87,88] Adapted for use in diaphyseal bone, this model reproduces the scintigraphic and radiographic changes typically observed with stress fractures, including progressive increase in ^{99m}Tc uptake in bone, periosteal callus formation, and presence of microscopic cracks within the bone.[12,102] In this model, hindlimbs of skeletally mature rabbits were loaded to produce tibial diaphyseal stress fractures. Briefly, right hindlimbs were subjected to repetitive impulsive loading, using a cam-driven loading device. Loading is at 1.5 time body weight for a 50 millisecond cycle duration at 1 Hz. Animals receive 2400 load cycles daily. This regime causes stress fracture in the distal tibial diaphysis after five to six weeks of loading.

In the first series of experiments using this model, Burr et al.[12] showed that stress fractures in rabbits result from repetitive cyclic loading at low stresses. The lesions, which occurred in the distal third of the tibial diaphysis, were characterized at the organ level by progressive increases in bone ^{99m}Tc activity, followed later and variably by a periosteal reaction (Figure 6). In subsequent studies,[16] we measured tibial diaphyseal strains at the stress fracture site in the range of 500 to 1000 microstrain, which is within the normal physiological strain range (see above discussion). Strain rates, though increased somewhat over normal, were also within the range reported for normal locomotor activities.[93]

Recently, Schaffler and Boyd[102] examined bone tissue-level responses in the development of stress fracture in the rabbit stress fracture model. They showed that increases in intracortical porosity precede the accumulation of bone microdamage in experimentally induced stress fracture in this model. Intracortical remodeling at the stress fracture site was markedly increased by three weeks of loading, with the number of resorbing sites increased almost sixfold over control levels (Figure 7a). Intracortical remodeling activity was further increased by six weeks of loading, with resorption number increased more than tenfold over control levels). Resorption

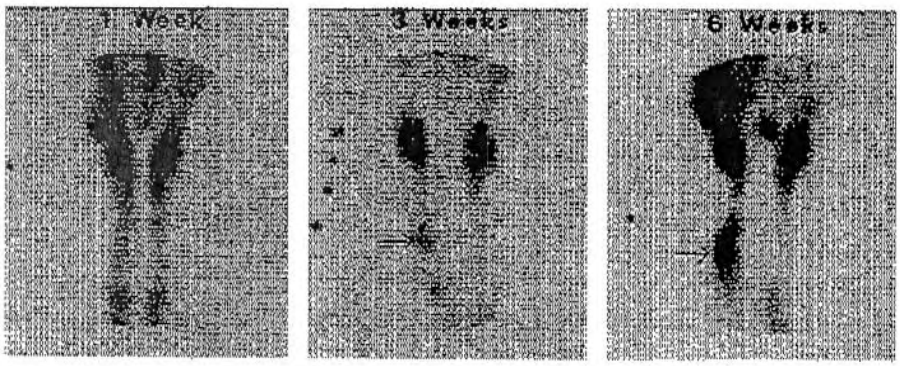

Figure 6 ^{99m}Tc bone scans of rabbit tibiae during development of experimental stress fracture. Arrows indicate increased isotope uptake in distal diaphyses of loaded limbs after 3 and 6 weeks of loading. Lesion severity progresses from 3 to 6 weeks.

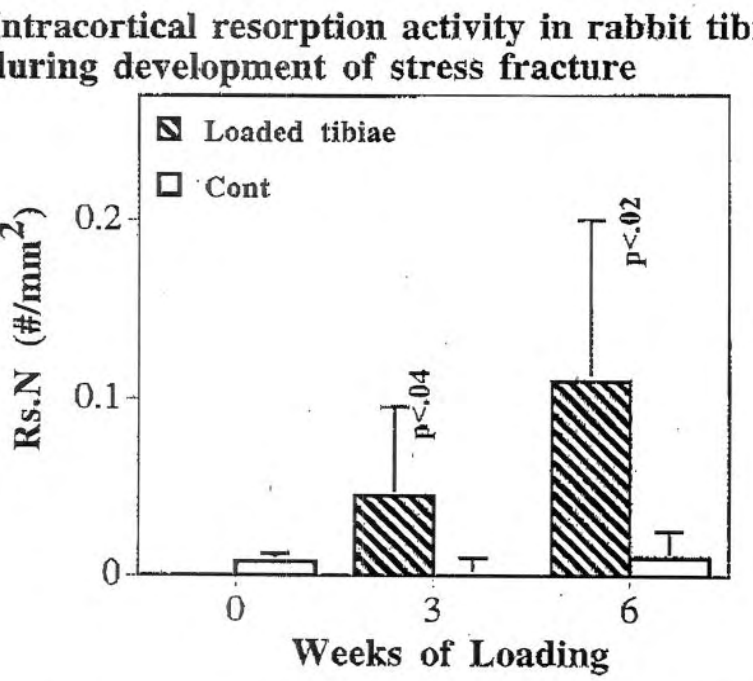

Figure 7a Intracortical resorption activity, as measured from resorption space number, at stress fracture site in rabbit distal tibial diaphyses after 3 and 6 weeks of repetitive loading. Significance values are shown relative to internal, nonloaded control limbs.

occurred primarily in the anterior and posterior tibial cortices, corresponding to the location of stress fracture and highest strain rate in this model. Bone microdamage was not observed in control bones or experimentally after three weeks of loading. By six weeks of loading, there was a significant increase in the number of microcracks observed in diaphyses Figure 7b. Typically, these were small cracks (mean length = 24 ± 7 μm). In addition, microcracks were observed only in those areas of the cortex that were undergoing intracortical remodeling (Figure 7c). Acute fatigue loading experiments, in which the equivalent of six weeks of loading was performed in one day, showed little microdamage induced by the loading alone (Figure 7b), confirming that rapid microdamage accumulation occurred only in the presence of increased bone remodeling.

The stimulus for activation of new remodeling sites in these experiments is not clear, as the experimental stress fracture site experiences a complicated series of changes relative to baseline in normal rabbit tibiae. These changes include altered strain distribution, increased loading rate with concomitant high frequency signal, and small amounts of microdamage, all of which have been shown to activate intracortical remodeling. Otter and co-workers[82] recently put forth the intriguing hypothesis that inadequate bone perfusion and reperfusion type injury in bone under chronic loading also might be a stimulus to activate bone remodeling in stress fracture. Thus, several lines of clinical, histopathological, and experimental data

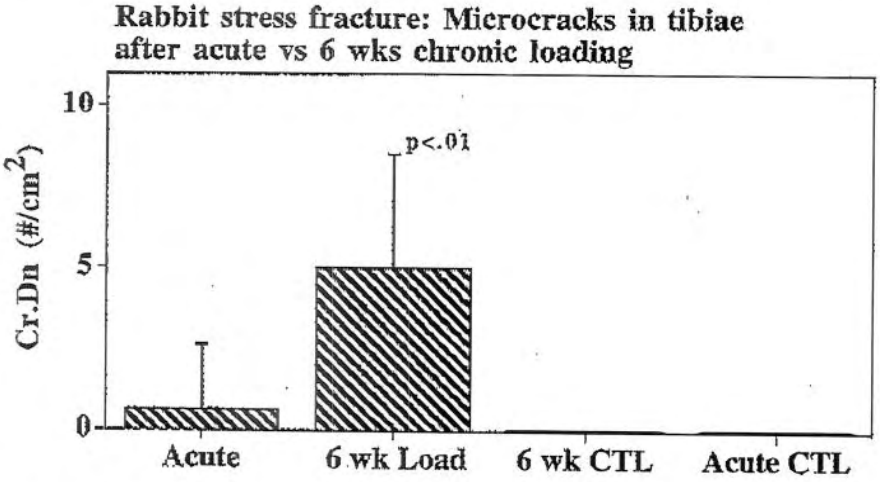

Figure 7b Microcrack content at stress fracture site in rabbit distal tibial diaphyses after 6 weeks of daily (chronic) loading versus acute loading (continuous loading for 20 hours to produce equivalent number of cycles to 6 weeks of daily loading). Acute loading, which occurs without increases in intracortical remodeling, results in a slight increase in bone microdamage content. Chronic loading, which occurs in the presence of significant increases in bone remodeling, causes a dramatic increase in microdamage.

show that increased bone remodeling occurs early in the stress fracture process. Activation of local remodeling activity results in focally increased bone porosity. Accordingly, increased intracortical porosity may be necessary for the later rapid accumulation of bone microdamage and development of stress fracture.

HOW CAN INCREASED REMODELING DRIVE MICRODAMAGE ACCUMULATION IN BONE?

A number of studies demonstrate that increased intracortical remodeling results from increased cyclic loading,[7,14,50,77] with direct mechanical effects (strain distribution, strain rate, frequency), matrix microdamage, and local cytokines among the possible stimuli for activating turnover. While the specific stimulus for activation of increased intracortical remodeling remains unclear, these studies all support the idea that early remodeling occurs with increased mechanical usage. In 1990, Schaffler, Radin, and Burr proposed a hypothesis for how elevated intracortical remodeling might drive the stress fracture process. They argued that increases in intracortical porosity, resulting from activation of intracortical remodeling, will have a dramatic effect on decreasing the stiffness of cortical bone. Continued loading of this focally osteoporotic bone will increase local stresses and strains, accelerate bone microdamage accumulation, cause periosteal hypertrophy and, ultimately, result in stress fracture. In essence, stress fracture would result when mechanical loading is sustained on a region of high turnover bone, creating a positive feedback loop leading to fracture, as summarized in Figure 8 (see Chapter 12).

Figure 7c Confocal photomicrograph of rabbit tibial compact bone at 6 weeks of loading, showing intracortical resorption (Rs) and new osteon (Os) in association with bone microdamage (Mdx arrows) (Field width = 400 μm).

Intracortical remodeling begins by activation of new remodeling sites and recruitment of bone cells to the active surface. In the first phase of remodeling, osteoclasts resorb pre-existing bone, resulting in more and larger porosity within the cortex. In humans, the resorption phase is estimated to last for about six to seven weeks.[34,57] Thus, increased intracortical remodeling results in increased bone porosity, which lasts several months after onset. As a consequence of the increase in remodeling space, void (i.e., porosity) volume in bone expands at the expense of bone tissue volume (total tissue volume = bone volume + porosity). Numerous investigations have shown that stiffness of bone decreases with decreasing bone volume (or increasing porosity), following a power-law type relationship. In trabecular bone, stiffness is proportional to the cube of bone volume.[23] Compact bone stiffness is even more highly dependent on mass. Schaffler and Burr found that stiffness in compact bone decreases to the seventh power of decreasing bone volume, indicating that the stiffness of compact bone is profoundly sensitive to its porosity or bone volume.[95] Similar exponential relationships for compact bone stiffness and density/porosity

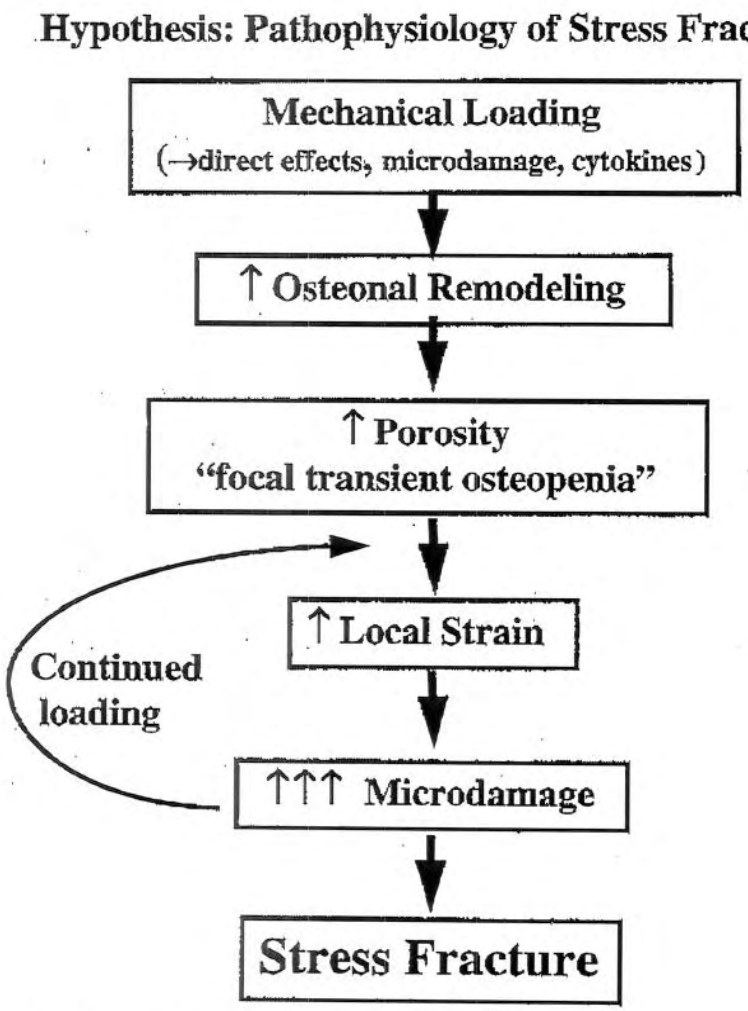

Figure 8 Schematic diagram summarizing the mechanism hypothesized for development of stress fracture, wherein increased bone remodeling and porosity (resulting from increased mechanical usage) are a prerequisite for the development of stress fractures. Increased local strains during continued loading would accelerate the accumulation of bone microdamage and the development of stress fracture in a positive feedback type manner.

were reported recently by Les et al.,[65] confirming that compact bone stiffness changes dramatically in response to small changes in intracortical porosity or bone volume.

The recent mathematical model for stress fracture development by Martin[68] is of particular interest in this regard (Chapter 12). Using a feedback model to examine the effects of increasing porosity on the mechanical properties of compact bone and development of stress fracture, Martin showed that there is a critical porosity — load interaction threshold. Once this point is reached, through increased bone porosity

and/or through increased local loading, Martin demonstrates that the system becomes unstable (i.e., positive feedback), and bone fails rapidly and catastrophically.

In summary, experimental data and several lines of clinical, histopathological data support the idea of a complex interplay between mechanical loading and bone remodeling in the etiology of stress fractures. While bone readily sustains fatigue microdamage during the course of repeated loading at the stresses or strains encountered in normal activities, it does not lead to fracture in the time course seen for the development of stress fracture. The model that best explains the development of stress fracture is that of a biologically (remodeling) driven damage accumulation system. In this model, stress fracture occurs as a positive feedback mechanism (Figure 8), wherein increased mechanical usage stimulates bone turnover, which results in focally increased bone remodeling space (porosity) and decreased bone mass. There is a wide range of factors (low level fatigue, altered mechanical loading, injury, cytokines, vascular) that can potentially activate local bone remodeling. All of these can occur in the development of stress fracture. With continued loading of this focally, transiently osteopenic bone, local stresses would be markedly elevated, leading to accelerated matrix damage and failure. Fracture is the result of continued repetitive loading superimposed on the decreased bone mass caused by more and larger resorption spaces

REFERENCES

1. Agarwal, B.D. and Broutman, L.J. *Analysis and Performance of Fiber Composites*, John Wiley & Sons, New York, 1980.
2. Antic, V.N., Fleisch, H., and Mulbauer, R.C., Effect of bisphosphonates on the increase in bone resorption induced by a low calcium diet, *Calcif. Tissue Int.*, 58, 443, 1996.
3. Balena, R., et al., The effects of 2-year treatment with the aminobisphosphonate alendronate on bone metabolism, bone histomorphometry and bone strength in ovariectomized nonhuman primates, *J. Clin. Invest.*, 92, 2577, 1993.
4. Beck, T.J., et al., Dual-energy x-ray absorptiometry derived structural geometry for stress fracture prediction in male U.S. Marine Corps recruits, *J. Bone Miner. Res.*, 11, 645, 1996.
5. Bentolila, V., et al., Intracortical remodeling in adult rat long bones after fatigue loading, *Bone*, 23, 275, 1998.
6. Berry, B.H., et al., Fractures of allografts: frequency, treatment and end results, *J. Bone Jt. Surg.*, 72A, 825, 1990.
7. Bouvier, M. and Hylander, W.L., Effect of bone strain on cortical bone structure in macaques (*Macaca mulatta*), *J. Morphol.*, 167, 1, 1981.
8. Boyce, T.M., et al., Residual mechanical properties of human cortical bone following fatigue loading, *Am. Soc. Biomech.*, 20, 23, 1996.
9. Bronckers, A.L.J.J., et al., DNA fragmentation during bone formation in neonatal rodent assessed by transferase mediated end labeling, *J. Bone Miner. Res.*, 11, 1281, 1996.
10. Buja, L.M., Eigenbrodt, M.L., and Eigenbrodt, E.H., Apoptosis and necrosis — basic types and mechanisms of cell death, *Arch. Pathol. Lab. Med.*, 117, 1208, 1993.
11. Burr, D.B. and Stafford, T., Validation of the bulk-staining technique to separate artifactual from *in vivo* bone microdamage, *Clin. Orthop.*, 260, 305, 1991.

12. Burr, D.B., et al., Experimental stress fractures of the tibia, *J. Bone Jt. Surg.*, 72B, 370, 1990.
13. Burr, D.B., et al., Skeletal change in response to altered strain environments: Is woven bone a response to elevated strain, *Bone*, 10, 223, 1989.
14. Burr, D.B., et al., The effects of altered strain environments on bone tissue kinetics, *Bone*, 10, 215, 1989.
15. Burr, D.B., et al., Bone remodeling in response to *in vivo* fatigue microdamage, *J. Biomechan.*, 18, 189, 1985.
16. Burr, D.B., et al., High strain rates are associated with stress fractures, *Trans. Orthop. Res. Soc.*, 20, 526, 1995.
17. Burr, D.B., et al., Does bone microdamage accumulation affect the normal mechanical properties of bone, *J. Biomech.*, 31, 337, 1998.
18. Burr, D.B., et al., *In vivo* measurement of human tibial strains recorded during dynamic loading, *Bone*, 19, 405, 1996.
19. Burr, D.B., et al., Bone microdamage and skeletal fragility in osteoporotic and stress fractures, *J. Bone Miner. Res.*, 12, 6, 1997.
20. Caler, W.E. and Carter, D.R., Bone creep-fatigue damage accumulation, *J. Biomechan.*, 22, 625, 1990.
21. Carter, D.R. and Caler, W.E., Cumulative damage model for bone fracture, *J. Orthop. Res.*, 3, 84, 1985.
22. Carter, D.R. and Hayes, W.C., Compact bone fatigue damage: a microscopic examination, *Clin. Orthop.*, 127, 265, 1977.
23. Carter, D.R. and Hayes, W.C., The compressive behavior of bone as a two phase porous structure, *J. Bone Jt. Surg.*, 59A, 954, 1977.
24. Carter, D.R., et al., Fatigue behavior of adult cortical bone: the influence of mean strain and strain range, *Acta Orthop. Scand.*, 52, 481, 1981.
25. Carter, D.R., et al., Uniaxial fatigue of human cortical bone: the influence of tissue physical characteristics, *J. Biomechan.*, 14, 461, 1981.
26. Charnay, A. and Tschantz, P., Mechanical influences in bone remodeling: experimental research on Wolff's law, *J. Biomechan.*, 5, 173, 1972.
27. Chestnut, C.H., Drug Therapy: Calcitonin, bisphosphonates, anabolic steroids, and hPTH, in *Osteoporosis: Etiology, Diagnosis, and Management*, Riggs, R.L. and Melton, L.J., Eds., Raven Press, New York, 1988, 1.
28. Clement, D.B., A survey of overuse running injuries, *Phys. Sportsmed.*, 9, 47, 1981.
29. Currey, J.D., *The Mechanical Adaptation of Bones*, University Press, Princeton, 1984.
30. Devas, M., *Stress Fractures*, Charles Blackstone, London, 1975.
31. Doty, S.B., Morphological evidence of gap junctions between bone cells, *Calcif. Tissue Int.*, 33, 509, 1981.
32. Doty, S.B., Robsinson R.A., and Schofield B., Morphological and histochemical staining characteristics of bone cells, in *Handbook of Physiology*, Auerbach, G.D., Ed., American Society of Physiology, Washington, 1976, 3.
33. Dunstan, C.R., Somers, N.M., Evans, R.A., Osteocyte death and hip fracture, *Calcif. Tiss. Int.*, Suppl. 53, 113, 1993.
34. Eriksen, E.F., Axelrod, D.W., and Melsen, F., *Bone Histomorphometry*, official publication of the American Society of Bone and Mineral Research, Raven Press, New York, 1995.
35. Evans, F.G. and Riolo, M.L., Relations between the fatigue life and histology of adult human cortical bone, *J. Bone Jt. Surg.*, 52A, 1579, 1970.
36. Farkas, T.A., et al., Early vascular changes in rabbit subchondral bone after repetitive impulsive loading, *Clin. Orthop.*, 219, 259, 1987.

37. Flora, L., et al., The long-term skeletal effects of EHDP in dogs, *Metab. Bone Dis. Rel. Res.*, 3, 289, 1981.
38. Forwood, M.R. and Parker, A.W., Microdamage in response to repetitive torsional loading in the rat tibia, *Calcif. Tissue Int.*, 45, 47, 1989.
39. Fraser, W.D., Paget's disease of bone, *Curr. Opin. Rheumatol.*, 9, 347, 1997.
40. Frost, H.M., Presence of microscopic cracks *in vivo* in bone, *Henry Ford Hosp. Med. Bull.*, 8, 27, 1960.
41. Frost, H.M., *Bone Dynamics in Osteoporosis and Osteomalacia*, Charles C. Thomas, Springfield, IL, 1966.
42. Frost, H.M. Bone microdamage: factors that impair its repair, in *Current Concepts in Bone Fragility*, Uhthoff, H.K., Ed., Springer-Verlag, Berlin, 1985.
43. Frost, H.M., *Intermediary Organization in the Skeleton*, CRC Press, Boca Raton, 1985.
44. Fyhrie, D.P., Effect of fatiguing exercise on longitudinal bone strain as related to stress fracture, *Ann. Biomed. Eng.*, 26, 660, 1998.
45. Genant, H.K., Bone-seeking radionuclides: an *in vivo* study of factors affecting skeletal uptake, *Radiology*, 113, 373, 1984.
46. Geslien, G.E., et al., Early detection of stress fractures using ^{99m}Tc polyphosphonate, *Radiology*, 121, 683, 1976.
47. Gibson, V.A., et al., Fatigue behavior of the equine third metacarpus, *J. Orthop. Res.*, 13, 861, 1995.
48. Grazier, K.L., et al., *The Frequency of Occurrence, Impact and Cost of Musculoskeletal Conditions in the United States*, American Academy of Orthopedic Surgeons, Chicago, 1984.
49. Griffiths, W.E.G., Swanson S.A.V., and Freeman M.A.R., Experimental fatigue fracture of the human cadaveric femoral neck, *J. Bone Jt. Surg.*, 53B, 136, 1971.
50. Hert, J., Liskova, M., and Landgrot, B., Influence of long-term continuous bending on bone, *Folia Morphol.*, 17, 389, 1969.
51. Hert, J., Pribylova, E., and Liskova, M., Reaction of bone to mechanical stimuli: microstructure of compact bone after intermittent loading, *Acta Anat.*, 82, 218, 1971.
52. Hise, L., et al., Quantitative ultrasound predicts stress fracture risk during basic training in female soldiers, *Trans. Orthop. Res. Soc.*, 22, 186, 1997.
53. Hoshaw, S.J., et al., A method for *in vivo* measurement of bone strains in humans, *J. Biomech.*, 30, 521, 1997.
54. Hoshaw, S.J., Fyhrie, D.P., and Schaffler, M.B., The effect of implant insertion and design on bone microdamage, in *The Biological Mechanisms of Tooth Eruption, Resorption and Replacement by Implants*, Davidovitch, Z., Ed., Harvard Society for the Advancement of Orthodontics, Boston, 1994, 735.
55. Hulkko, A. and Orava, S., Stress fractures in athletes, *Int. J. Sports Med.*, 8, 221, 1987.
56. Igarashi, K., et al., Anchorage and retentive effects of a bisphophonate (AHBuBP) on tooth movements in rats, *Am. J. Orthod. Dentofacial Orthopaed.*, 106, 279, 1994.
57. Jee, W.S.S., The skeletal tissues, in *Cells and Tissues*, Weiss, L.J., Ed., Elsevier Press, Amsterdam, 1989.
58. Johnson L.C., et al., Histogenesis of stress fractures, *J. Bone Jt. Surg.*, 45A, 1542, 1963.
59. Jones B.H., et al., Exercise-induced stress fractures and stress reactions in bone: epidemiology, etiology, and classification, *Exerc. Sport Sci. Rev.*, 17, 379, 1993.
60. Kenzora, J.E., et al., Experimental osteonecrosis of the femoral head in adult rabbits, *Clin. Orthop.*, 130, 8, 1978.
61. Kerr, J.F.R., Wyllie, A.H., and Currie, A.R., Apoptosis: a basic phenomenon with wide-ranging implications for tissue kinetics, *Br. J. Cancer*, 26, 239, 1972.

62. Lanyon, L.E., et al., Bone deformation recorded in vivo from strain gages attached to the human tibial shaft, *Acta Orthop. Scand.*, 46, 256, 1975.
63. Lanyon, L.E., Osteocytes, strain detection and bone modeling and remodeling *Calcif. Tiss. Int.*, Suppl. 53, 102, 1993.
64. Lee, T.C., Myers, E.R., and Hayes, W.C., Fluorescence-aided detection of microdamage in compact bone, *J. Anat.*, 193, 179, 1998.
65. Les, C.M., et al., Estimation of material properties in the equine metacarpus with use of quantitative computed tomography, *J. Orthop. Res.*, 12, 822, 1994.
66. Li, G., et al., Radiologic and histological analysis of stress fracture in rabbit tibias, *Am. J. Sports Med.*, 13, 285, 1985.
67. Martin R.B., Porosity and specific surface of bone, *CRC Crit. Rev. Biomed. Eng.*, 10, 3, 179.
68. Martin, R.B., Mathematical model for repair of fatigue damage and stress fracture in osteonal bone, *J. Orthop. Res.*, 13, 309, 1995
69. Martin, R.B. and Burr, D.B., A hypothetical mechanism for the stimulation of osteonal remodeling by fatigue damage, *J. Biomechan.*, 15, 137, 1982.
70. Mashiba, T., et al., Suppressed bone turnover by bisphosphonates increases microdamage accumulation and reduces some biomechanical properties in dog rib, *J. Bone Miner. Res.*, 15, 613, 2000.
71. Matheson, G.O., et al., Stress fractures in athletes: a study of 320 cases, *Am. J. Sports Med.*, 15, 46, 1987.
72. Mellanotte, P.L. and Follis, R.H., Early effects of x-radiation on cartilage and bone, *Am. J. Pathol.*, 39, 1, 1961.
73. Meunier, P.J. and Vignot, E., Therapeutic strategy in Paget's disease of bone, *Bone*, 17, 489S, 1995.
74. Milgrom, C., et al., Multiple stress fractures: a longitudinal study of a soldier with 13 lesions. *Clin. Orthop.*, 192, 174, 1985.
75. Milgrom, C., et al., Stress fractures in military recruits: a prospective study showing an unusually high incidence, *J. Bone Jt. Surg.*, 67B, 732, 1985.
76. Mills, G.Q., Marymount, J.H., and Murphy, D.A., Bone scan utilization in the differential diagnosis of exercise-induced lower extremity pain, *Clin. Orthop.*, 149, 207, 1980.
77. Mori, S. and Burr, D.B., Increased intracortical remodeling following fatigue damage, *Bone*, 14, 103, 1993.
78. Morris, J.M. and Blickenstaff, L.D., *Fatigue Fractures*, Charles C. Thomas, Springfield, IL, 1967.
79. Noble, B.S., et al., Identification of apoptotic changes in osteocytes in normal and pathological human bone, *Bone*, 20, 273, 1997.
80. Nunamaker, D.M., Butterweck, D.M., and Provost, T.M., Fatigue fractures in thoroughbred racehorses: relationship with age, peak bone strain and training, *J. Orthop. Res.*, 8, 604, 1990.
81. Orava, S. and Hulkko, A., Stress fractures of the mid-tibial shaft, *Acta Orthop. Scand.*, 55, 35, 1984.
82. Otter, M.W., et al., Does bone perfusion/reperfusion initiate bone remodeling and the stress fracture syndrome, *Med. Hypotheses*, 53, 363, 1999.
83. Parfitt, A.M., Stereologic basis of bone histomorphometry: theory of quantitative microscopy and reconstruction of the third dimension, in *Bone Histomorphometry: Techniques and Interpretation*, Recker, R.R., Ed., CRC Press, Boca Raton, 1983.
84. Parfitt, A.M., A new model for the regulation of bone resorption with particular reference to the effect of bisphosphonates, *J. Bone Miner. Res.*, 11, 150, 1996.

85. Pattin, C.A., Caler, W.E., and Carter, D.R., Cyclical mechanical property degradation during fatigue loading of compact bone, *J. Biomechan.*, 29, 69, 1996.
86. Qiu S.J., Boyce, T.M., and Schaffler, M.B., Osteocyte loss and microdamage in aging human compact bone, *Trans. Orthop. Res. Soc.*, 22, 88, 1997.
87. Radin, E.L., et al., Response of joints to impact loading. 3. Relationship between trabecular microfractures and cartilage degeneration, *J. Biomechan.*, 6, 51, 1973.
88. Radin, E.L., et al., Effects of mechanical loading on the tissues of the rabbit knee, *J. Orthop. Res.*, 2, 221, 1984.
89. Reifsnider, K.L., Schultz, K., and Duke J.C., Long-term fatigue behavior of composite materials, in *Long Term Behavior of Composites*, ASTM STP, Philadelphia, 1983, 813, 136.
90. Rice, J.C., Cowin, S.C., and Bowman, J.A., On the dependence of the elasticity and strength of cancellous bone on apparent density, *J. Biomechan.*, 21, 155, 1988.
91. Roub, L.W., et al., Bone stress: a radionuclide imaging perspective, *Radiology*, 132, 431, 1979.
92. Rubin, C.T., Skeletal strain and the functional significance of bone architecture, *Calcif. Tissue Int.*, Suppl. 36, 11, 1984.
93. Rubin, C.T. and Lanyon, L.E., Limb mechanics as a function of speed and gait: a study of functional strains in the radius and tibia of horse and dog, *J. Exp. Biol.*, 101, 187, 1982.
94. Rubin, C.T., et al., The correlation of metabolic fatigue to changes in the skeleton's milieu, *13th Annu. Am. Soc. Biomech.*, 246, 1989.
95. Schaffler, M.B. and Burr, D.B., Stiffness of compact bone: effects of porosity and density, *J. Biomechan.*, 21, 13, 1988.
96. Schaffler, M.B., et al., Skeletal tissue responses to thermal injury: an experimental model, *Bone*, 9, 397, 1988.
97. Schaffler, M.B., Burr, D.B., and Radin, E.L., Mechanical and morphological effects of strain rate on fatigue in compact bone, *Bone*, 10, 207, 1989
98. Schaffler, M.B., Radin, E.L., and Burr, D.B., Long-term fatigue behavior of compact bone at low strain magnitude and rate, *Bone*, 11, 321, 1990
99. Schaffler, M., Examination of compact bone microdamage using back-scattered electron microscopy, *Bone*, 15, 483, 1994.
100. Schaffler, M.B., Boyce, T.M., and Fyhrie, D.P., Tissue and matrix failure modes in human compact bone during tensile fatigue, *Trans. Orthop. Res. Soc.*, 21, 57, 1996.
101. Schaffler, M.B., Choi, K., and Milgrom, C., Aging and microdamage accumulation in human compact bone, *Bone*, 17, 521, 1995.
102. Schaffler, M.B. and Boyd, R.D., Bone remodeling and microdamage accumulation in experimental stress fracture, *Trans. Orthop. Res. Soc.*, 22, 113, 1997.
103. Skerry, T.M., et al., Early strain related changes in enzyme activity in osteocytes following bone loading *in vivo*, *J. Bone Miner. Res.*, 4, 783, 1989.
104. Stover, S., Spontaneous fractures in equine long bone, First International Workshop on Overuse in the Equine and Human Athletes, Tufts University, 1996.
105. Sullivan, D., et al., Stress fractures in 51 runners, *Clin. Orthop.*, 187, 188, 1984.
106. Tomkinson, A., et al., The role of estrogen in the control of rat osteocyte apoptosis, *J. Bone Miner. Res.*, 13, 1243, 1998.
107. Tschantz, P. and Rutishauser, E., La surcharge mechanique de l'os vivant, *Ann. Anat. Pathol.*, 12, 223, 1967.
108. Verborgt, O., Gibson, G.J., and Schaffler, M.B., Loss of osteocyte integrity in association with microdamage and bone remodeling after fatigue *in vivo*, *J. Bone Miner. Res.*, 15, 60, 2000.

109. Wang, D.C., Kottamasu, S.R., and Karvelis, K., Scintigraphy in metabolic bone disease, in *Primer on Metabolic Bone Disease and Disorders of Mineral Metabolism*, Fauvas, M.J., Ed., American Society of Bone and Mineral Research, Kelseyville, CA, 1990.
110. Weibel, E.R., *Stereological Methods*, Academic Press, New York, 1980.
111. Weinreb, M., et al., Histomorphometrical analysis of the effects of the bisphosphonate alendronate on bone loss caused by experimental periodontitis in monkeys, *J. Periodontal Res.*, 29, 35, 1994.
112. Wyllie, A.H., Cell death: the significance of apoptosis. *Int. Rev. Cytol.*, 68, 251, 1980.
113. Zioupos, P. and Currey, J.D., The extent of microcracking and the morphology of microcracks in damaged bone, *J. Mater. Sci.*, 29, 978, 1994.
114. Zwas, S.T., et al., Early diagnosis of stress fractures in soldiers by ^{99m}Tc-MDP bone scan: evaluation of efficiency and scintigraphic patterns of appearance and resolution, in *Fifth Congress of Nuclear Medicine in Israel*, 4, Czerniak, P. and Noam, N., Eds., Ramat Aviv: Baruk Institute for Radioclinical Research and Publication Sale Division, Tel Aviv University, 1980, 52.
115. Zwas, S.T., Elkanovitch, R., and Frank, G., Interpretation and classification of bone scintigraphic findings in stress fracture, *J. Nucl. Med.*, 28, 452, 1987.

Annals of Biomedical Engineering, Vol. 30, pp. 217–225, 2002
Printed in the USA.

0090-6964/2002/30(2)/217/9/$15.00

Prestress Due to Dimensional Changes Caused by Demineralization: A Potential Mechanism for Microcracking in Bone

YENER N. YENI,[1] MITCHELL B. SCHAFFLER,[2] GARY GIBSON,[1] and DAVID P. FYHRIE[1]

[1]Breech Research Laboratory, Bone and Joint Center, Henry Ford Hospital, 2799 West Grand Boulevard, Detroit, MI and [2]Leni and Peter W. May Department of Orthopaedics, Box 1188, The Mount Sinai School of Medicine, New York, NY

(Received 22 February 2000; accepted 4 December 2001)

Abstract—Microcracking in bone due to internal strains caused by mineralization is a possible mechanism of damage. Similar damage can be seen in other biological composites such as trees experiencing growth-related prestresses. Dimensional changes in cortical bone due to demineralization and experimental glycation were studied to test whether mineralization-related prestrains are consistent with observed microcracking patterns in bone. A microscopy technique that enables wet measurements of length and angle of milled bone specimens was used. Demineralization of bovine and human bones caused significant anisotropic changes in tissue size. Dimensional changes due to demineralization in bovine bone were prevented or reduced when collagen cross linking was increased by glycation. The dimensional changes of bone caused by demineralization are consistent with the hypothesis that mineralization-caused stresses in remodeling tissue can cause microcracks. © *2002 Biomedical Engineering Society.* [DOI: 10.1114/1.1451078]

Keywords—Cortical bone, Demineralization prestress, Microcracking, Collagen cross-linking, Glycation, Anisotropy.

INTRODUCTION

Bone microdamage has been of considerable interest during the past few decades due to its deleterious effect on mechanical properties and fracture susceptibility.[11] Studies of *in vivo* microdamage show that microdamage content increases with age in human cortical bone, suggesting that age-related bone fragility may be associated with microdamage.[33,37] It is believed that the microcracks in bone are fatigue cracks caused by physiological loading activities.[8–10,13,16,29,30,36]

The majority of *in vivo* microcracks of human cortical bone are found in the interstitial bone and the osteonal cement lines.[33,37] These sites of *in vivo* microcracking are also common in human trabecular bone.[44] It is believed that cracks initiate in the interstitial matrix as a result of fatigue loading or overload and become trapped in cement lines that are thought to be compliant interfaces.[10,13,35,36] Microcrack morphology due to experimental loading, however, can be different from the *in vivo* pattern depending on the loading regime and loading rate.[8,13,21] Although it is clear that loading causes microcracks in bone, it is not certain that loading is the only cause of the large number of *in vivo* microcracks found in and around the cement lines.

In biological composites, internal stresses can be generated by the growing material. A typical example of this are the growing stresses in trees.[1,31,32,42] There are longitudinal compressive and tensile stresses in the inner and outer part of a tree trunk and circumferential stresses that prevent splitting along the rays that are the radial load carrying structures.[17,31] Although these stresses are usually attributed to the mass of the growing tree, nonzero prestrains observed in the roots suggest that some of them are a result of wood development.[19]

A mechanism for microcracking at osteonal cement lines in cortical bone is stress between the new osteon and the old matrix generated by the mineralization process analogous to growing stresses in trees. Bone is known to be a prestrained material[3,39,45] and the results of previous studies, showing dimensional changes in demineralized bone, suggest that increasing mineralization plays a role in generating prestrains in bone.[15,26,27] In this study we performed a series of experiments to gain more insight into mineralization-related strains in bone by studying the inverse problem of dimensional changes related to demineralization. In particular, we concentrated on different anatomical orientations in miniaturized specimens of human and chemically altered bovine bone. We expected to find significant strains upon demineralization and that these strains would suggest mechanisms of matrix expansion during mineralization consistent with observed *in vivo* microcracking patterns.

MATERIALS AND METHODS

In order to assess the relative contribution of mineralization and cross linking on the prestresses in bone, bone dimensions were measured before and after decal-

Address correspondence to Yener N. Yeni, Ph.D., Bone and Joint Center, Henry Ford Hospital, 2799 West Grand Boulevard, Detroit, MI 48202. Electronic mail: yeni@bjc.hfh.edu

cification on cortical bone specimens with standardized geometry machined from bovine tibiae and a human femur. Specimens with 500 μm thickness were sliced from rectangular cortical bone beams, height and width of which depended on the source bone, using a low-speed diamond saw (model 660, South Bay Technology, Inc., Temple City, CA). Although the values of height and width were scattered between experimental groups (the mean values were 2.73–5.46 mm; the coefficient of variation of means between groups was 0.22), the variability within groups was low (coefficient of variation was <0.06 in each group). A pencil mark was made on a corner of each specimen as a reference point for the anatomical orientation of that specimen. Measurements of initial and postdecalcification specimen dimensions were performed using an inverted microscope (Diaphot TMD, Nikon, Tokyo, Japan) with the specimens in 40 ml of saline or decalcifying solution in a Petri dish. The images were captured using NIH IMAGE software (version 1.61, National Institutes of Health) and a charge-coupled-device (CCD) camera (C2400-60, Hamamatsu Photonics K. K., Hamamatsu City, Japan). The light intensity on the microscope was kept at the same value for all measurements. Lengths from four edges and angles from four corners were measured before and after each procedure using NIH IMAGE. The calibration of the whole system was done with a standard calibration slide. The length and angle measurements were repeated five times on one of the specimens at different times, by mounting and remounting the specimen. The measurement error was less than 0.007 (coefficient of variation of the measured values) for both length and angle measurements.

To test the idea that mineral significantly contributes to prestresses in bone, measurements of bone dimensions were performed before and after removal of the mineral with a formic acid (22.5%)–sodium citrate solution (100 g/l). The choice of formic acid–sodium citrate solution was based on the fact that decalcification of specimens with a formic acid–sodium citrate solution is faster than using ethylenediamine tetraacedic acid (EDTA) procedures. The formic acid procedure also allows testing for decalcification by simple chemical methods.[38] However, we were concerned that the formic acid procedure might damage the collagen during decalcification. In order to determine whether this would be significant in our experiments we conducted a separate experiment comparing the amount of collagen denatured by the formic acid decalcification to that denatured by EDTA decalcification.

For comparison of the amount of collagen denatured by the formic acid decalcification to that denatured by EDTA decalcification, cubic specimens of approximately 4 mm edge length were machined from bovine cortical bone. There were six and four specimens in the formic acid and EDTA groups, respectively. Measurement of degraded collagen was performed on the specimens, decalcified with formic acid or EDTA, using selective digestion of collagen by α-chymotrypsin, as outlined by Bank *et al.*[5] The difference in degraded collagen between the treatment groups was not statistically significant ($7.0\% \pm 1.6\%$ and $8.9\% \pm 1.6\%$ for EDTA and formic acid, respectively; t-test, $p = 0.10$). A power analysis revealed that the power of the t-test was 0.37 and a sample size of 13 would be necessary to achieve statistical significance with power $= 0.80$.

In a recent study,[43] the difference in degraded collagen between females and males was up to 2.2% in baboon cortical bone but the differences were not statistically significant. In addition, there was no difference in mechanical properties of bone that might have been caused by differences in degraded collagen between males and females. Significant differences in degraded collagen and mechanical properties were noted in different age groups. The difference in degraded collagen between age groups was from 2.6% to 5.3%, which is larger than the nonsignificant difference between genders in the same study and between acid treatments in the current study. Therefore, the 1.9% difference in degraded collagen between acid treatments is within normal biologic variability. Although it is possible that a 1.9% difference in degraded collagen between the treatment groups will achieve statistical significance with a large number of specimens, it is reasonable to accept this variability as a limitation in the protocol because of the very long time involved in decalcification with EDTA and the advantage of being able to use a decalcification end-point test for the formic acid treatment.

Postdecalcification measurements in the decalcifying solutions were performed immediately after decalcification was complete. The specimens were stored in saline for a day before repeating the postdecalcification measurements in saline. The time required to completely decalcify the specimens was slightly different between experiment groups as explained below. However, each specimen in the same experiment group was subjected to the same duration of treatment.

Experiment 1 (Bovine Bone)

In order to develop and test the methodology and also examine the variations in measured parameters in comparison with available literature, this initial experiment was conducted with bovine bone. Tibiae from the same animal (unknown gender and age, although approximately two-year-old animals are typical in the slaughter house) were used to minimize interspecimen variability. Ten longitudinal [radial–axial (RZ)] and ten transverse [radial–tangential (RT)] (Fig. 1) specimens were prepared. The planes were named by the two axes that lay in the plane, R and T being radial and tangential, respec-

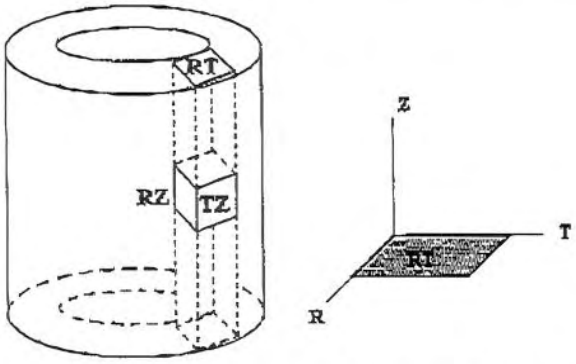

FIGURE 1. Radial–tangential (RT), radial–axial (RZ), and tangential–axial (TZ), planes with reference to a cylindrical bone section.

tively. The Z axis was chosen to represent the axial direction as customary in cylindrical coordinates. The lengths of edges and corner angles were measured in saline solution as explained above. Following the initial measurements, the specimens were demineralized in a formic acid (22.5%)–sodium citrate solution (100 g/l). The end of the decalcification procedure was determined chemically using standard precipitation methods.[38] Briefly, 5 ml of 0.5N sodium hydroxide was added to 5 ml of decalcifying solution followed by 1 ml of 5% ammonium oxalate. The final mixture was observed for turbidity which indicates the presence of calcium ions. The procedure was repeated until the test mixture was clear indicating that decalcification was over. After this, the decalcifying solution was replaced once more and the specimens were kept in the fresh solution for an extra day. The total amount of time between the initial and postdemineralization measurements, which was immediately after decalcification was complete, was 10 days. The demineralized dimensions and angles were measured on the same specimens in the decalcifying solution.

As the dimensional changes can be affected by the medium in which the measurements are conducted, we repeated this experiment with postdemineralization measurements in saline solution (0.9% NaCl) using another set of bovine bone specimens in order to assess the dimensional changes due to demineralization in an environment more closely resembling the physiological environment of bone. Five longitudinal (RZ) and five transverse (RT) specimens were used. Decalcification was complete after 7 days in this group.

Experiment 2 (Human Bone)

The previous experiment was repeated using human bone. Five longitudinal (RZ) and five transverse (RT) specimens were machined from the distal cortex of a human femur of unknown age and gender. Following the edge and angle measurements, specimens were decalcified and the measurements were repeated once in the decalcifying solution and once in saline to determine the response of demineralized human bone in its physiological environment. Decalcification was complete after 7 days.

In order to check whether the observed dimensional changes can be possible by simply storing the specimens in saline, an additional group of undecalcified specimens (five RZ and five RT) were prepared as a control group. Following initial measurements, the specimens were left in saline for the same amount of time as the demineralization specimens stayed in the formic acid solution and the measurements were repeated after this period. The saline solution was supplemented with Gentamicin (3 $\times$Gentamicin 0.6 ml + 1 $\times$PBS 200 ml) to prevent degradation of bone due to bacterial growth.

Experiment 3 (Glycated Bovine Bone)

In order to determine how the dimensions of bovine bone with increased cross-link content change upon decalcification, four RT, two RZ, and one tangential–axial (TZ) specimens were machined from a bovine tibia. Following the reference measurements, the specimens were glycated (to increase the cross-link content) with 100 mg/ml of ribose in 1 $\times$Hanks buffer/1.3 mM $CaCl_2$ at 37 °C for 7 days[6] and edge-length and angles were re-

TABLE 1. Changes in length, area, and angle parameters in decalcifying solution after demineralization of bovine bone. Significant results are highlighted and indicated by a "†" sign. Blank entries: no corresponding measurement; positive numbers indicate enlargement after respective treatment.

Specimen	Axial (%)	Tangential (%)	Radial (%)	Angle (°)	Area (%)
RZ	**−20.1†**		**4.7†**	0.256	−16.6
	(2.5)		**(4.5)**	(0.973)	(4.7)
$n=10$	**$p<0.0001$**		**$p=0.002$**	$p>0.7$	$p<0.0001$
RT		−0.048	**17.8†**	0.823	**17.8†**
		(2.372)	**(2.5)**	(0.617)	**(1.9)**
$n=9$		$p>0.9$	**$p<0.0001$**	$p>0.2$	**$p<0.0001$**

TABLE 2. Changes in length, area, and angle parameters in saline solution after demineralization of bovine bone. Significant results are highlighted and indicated by a "†" sign. Blank entries: no corresponding measurement; positive numbers indicate enlargement after respective treatment.

Specimen	Axial (%)	Tangential (%)	Radial (%)	Angle (°)	Area (%)
RZ	−7.15†		4.37†	3.100	−3.44
	(1.03)		(1.52)	(1.421)	(1.08)
$n=5$	p<0.001		p=0.003	$p=0.008$	$p=0.002$
RT		2.33†	6.19†	0.250	8.67†
		(0.98)	(1.13)	(0.637)	(0.89)
$n=5$		p=0.006	p<0.001	$p>0.4$	p<0.001

measured in saline. Then, the specimens were demineralized following the procedure stated above. Decalcification was complete after 7 days. Length and angle measurements were repeated after demineralization, once in saline and once in the decalcifying solution.

Multiple length and angle measurements were averaged and one value was used for each specimen. The results were compared using repeated measures of analysis of variance (ANOVA) in experimental groups subjected to more than one treatment or measurement (base line, postdemineralization in decalcifying solution and postdemineralization in saline solution measurements in experiment 2 and base line, postglycation, postdemineralization in decalcifying solution and postdemineralization in saline solution measurements in experiment 3). When the data failed normality or equal variance tests, nonparametric repeated measures of ANOVA on ranks (Friedman) was used. To isolate treatments that differed significantly from the others, Bonferroni (Tukey's test in case of nonparametric ANOVA) procedures were used. In experiment groups subjected to one treatment only (experiment 1 and the control group in experiment 2), the results were compared using paired t-tests following a normality test (Kolmogorov–Smirnov). For a few variables that failed the normality test the comparison of groups were made using a Wilcoxon signed rank test. Pre- and postprocedure values of the same specimen were the paired variables. Treatment effects were examined with respect to base-line measurements in all experiment groups.

RESULTS

The changes in demineralized length, area, and angle are presented in Tables 1–6. In Tables 1–6, changes in length and area are reported as percent changes with standard deviations. Changes in angle are presented in terms of degrees as mean difference (with standard errors indicated parenthetically) between pre- and postdemineralization since this is equivalent to shear strains. Note that positive values in percent changes correspond to an increase in the measured quantity.

Experiment 1 (Bovine Bone)

The changes in demineralized length, area, and angle are presented in Tables 1 and 2. Demineralized length was significantly smaller than base line in the axial direction, whereas demineralized length in the radial direction was significantly greater in both decalcifying and saline solutions (Tables 1 and 2, Fig. 2). Values in one of the RT specimens were more than 2 standard deviations different than the mean values (both radial and tangential) in the group measured in the decalcifying solution. Therefore, this specimen was discarded. Significance level of the statistics did not change by excluding this

TABLE 3. Changes in length, area, and angle parameters in decalcifying solution after demineralization of human bone. Significant results are highlighted and indicated by a "†" sign. Blank entries: no corresponding measurement; positive numbers indicate enlargement after respective treatment.

Specimen	Axial (%)	Tangential (%)	Radial (%)	Angle (°)	Area (%)
RZ	−4.4†		−0.22	0.0415	−4.6†
	(0.47)		(1.40)	(0.271)	(1.6)
$n=5$	p<0.001		$p>0.4$	$p>0.6$	p<0.001
RT		0.63	1.47†	0.235	2.0†
		(0.65)	(0.93)	(0.185)	(0.67)
$n=5$		$p>0.2$	p=0.036	$p<0.6$	p=0.014

TABLE 4. Changes in length, area, and angle parameters in saline solution after demineralization of human bone. Significant results are highlighted and indicated by a "†" sign. Blank entries: no corresponding measurement; positve numbers indicate enlargement after respective treatment.

Specimen	Axial (%)	Tangential (%)	Radial (%)	Angle (°)	Area (%)
RZ	−2.05†		0.40	0.208	−1.71†
	(0.99)		(0.72)	(0.127)	(1.25)
$n=5$	p<0.001		$p>0.4$	$p>0.6$	p=0.033
RT		0.37	1.03	0.239	1.33
		(0.71)	(0.87)	(0.256)	(1.19)
$n=5$		$p>0.2$	$p=0.148$	$p>0.6$	$p=0.096$

specimen. In addition to the axial and radial changes, there was a significant expansion in the tangential direction when the dimensions were measured in saline, but not in decalcification solution, after demineralization (Table 2).

There was a significant distortion (change in corner angles) in the RZ plane as measured in saline after demineralization (Table 2), whereas no significant difference in corner angles between pre- and postdemineralization measurements was observed in decalcifying solution nor in the RT plane in saline after demineralization (Table 1).

The area of the specimens were significantly different than normal after demineralization both in decalcifying (Table 1) and saline (Table 2) solutions in accordance with length changes.

Experiment 2 (Human Bone)

The changes in demineralized length, area and angle as measured in the decalcifying and saline solutions are presented in Tables 3 and 4, respectively.

Demineralized length was significantly decreased in the axial direction for both decalcifying and saline solutions (Tables 3 and 4, Fig. 2).

Demineralized length in the radial direction, measured in decalcifying solution, was significantly greater than normal in the RT plane (Table 3). The difference was smaller and the significance was lost when demineralized specimens were measured in saline (Table 4). No significant change was observed in the radial direction in the RZ plane ($p>0.4$) and in the tangential direction in the RT plane ($p>0.2$).

The difference in areas between pre- and postdemineralization measurements was significant on both the RT and RZ planes when demineralized specimens were measured in the decalcifying solution (Table 3). In saline, shrinkage in the RZ specimens was still significant ($p=0.0361$) but smaller, whereas the swelling in the RT specimens was no longer significant (Table 4).

No significant difference in any of the measured parameters was observed between initial and postsaline measurements in the undecalcified control group specimens that were stored in saline (Table 5).

Experiment 3 (Glycated Bovine Bone)

The changes in measured parameters after glycation and after demineralization are presented in Table 6. There was no difference between pre- and postglycation measurements ($p>0.09$ for all tests). The difference in the area was less than 1% in all planes.

Significant changes in the tangential direction, measured in the decalcifying solution, were no longer significant when measured in saline. The only significant measurement in saline was the shrinkage in the axial direction when the axial measurements are combined from two planes (Table 6, Fig. 2).

TABLE 5. Changes in length, area, and angle parameters for the control specimens (human bone specimens stored in saline without decalcification). Blank entries: no corresponding measurement.

Specimen	Axial (%)	Tangential (%)	Radial (%)	Angle (°)	Area (%)
RZ	0.19		−0.19	0.15	−0.17
	(0.78)		(1.07)	(0.80)	(1.26)
$n=5$	$p>0.6$		$p>0.7$	$p>0.6$	$p>0.8$
RT		1.63	−0.91	0.50	0.70
		(1.67)	(0.96)	(1.32)	(1.62)
$n=5$		$p>0.06$	$p>0.1$	$p>0.4$	$p>0.3$

TABLE 8. Changes in length, area, and angle parameters after glycation and subsequent demineralization of glycated bovine bone. Blank entries: no corresponding measurement; significant results are highlighted and indicated by a "†" sign; positive numbers indicate enlargement after respective treatment; and "*q*" value is reported as a measure of significance by multiple comparison tests following nonparametric repeated measures of ANOVA (the higher, the more significant).

	After glycation					After decalcifying, in decalcifying solution					After decalcifying, in saline solution				
Specimen	Axial (%)	Tangential (%)	Radial (%)	Angle (°)	Area (%)	Axial (%)	Tangential (%)	Radial (%)	Angle (°)	Area (%)	Axial (%)	Tangential (%)	Radial (%)	Angle (°)	Area (%)
RZ $n=2$	−0.26 (0.37) $p>0.1$		−0.31 (0.45) $p>0.1$	0.348 (0.380) $p>0.7$	−0.29 (0.03) $q<1.1$	−1.31 (0.37) $p>0.1$		−1.00 (0.11) $p>0.1$	0.129 (0.276) $p>0.7$	−0.60 (0.23) $q<2.2$	−0.91 (0.36) $p>0.1$		0.11 (0.09) $p>0.1$	0.0988 (0.416) $p>0.7$	−0.95 (0.24) $q<3.3$
RT $n=4$		−0.14 (0.25) $q<0.8$	0.41 (0.39) $p>0.6$	0.109 (0.158) $p>0.2$	0.16 (0.27) $p>0.5$		**−1.56† (0.69) q=3.873**	−0.07 (1.17) $p>0.6$	0.639 (0.332) $p>0.2$	−0.53 (0.75) $p>0.5$		−0.25 (2.02) $q<1.8$	−0.06 (0.97) $p>0.6$	0.843 (0.688) $p>0.2$	−0.16 (1.44) $p>0.5$
TZ $n=1$	−0.97	−0.99		0.0025	−0.97	−1.11	−1.18		0.683	−1.11	−0.69	−1.02		0.663	−0.83
Combined	−0.50 (0.49) $p>0.2$	−0.31 (0.44) $p>0.08$	0.17 (0.52) $p>0.2$			**−1.24† (0.28) p=0.005**	**−1.47† (0.53) p>0.08**	0.26 (0.78) $p>0.2$			**−0.84† (0.29) p=0.035**	−0.34 (1.75) $p>0.08$	−0.36 (0.89) $p>0.2$		

DISCUSSION

Dimensional change in cortical bone due to demineralization was studied in order to address the question of whether mineralization may contribute to prestress mechanisms in a way consistent with *in vivo* cracking patterns. Significant and anisotropic changes in the size of bovine and human cortical bone specimens were caused by demineralization. The results indicate that human bone shows a reduction in axial length with demineralization and bovine bone exhibits a similar behavior. The measurements were conducted in solution (eliminating drying effects) but making the results dependent on the ionic content of the solution.[15,26] The magnitude of the change in measured dimensions was dependent upon the bathing solution consistent with previous studies.[15,27] In order to reduce uncontrolled variability, specimen donors were limited to one bovine and one human cadaver, thus, likely effects of interindividual variations, gender, and age were not examined.

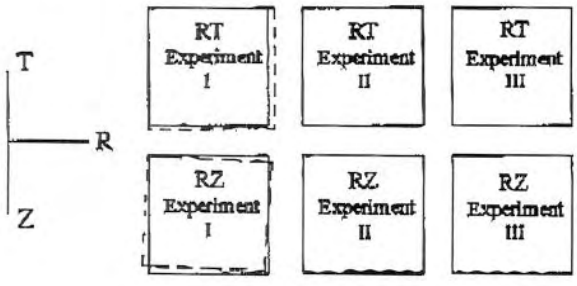

FIGURE 2. Dimensional changes caused by demineralization of cortical bone are drawn on a scale relative to the original size of the specimen as measured in saline solution. Bovine bone is distorted in the longitudinal plane in addition to shrinking axially and expanding radially (I). Human bone axially shrinks (II) and bovine bone behaves similarly when cross linking is increased (III).

Human bone in saline solution (Table 4), which more closely resembles the *in vivo* situation, showed a reduction in axial length with demineralization. Bovine bone exhibited similar results to human in both bathing solutions tested. The observed axial shrinkage in both bovine and human bones of different microstructures supports the idea that mineralization-related dimensional changes occur at a finer level than microstructural.[27] As mineral crystals grow in the hole regions of fibrils[22] and become larger than the axial gap,[24] collagen molecules will be pushed away. As the mineralization proceeds to fill the extrafibrillar spaces, the fibrils will straighten. Bone collagen is laid down in the form of sheets, resulting in different microstructures such as plexiform, circumferential lamellae, trabecular packets and osteons. The majority of collagen and mineral is aligned with the long axis of bone, therefore, our results suggest that a newly formed microstructure would tend to lengthen along the axis of principal collagen orientation during mineralization; in long bones along the anatomical axis consistent with previous observations[26] and the current results. As it lengthens, the new microstructure will put the old bone in tension by pulling the surrounding tissue apart and the reaction from the old bone will put the new microstructure in compression. A simple analogy of this situation is embedding an elastic bar in another material and pulling the bar from both ends. As the bar is stretched from both ends, it will apply tension to the embedding material through shearing at the interface between the bar and the embedding material. The reaction from the embedding

material on the bar will be compressive, again through shear.

It has been shown, by examining the primary bone tissue in humans, that a mature level of fluorescent (fluorescence resulting from the presence of nonenzymatic glycation end products) collagen cross links is achieved for a tissue age of approximately 15 years,[20] whereas bovine bone found in abattoirs is typically 1.5–2 years old. Therefore, the amount of collagen cross linking is expected to be different between bovine and mature human bones. To test whether increased cross linking in bovine bone would address the observed differences in dimensional changes between bovine and human bones, bovine bone was nonenzymatically glycated which is a natural way of forming cross links resulting from a reaction of reducing sugars with collagen.[25] Although no direct quantification of increased cross links was performed on the glycated specimens of this study it was expected that glycation of bovine bone would increase collagen cross linking based on the previous work in our laboratory.[40] When the cross-link content of the matrix of bovine bone was increased using nonenzymatic glycation *in vitro*, it became similar to human bone; instead of large dimensional changes in all directions, there was a reduction of length only in the axial direction when measured in saline (Table 6).

The presence of prestrains in bone has been demonstrated previously using hole drilling[45] and saw cutting.[39] Ascenzi and Benvenuti[2] presented evidence for prestrain also at the osteonal lamellar level by demonstrating that osteonal lamellae assumed a distorted cylindrical shape upon isolation and a helicoidal arrangement upon cutting after isolation. Isolation would remove constraints and, therefore, relieve stresses that may have been formed by mineralization of neighboring microstructures at different times. Relief of the constraint could cause the observed shape changes in lamellae in accordance with our larger-scale experiment. Because specimens with different levels of calcification and decalcified specimens assumed a similar helicoidal arrangement upon cutting, Ascenzi and Benvenuti[2] concluded that mineralization did not have an essential effect on prestresses. However, isolation and cutting could relieve prestresses that are built by the mineral phase even though relieving them does not involve removing the mineral. This is possible in a structure as that of the mineral/collagen network which can be considered as nonhomogeneously stretched and interconnected elastic sheets. Nevertheless, the involvement of mineralization in building prestresses may be different between and within bone microstructure. More recently, Ascenzi[3] analyzed the helicoidal arrangement of osteonal lamellae and dimensional changes upon isolation and cutting in more detail and estimated large shear and axial strains in osteons. In our macroscale measurements, shear deformation (or distortion) was observed for bovine bone in a longitudinal plane measured in saline only, whereas axial pretension of the bone collagenous matrix could be demonstrated for both human and bovine bones in different media consistent with Ascenzi's findings. The dimensional changes caused by demineralization found in this study suggest that prestrains could occur during mineralization. This way, bone builds itself into a self-reinforced prestressed composite material. In the case of plexiform bone, the tension–compression prestrain patterns would be variable. In the case of circumferential lamellae, the outer rings would be expected to be in tension while the inner rings would be prestrained in compression. Prestresses, generated by lengthening osteons, would put the interstitial bone in tension while the new osteon is in compression. In composites where one phase is coated with another phase prestressed in tension, the failure of the composite is by fracture of the prestressed phase and the cracking of the adhesive layer is prevented whereas composites of the same kind without the prestress fail at the interface between the phases under bending.[18] Analogous to these composites, tensile prestresses in the interstitial bone and compressive prestresses in the new osteon would ensure that the cracks will initiate in the interstitial bone and stop at the osteonal cement line thus protecting the more viable bone.

The demineralization results are consistent with a possible damage mechanism resulting from axial expansion during mineralization. For a mineralizing osteon bonded to interstitial bone that is already mineralized (or a mineralizing remodeling packet in trabecular bone), axial expansion of the osteon could cause debonding of the cement line due to shear. This would cause microstructural damage in the cement line as is often seen *in vivo*.[33,37] If the axially expanding osteons cause enough tensile stresses on the surrounding bone matrix, cracks could also form directly in the interstitial matrix. These possible mechanisms of mineralization-caused microcracking are analogous to the interstitial matrix cracking and fiber debonding in a fiber ceramic composite subjected to thermal residual stresses.[14,23]

A possible implication of microdamage produced by mineralization is that it could be a remodeling signal for unloaded or lightly loaded bones.[4,12] If mineralization can cause matrix damage and, consequently, engender more remodeling, it would be expected that osteons would cluster together. This is what was found by Lee *et al.*[28] where osteons of the horse third metacarpal bone were demonstrated to associate with one another at a much greater than random level.

The difference in the magnitude of the observed dimensional changes between bovine and human bones suggests that human and bovine bones are somewhat different in their response to decalcification. The differences may be caused by greater volume percentage of

mineral and less porosity of bovine bone than human bone,[7] and differences in the microstructure, anisotropy, and cross linking. The large swelling in the transverse plane in bovine bone compared to human bone may be attributed to different amounts of collagen cross linking between bovine and human bones. Since highly cross-linked human bone is constrained for swelling, it would be expected that relatively less cross-linked bovine bone would have a larger swelling than human bone in the transverse plane. Large swelling in the transverse plane may allow kinking of collagen fibers and cause axial shrinkage to be larger than expected. Consistent with the above argument, when the cross-link content of the matrix was increased using *in vitro* glycation, the changes in radial size were reduced significantly or eliminated and bovine bone became similar to human bone (Table 6).

Further expansion in both bovine and human bones in the transverse plane (RT) in decalcifying solution and the change in this behavior upon altering the cross-link content can be attributed to the polymeric nature of the collagen. A polymer network tends to swell in the presence of a solvent, the swelling being limited by cross linking among polymer chains or by constraints from the presence of crystallites. A part of the mineralization-caused prestresses may be due to the constraint by the mineral on the swelling of the collagen. Larger expansion in bones in the transverse plane (RT) measured in acidic decalcifying solution compared with that measured after returning to saline solution can be attributed to the low pH of the solution since collagen fibrils tend to swell more in the presence of either an acidic or basic solvent.[41]

Volume change in collagen due to swelling is reversible provided that the system is below a characteristic temperature which is 36–37 °C for bovine and human tendon.[34] Our experiments were conducted at room temperature, therefore, it is likely that swelling of the collagen network in acidic decalcifying solution was reversible and no permanent change was caused in collagen structure.

Dimensional changes due to demineralization were different in magnitude and direction in different anatomical orientations. This anisotropic response to demineralization is consistent with previous results from examination of cylindrical specimens.[26] Lees also reported a demineralization-caused axial shrinkage in the same order of magnitude with our results for wet bovine bone. However, the results are not directly comparable due to differences, such as a drying step between wet and demineralized bone in Lees *et al.*,[27] in the methodology between the current study, and others. The magnitude of the dimensional change in a given anatomical direction was also different depending on which plane was used for measurement (such as the radial direction measured on the TZ plane as compared to the RT plane), suggesting that the characteristic size of the microstructure (plexus or osteon) plays a role in the mechanics of dimensional changes even if the underlying mechanisms are present at a finer level. In this regard, the differences in the initial dimensions of the specimens might have contributed to the differences in dimensional changes between the experiment groups. However, this is expected to be small as all dimensions of specimens were an order of magnitude larger than the microstructural dimensions.

In conclusion, there is significant shrinkage in cortical bone in the direction of the long axis upon demineralization. This shrinkage is consistent with a tendency for axial elongation of the matrix during mineralization. Cement line and interstitial matrix cracks in cortical and cancellous bone are consistent with an hypothesis that axial expansion of osteons and remodeling packets resulting from mineralization can increase the possibility that bone will crack at the cement line or through the interstitial bone.

ACKNOWLEDGMENTS

NIH AR40776, NIH AR41210, and DAMD 17-18-18515. The authors thank Chen Young for preparing the glycation solution, John Khoury for performing the measurements of denatured collagen, Dr. S. Tashman for providing the human femur and Dr. C. Les and Dr. D. Vashishth for helpful comments.

REFERENCES

[1] Archer, R. R. Growth Stresses and Strains in Trees. New York: Springer, 1987.

[2] Ascenzi, A., and A. Benvenuti. Evidence of a state of initial stress in osteonic lamellae. *J. Biomech.* 10:447–453, 1977.

[3] Ascenzi, M. G. A first estimate of prestress in so-called circularly fibered osteonic lamellae. *J. Biomech.* 32:935–942, 1999.

[4] Baltadjiev, G. Micromorphometric characteristics of osteons in compact bone of growing tibiae of human fetuses. *Acta Anat. (Basel)* 154:181–185, 1995.

[5] Bank, R. A., M. Krikken, B. Beekman, R. Stoop, A. Maroudas, F. P. J. G. Lafeber, and J. M. Tekoppele. A simplified measurement of degraded collagen in tissues: Application in healthy, fibrillated, and osteoarthritic cartilage. *Matrix Biol.* 16:233–243, 1997.

[6] Bank, R. A., M. T. Bayliss, F. B. Lafeber, A. Maroudas, and J. M. Tekoppele. Aging and zonal variation in post-translational modification of collagen in normal human articular cartilage. The age-related increase in nonenzymatic glycation affects biomechanical properties of cartilage. *Biochem. J.* 330(Pt 1):345–351, 1998.

[7] Biltz, R. M., and E. D. Pellegrino. The chemical anatomy of bone. I. A comparative study of bone composition in sixteen vertebrates. *J. Bone Jt. Surg., Am.* 51:456–466, 1969.

[8] Boyce, T. M., D. P. Fyhrie, M. C. Glotkowski, E. L. Radin,

and M. B. Schaffler. Damage type and strain mode associations in human compact bone bending fatigue. *J. Orthop. Res.* 16:322–329, 1998.

[9] Burr, D. B., R. B. Martin, M. B. Schaffler, and E. L. Radin. Bone remodeling in response to *in vivo* fatigue microdamage. *J. Biomech.* 18:189–200, 1985.

[10] Burr, D. B., M. B. Schaffler, and R. G. Frederickson. Composition of the cement line and its possible mechanical role as a local interface in human compact bone. *J. Biomech.* 21:939–945, 1988.

[11] Burr, D. B., M. R. Forwood, D. P. Fyhrie, R. B. Martin, M. B. Schaffler, and C. H. Turner. Bone microdamage and skeletal fragility in osteoporotic and stress fractures. *J. Bone Miner. Res.* 12:6–15, 1997.

[12] Burton, P., C. Nyssen-Behets, and A. Dhem. Haversian bone remodeling in human fetus. *Acta Anat. (Basel)* 135:171–175, 1989.

[13] Carter, D. R., and W. C. Hayes. Compact bone fatigue damage. A microscopic examination. *Clin. Orthop. Relat. Res.* 127:265–274, 1977.

[14] Clegg, W. J. Controlling cracks in ceramics. *Science* 286:1097–1098, 1999.

[15] Finlay, J. B., and W. R. Hardie. Anisotropic contraction of cortical bone caused by dehydration of samples of the bovine femur *in vitro*. *Proc. Inst. Mech. Eng., Part H: J. Eng. Med.* 208:27–32, 1994.

[16] Forwood, M. R., and A. W. Parker. Microdamage in response to repetitive torsional loading in the rat tibia. *Calcif. Tissue Int.* 45:47–53, 1989.

[17] Fournier, M., B. Chanson, B. Thibaut, and D. Guitard. Mechanics of standing trees—Modeling a growing structure submitted to continuous and fluctuating loads. 2. Tridimensional analysis of maturation stresses—case of standard hardwood. *Ann. Sci. Forest.* 48:527–546, 1991.

[18] Garden, H. N., and L. C. Hollaway. An experimental study of the failure modes of reinforced concrete beams strengthened with prestressed carbon composite plates. *Composites, Part B* 29:411–424, 1998.

[19] Gartner, B. L. Trees have higher longitudinal growth strains in their stems than in their roots. *Int. J. Plant Sci.* 158:418–423, 1997.

[20] Gibson, G., M. Glotkowski, D. Fyhrie, M. Schaffler, C. Les, and S. Tashman. Fluorescence provides a measure of local tissue age and remodeling history in human compact bone. Transactions of the 46th Annual Meeting. Orthopaedic Research Society, 2000, p. 691.

[21] Griffin, L. V., J. C. Gibeling, R. B. Martin, V. A. Gibson, and S. M. Stover. Model of flexural fatigue damage accumulation for cortical bone. *J. Orthop. Res.* 15:607–614, 1997.

[22] Hodge, A. J. Molecular models illustrating the possible distributions of "holes" in simple systematically staggered arrays of type I collagen molecules in native-type fibrils. *Connect Tissue Res.* 21:137–147, 1989.

[23] Hsueh, C. H. Matrix cracking with frictional bridging fibres in continuous fibre ceramic composites. Part II. Cracking due to residual stresses. *J. Mater. Sci.* 30:4793–4800, 1995.

[24] Katz, E. P., E. Wachtel, M. Yamauchi, and G. L. Mechanic. The structure of mineralized collagen fibrils. *Connect Tissue Res.* 21:149–158, 1989.

[25] Knott, L., and A. J. Bailey. Collagen cross links in mineralizing tissues: A review of their chemistry, function, and clinical relevance. *Bone (N.Y.)* 22:181–187, 1998.

[26] Lees, S. A mixed packing model for bone collagen. *Calcif. Tissue Int.* 33:591–602, 1981.

[27] Lees, S., J. D. Heeley, and P. F. Cleary. Some properties of the organic matrix of a bovine cortical bone sample in various media. *Calcif. Tissue Int.* 33:83–86, 1981.

[28] Les, C. M., M. R. Simon, G. J. Pijanowski, and J. C. Eurell. A technique for evaluating secondary remodeling in the diaphysis of the equine third metacarpal bone. *Proc. Am. Soc. Biomech.* 13:84–85, 1989.

[29] Martin, R. B., and D. B. Burr. Structure, Function, and Adaptation of Compact Bone. New York: Raven, 1989.

[30] Martin, R. B., S. M. Stover, V. A. Gibson, J. C. Gibeling, and L. V. Griffin. *In vitro* fatigue behavior of the equine third metacarpus: Remodeling and microcrack damage analysis. *J. Orthop. Res.* 14:794–801, 1996.

[31] Mattheck, C., and H. Kubler. Wood—The Internal Optimization of Trees, edited by T. E. Timell. New York: Springer, 1995.

[32] Niklas, K. J. Plant Biomechanics: An Engineering Approach to Plant Form and Function. Chicago: The University of Chicago Press, 1992.

[33] Norman, T. L., and Z. Wang. Microdamage of human cortical bone: Incidence and morphology in long bones. *Bone (N.Y.)* 20:375–379, 1997.

[34] Rigby, B. J. Relation between the shrinkage of native collagen in acid solution and the melting temperature of the tropocollagen molecule. *Biochim. Biophys. Acta* 133:272–277, 1967.

[35] Saha, S. Longitudinal shear properties of human compact bone and its constituents and the associated failure mechanisms. *J. Mater. Sci.* 12:1798–1806, 1977.

[36] Schaffler, M. B., E. L. Radin, and D. B. Burr. Mechanical and morphological effects of strain rate on fatigue of compact bone. *Bone (N.Y.)* 10:207–214, 1989.

[37] Schaffler, M. B., K. Choi, and C. Milgrom. Aging and matrix microdamage accumulation in human compact bone. *Bone (N.Y.)* 17:521–525, 1995.

[38] Sheehan, D. C., and B. B. Hrapchak. Theory and Practice of Histotechnology. Columbus, OH: Battelle, 1980.

[39] Stanwyck, T. S., R. Fischer, M. Pope, and D. Seligson. Studies on prestress in bone. *Biorheology* 19:301–306, 1982.

[40] Vashishth, D., G. J. Gibson, J. I. Khoury, M. B. Schaffler, J. Kimura, and D. P. Fyhrie. Influence of nonenzymatic glycation on biomechanical properties of cortical bone. *Bone (N.Y.)* 28:195–201, 2001.

[41] Veis, A. Intact Collagen. In: Treatise on Collagen Volume 1: Chemistry of Collagen, edited by G. N. Ramachandran. London: Academic, 1967, pp. 368–439.

[42] Wainwright, S. A., W. D. Biggs, J. D. Currey, and J. M. Gosline. Mechanical Design in Organisms. Princeton: Princeton University Press, 1982.

[43] Wang, X., R. A. Bank, J. M. TeKoppele, G. B. Hubbard, K. A. Athanasiou, and C. M. Agrawal. Effect of collagen denaturation on the toughness of bone. *Clin. Orthop. Relat. Res.* 371:228–239, 2000.

[44] Wenzel, T. E., M. B. Schaffler, and D. P. Fyhrie. *In vivo* trabecular microcracks in human vertebral bone. *Bone (N.Y.)* 19:89–95, 1996.

[45] Wright, T. M., D. M. Barnett, and W. C. Hayes. Residual stresses in bone. *Recent Adv. Eng. Sci.* 8:25–32, 1977.